REACTOR MATERIALS

A Quarterly Technical Progress Review

Prepared for DIVISION OF TECHNICAL INFORMATION, USAEC, by
R. W. DAYTON, E. M. SIMONS, and ASSOCIATES, BATTELLE MEMORIAL INSTITUTE

Spring 1964

● VOLUME 7

● NUMBER 1

FEATURE ARTICLE:

Some Facts About Stress Corrosion of Austenitic Stainless Steels in Reactor Systems

TECHNICAL PROGRESS REVIEWS

To meet the needs of industry for concise summaries of current atomic developments, the Atomic Energy Commission is publishing this series, Technical Progress Reviews. Issued quarterly, each of the reviews digests and evaluates the latest findings in a specific area of nuclear technology and science.

The five journals published in this series are:

Isotopes and Radiation Technology, P. S. Baker, A. F. Rupp, and associates, Oak Ridge National Laboratory

Nuclear Safety, Wm. B. Cottrell, W. H. Jordan, and associates, Oak Ridge National Laboratory

Power Reactor Technology, W. H. Zinn and J. R. Dietrich, General Nuclear Engineering Corporation

Reactor Fuel Processing, Stephen Lawroski and associates, Chemical Engineering Division, Argonne National Laboratory

Reactor Materials, R. W. Dayton, E. M. Simons, and associates, Battelle Memorial Institute

Each journal may be purchased from the Superintendent of Documents, U. S. Government Printing Office, Washington, D. C., 20402. *Isotopes and Radiation Technology* at $2.00 per year for subscription or $0.55 for individual issues; the other four journals at $2.50 per year and $0.70 per issue. See back cover for remittance instructions and foreign postage requirements.

The views expressed in this publication do not necessarily represent those of the United States Atomic Energy Commission, its divisions or offices, or of any Commission advisory committee or contractor.

Availability of Reports Cited in This Review

Unclassified AEC reports are available for inspection at AEC depository libraries and are sold by the Office of Technical Services, Department of Commerce, Washington, D. C., 20230. Some of the reports cited are not available owing to their preliminary nature; however, the information contained in them will eventually be made available in formal progress or topical reports.

Unclassified reports issued by other Government agencies or private organizations should be requested from the originator.

Unclassified British and Canadian reports may be inspected at AEC depository libraries. British reports are sold by the British Information Service, 45 Rockefeller Plaza, New York, N. Y.; Canadian reports (AECL series) are sold by the Scientific Document Distribution Office, Atomic Energy of Canada, Ltd., Chalk River, Ontario, Canada.

Classified U. S. and foreign reports identified in this journal as Classified may be purchased by properly cleared Access Permit Holders from the Division of Technical Information Extension, U. S. Atomic Energy Commission, P. O. Box 1001, Oak Ridge, Tenn., 37831. Such reports may be inspected at classified AEC depository libraries.

REACTOR MATERIALS

A REVIEW OF RECENT DEVELOPMENTS

Prepared for DIVISION OF TECHNICAL INFORMATION, USAEC,
by R. W. DAYTON, E. M. SIMONS, and ASSOCIATES,
BATTELLE MEMORIAL INSTITUTE

SPRING 1964

VOLUME 7

NUMBER 1

Foreword

Reactor Materials is one of a series of quarterly technical progress reviews broadly covering the field of nuclear science and technology. Under the auspices of the AEC Division of Technical Information, *Reactor Materials* is prepared by Battelle personnel from worldwide literature. It covers properties, behavior, and fabrication processes of materials applicable to nuclear reactor components and associated equipment.

The reader will recognize that the scope of this Review is too broad to permit detailed coverage of every topic. Rather, the authors and editors attempt to combine the highlights of significant new developments into an informative summary of current research for both management and the technical specialist. As a rule, enough of the results are presented to define the research and summarize the findings. For readers desiring more information on any particular topic, a complete set of references is provided at the end of each section.

Each quarter a number of bibliographies, monographs, and books appear on subjects within the scope of *Reactor Materials*. Although the main purpose of this Review is to call attention to findings that are new and significant, such publications are noted in the text because they often represent excellent compilations of available information on important materials topics.

R. W. DAYTON
E. M. SIMONS
R. W. ENDEBROCK
Battelle Memorial Institute

DEPOSITED BY THE
UNITED STATES OF AMERICA

Contents

FEATURE ARTICLE

Some Facts About Stress Corrosion of Austenitic Stainless Steels in Reactor Systems. . . 1

by Warren E. Berry, Battelle Memorial Institute

Foreword

I FUEL AND FERTILE MATERIALS . 14
Unalloyed Uranium 14
Alpha-Phase Uranium Alloys . . . 14
Gamma-Phase Uranium Alloys . . 15
Plutonium 15
Plutonium Compounds 17
Thorium 18
Metal-Ceramic Fuels 18
Coated-Particle Fuel Materials . . 19
Uranium Oxides 29
Uranium Carbides, Nitrides, and Sulfides 29
Fuel-Water Reactions 31
Basic Studies of Irradiation Effects on Fuel Materials 32
References 33

II MODERATOR MATERIALS . . 36
Graphite 36
Beryllium Metal and Alloys . . . 37
Beryllium Oxide 41
Beryllium Compounds 42
Solid Hydrides 42
References 43

III NUCLEAR POISONS 45
Metallic Poison Materials . . . 45
Nonmetallic Poison Materials . . . 45
References 47

IV CLADDING AND STRUCTURAL MATERIALS 48
Corrosion 48
Radiation Effects in Nonfuel Materials . 53
Selected Mechanical Properties of Cladding and Structural Materials . 60
Selected Metallurgical Aspects of Cladding and Structural Materials . 61
Ceramic Technology 66
References 66

V SPECIAL FABRICATION TECHNIQUES 71
Melting, Hot and Cold Working . . 71
Cladding 72
Welding and Brazing 74
Explosive Forming 75
Nondestructive Testing 78
References 78

Issued quarterly by the U. S. Atomic Energy Commission. Use of funds for printing this publication approved by the Director of the Bureau of the Budget on October 14, 1963.

67 195A A 30

FEATURE ARTICLE

Some Facts About Stress Corrosion of Austenitic Stainless Steels in Reactor Systems

By Warren E. Berry*

(Editor's Note: Reliability through structural integrity is perhaps the most important consideration in the mechanical design of nuclear reactor systems. Ordinarily, the materials specialist need look no further if he finds a commercial material with nuclear properties that satisfy the reactor physicist, mechanical properties that are ample to withstand the expected stresses, and chemical properties that preclude excessive corrosion in the intended environment. In stainless steels, however, he must reckon with a phenomenon that can cause cracking under the combined action of tensile stresses and corrosion when neither is severe enough to produce a failure by itself. This phenomenon is stress-corrosion cracking.

The article that follows presents dramatic examples of stress-corrosion cracking encountered in established reactor systems. It describes the measures taken to circumvent the problem and concludes with an account of the various attempts to analyze and explain its cause both theoretically and experimentally. The reader will note that, although impressive strides have been made, stress corrosion has many ramifications, and complete understanding has not yet been achieved.)

Introduction

The austenitic stainless steels have been the workhorse of the nuclear reactor industry. They have been used in all reactor concepts—pressurized water, boiling water, nuclear superheaters, homogeneous, gas-cooled, and sodium-cooled reactors—and in almost all components, such as fuel diluent, fuel cladding, reactor-vessel lining, piping, heat exchangers, and structural members. One of the major reasons for their widespread use has been their excellent corrosion resistance and general compatibility with the reactor environments.

Despite their low corrosion rates, the stainless steels often exhibit a major shortcoming, namely, stress-corrosion cracking, a brittle fracture in a normally ductile material. This type of failure is not peculiar to nuclear reactors, having been recognized, reported, and researched prior to their advent. The novel and often stringent conditions of reactor operation only served to produce a well-known phenomenon in new ways.

Stress-corrosion cracking occurs as a result of the combined action of tensile stresses and corrosion, where the action of either variable by itself would not produce a failure, although, naturally, it occurs more readily at higher stress levels. The corroding media that cause stress-corrosion cracking are peculiar to a given alloy or alloying system. Chlorides and hydroxides are mainly responsible for cracking in the austenitic stainless steels. There are varying degrees of susceptibility, depending on the cation species. For example, stress-corrosion cracking occurs rapidly in the presence of chloride solutions such as $MgCl_2$, $CaCl_2$, and

*Assistant Chief, Corrosion Research Division, Battelle Memorial Institute.

$ZnCl_2$, which do not readily attack stainless steel. Stress-corrosion cracking occurs after long exposure to solutions that produce pitting (NaCl, KCl, and NH_4Cl); however, it does not normally occur at all in solutions that cause heavy general attack ($CrCl_3$, $FeCl_3$, and $HgCl_2$). The seriousness of stress corrosion of stainless steel in different alkaline solutions is in the tentative order: NaOH > KOH > LiOH > NH_4OH.

The cracking that occurs in stainless steels exposed to chloride solutions is predominantly transgranular. An example of this is shown in Fig. 1. Under certain conditions of sensitization (grain-boundary precipitation of chromium carbide as the result of heating in the 900 to 1500°F range), stress can produce cracking at grain boundaries in advance of intergranular attack. This is illustrated in Fig. 2. Cracking in caustic solutions can be transgranular or intergranular, depending on temperature, caustic concentration, associated chemicals, and whether the stainless steel is sensitized.

Examples of Failures

Some examples of stress-corrosion cracking, which have occurred in reactor operations or related conditions, are cited in the following paragraphs.

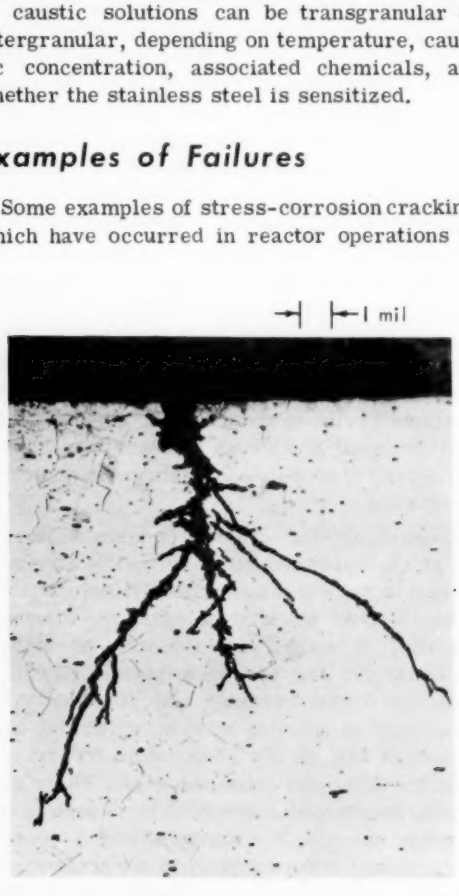

Fig. 1 Transgranular stress-corrosion crack in austenitic stainless steel.

Fig. 2 Intergranular stress-corrosion crack in type 304 stainless steel.[2] (Courtesy of *Nucleonics* magazine.)

Homogeneous Reactor

Transgranular stress-corrosion cracks were detected[1] in type 304 and type 347 stainless-steel components of the Homogeneous Reactor during tests of remote-maintenance procedure prior to actual startup of the reactor. The cracks were in the secondary system used for detecting leaks at the flanged joints of the primary system and in the grooves of the flanges in the primary system. Up to 1070 ppm chlorides were found in the fluid drained from the secondary system. This tubing was believed to have been contaminated with chlorides prior to installation. Apparently a chlorinated-hydrocarbon lubricating compound was not removed during fabrication and was baked in during subsequent annealing. The stress-corrosion cracking was attributed to these chlorides.

Savannah River Reactor Plant

Intergranular stress-corrosion cracking was detected in two type 304 stainless-steel outlet nozzles in high-purity heavy-water moderator service at the Savannah River Reactor plant.[3]

The cracks propagated from general intergranular attack that apparently occurred at sensitized grain boundaries as the result of acid pickling during initial fabrication of the nozzles. Cracking was attributed to chlorides, although the bulk heavy water contained only about 6 ppb chloride. The chloride ions were believed to have concentrated in the intergranular pickling cracks. Laboratory tests with sensitized U-bend specimens, pickled to produce intergranular attack, showing intergranular cracking within 450 hr in water containing only 2 ppm chloride at 90°C.

Additional work at Savannah River[4] indicated that chlorides concentrated (up to 1000 ppm) in aluminum-corrosion-product deposits in the reactor system. Transgranular cracks in type 304 stainless steel were found in conjunction with some of these deposits. The aluminum corrosion products apparently dissolved during corrosion of the aluminum cladding on the fuel elements and then deposited on the stainless steel in the lower temperature regions of the reactor temperature range. In laboratory tests, aluminum corrosion products exhibited ion-exchange properties, adsorbing both cations and anions from the solution.

Heat Exchanger at Capenhurst

Transgranular stress-corrosion cracking occurred in a niobium-stabilized austenitic stainless heat exchanger at Capenhurst, England.[5] The heat exchanger, a helical coil of tubing within a stainless-steel shell, cooled the bypass water of a corrosion test loop from 300 to 40°C prior to its entry into an ion-exchange-resin bed. Loop water was inside the tubing and cooling water was on the shell side. The cooling water contained 440 ppm chlorides. The cracking failure occurred on the outside surface of the tubing where the coil and shell were in close contact. Chlorides apparently became concentrated in this crevicelike area.

Nautilus Nonregenerative Heat Exchanger

Transgranular stress-corrosion cracks were also found[6] in the nonregenerative heat exchanger that cooled the reactor primary water prior to its entry into the ion-exchange-resin beds aboard the U. S. S. *Nautilus*. Cracks originated on the outside surface of the type 347 stainless-steel tubes. They were located at the crevice area on the drain side of the inner tube sheet of the double tube-sheet assembly. Crevices between the rolled-in tubes and the tube sheet apparently allowed sufficient leakage to concentrate the chlorides beyond the 15-ppm level of the bulk cooling water. Inlet temperature of the reactor water was 260°F, and the outlet temperature was 120°F.

S1W Reactor Plant

Ten tubes were reported[7] to have leaked in the S1W port stainless-steel steam generator within the first 16 months of operation. Tubes were of type 347 stainless steel rolled into a single tube sheet. Three out of four tubes examined exhibited transgranular cracks originating on the boiler (shell) side. The cracks occurred in the crevice area between the tube and tube sheet near the secondary (boiler water) side. The boiler water was treated with 50 to 200 ppm phosphate at *p*H 10.6 to 11.2, but contained up to 48 ppm chlorides and up to 0.1 ppm oxygen (boiler feedwater contained up to 6.5 ppm oxygen). Steam pressure ranged up to 340 psi (about 430°F). The cracks were attributed to chloride stress-corrosion cracking.

Superheat Advance Demonstration Experiment

Intergranular and transgranular cracking have been observed[2] in type 304 stainless-steel-clad fuel elements in superheater experiments conducted in the Vallecitos Boiling-Water Reactor. The intergranular cracks were related to sensitized areas in the stainless steel, whereas the transgranular cracks were found in areas of little or no sensitization (maximum cladding temperature ranged from 1200 to 1350°F). Chloride deposits were found on the surface at crack sites. Cracking was attributed to concentration of chlorides carried over from the reactor water in conjunction with moisture and oxygen in the steam and to high operating and residual stresses in the cladding.

Pressurized-Water Reactor

Leaks occurred in several type 304 stainless-steel tubes in one of the Pressurized-Water Reactors (PWR) (Shippingport, Pa.) steam generators after about 200 hr of power operation and 2 weeks of steaming and miscellaneous high-temperature conditions.[8] The cracks were transgranular and originated from the outside (boiler water) of the tubes. Cracking was attributed to steam blanketing in a localized area, which resulted in concentrating the free caustic in the treated boiler water.

Dresden Control-Rod Components

Intergranular cracks were found[9] in semi-austenitic 17-4 PH stainless-steel tubes in the control-rod mechanism of the Dresden reactor after about 1500 hr of operation. Cracking was attributed to high residual stresses and to the 900°F aging heat-treatment, which produces maximum hardness in this alloy. The tubes that cracked had been exposed to high-purity water at temperatures ranging from 200 to 550°F.

Preventive Measures

Measures to eliminate stress-corrosion-cracking susceptibility include: reducing stress levels, altering the chemistry of the environment, cathodic protection, changing the design or operating conditions, substituting alternative materials and, on a long-range basis, understanding the mechanism of cracking. Frequently the control of only one variable will eliminate susceptibility, whereas on other occasions the rigid control of all variables is required.

Stress Level

It is a well-known fact that reduction of tensile stress, either applied or residual, will lower cracking susceptibility. However, because of the interaction of environmental factors and the composition of the stainless steel itself, it is not possible to specify a universal threshold stress level below which no cracking will occur. For example,[10] Fig. 3 dramatically illustrates the relative susceptibility of various types of stainless steels to cracking in boiling 42% $MgCl_2$ as well as the beneficial effect of reducing stress levels. However, it does not necessarily follow that comparable times to failure will be obtained with these alloys in other environments.

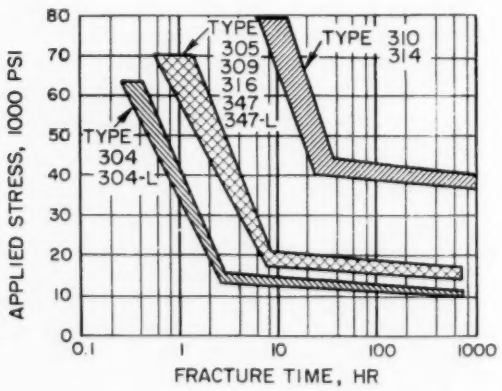

Fig. 3 Relative stress-corrosion cracking resistance of commercial stainless steels in boiling 42% magnesium chloride.[10]

Unfortunately in some environments there does not appear to be any threshold stress level. Stress-corrosion cracking of type 347 stainless steel has been reported[11] at 2000 psi tensile stress in the condensing vapors above a solution containing 50 ppm chloride at 400°F. From a practical standpoint, even under load-free conditions, it would be extremely difficult to reduce residual (internal) stresses to such low levels.

However, in many applications, solution annealing at 1850 to 1900°F after fabrication or welding can reduce residual stresses sufficiently to eliminate cracking. Electrical resistance heating has been demonstrated[12] to be a possible field method for reducing residual stresses in order to decrease cracking susceptibility in type 347 stainless-steel tubing.

Chemistry of the Environment

It naturally follows that reduction or elimination of the offending species in the corrodent will reduce susceptibility to cracking. For example, in reactor waters contaminated with chlorides, both oxygen and chloride must be present for stress-corrosion cracking to occur. It has been demonstrated[13] in tilting autoclave tests, using alkaline phosphate treated 500°F water, that U-bend specimens of type 347 stainless steels will not crack when chloride content is high and oxygen content is low, or vice versa. These results are shown graphically in Fig. 4.

Oxygen is not a requisite for caustic cracking of stainless steels. However, caustic cracking does not occur so readily as chloride cracking. Tilting autoclave tests using aqueous solutions at 500°F have revealed[13] that greater than 50,000 ppm NaOH was required to crack type 347 stainless-steel U-bend specimens, whereas similar specimens cracked readily in 10 ppm chloride, provided that sufficient oxygen was present. However, under concentrating conditions, cracking has been observed[14] in dilute NaOH solutions at 488°F.

The use of inhibitors to prevent cracking has been studied to some extent. Increasing *p*H to

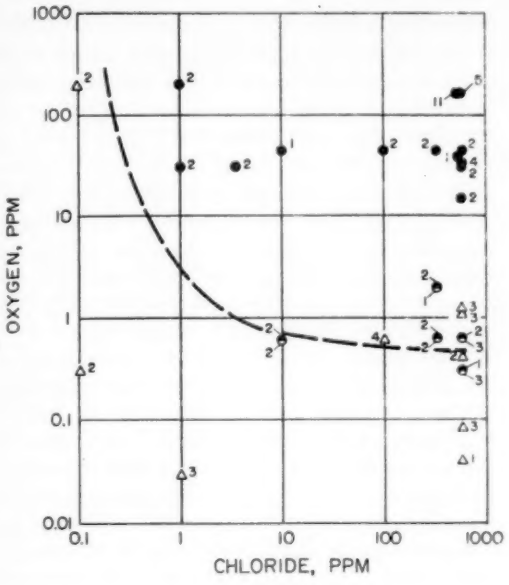

Fig. 4 Relation between chloride and oxygen content of alkaline phosphate-treated boiler water and susceptibility to stress corrosion of austenitic stainless steel exposed to the steam phase with intermittent wetting at 500°F.[13] ●, failure; △, no failure. Figures denote number of specimens.

11 and adding phosphate or chromate ion have inhibited cracking in very dilute chloride solutions at temperatures to 200°F.[15] Alkaline phosphate boiler-water treatment has inhibited stress-corrosion cracking in water containing chlorides.[13] Additions of Na_2HPO_4 or $NaNO_2$ greatly prolonged the time to cracking but did not prevent it entirely in chloride-contaminated solutions and wet or superheated steam at temperatures of 250 to 330°C.[16] Na_2HPO_4 has been found to be an effective inhibitor of caustic cracking,[13,16] particularly under some conditions where NaOH is being concentrated by evaporation.[14]

Of particular interest is the regulation of the coordinated-phosphate boiler-water treatment to prevent free caustic formation on evaporating surfaces. Operation at *p*H and phosphate levels above the curve shown in Fig. 5 results in free caustic,[8,13] and this caustic is believed to be the cause of the cracking that occurred in the PWR steam generator.[8] Subsequent practice at the PWR called for operation at 0.2 *p*H units below this curve.

Cathodic Protection

Many laboratory experiments have demonstrated that cathodic protection can prevent stress-corrosion cracking. However, large-scale protection in reactor environments is difficult. Arrangement of anodes to provide sufficient protection is virtually impossible, particularly in piping and heat exchangers. The problem is further complicated by the low conductivity of the water, especially on the primary side. Sacrificial anodes are usually undesirable because of the corrosion products they introduce into the coolant.

Design Considerations

As mentioned earlier, design changes that result in lower operating and residual stresses can eliminate stress-corrosion cracking. Of particular concern are stagnant areas and crevices in heat-transfer areas where chlorides or caustic can become concentrated. Almost all the failures reported to date have been related to concentrating conditions.

Typical of concentrating areas is the crevice between rolled-in tubes and tube sheets as shown in Fig. 6. This contains all the ingredients conducive to stress-corrosion cracking—a combination of high residual stresses, heat transfer, and a crevice area where evaporation and concentration can occur. To avoid solids concentration in this design, it is desirable to

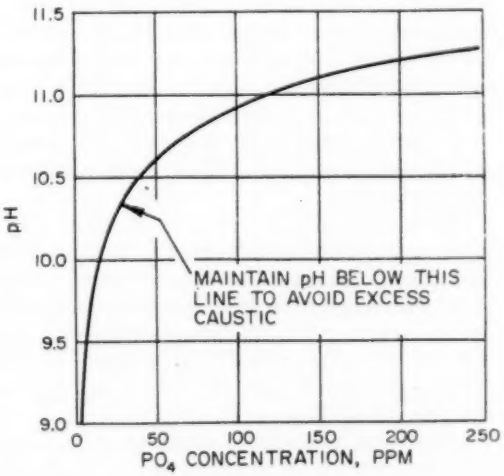

Fig. 5 Relation between *p*H and phosphate concentration, defining areas of phosphate vs. free caustic residues on evaporating surfaces.[8,13]

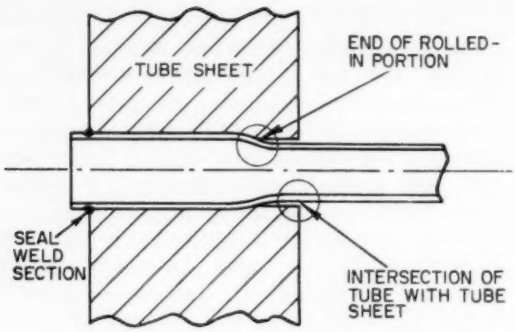

Fig. 6 Areas susceptible to stress-corrosion cracking in austenitic stainless-steel tube-to-tube-sheet joints.

have the more corrosive water (high in caustic or chlorides and oxygen) inside the tubes, and the less corrosive (high purity) water outside the tubes. However, this is not always practical.

A major contributing factor in the cracking failures in the PWR steam generator is believed to be steam blanketing and concentration of free caustic in a localized area.[8] Additional steam risers were installed to eliminate steam blanketing. The elimination of free caustic has already been discussed.

The cracking in the stainless-steel fuel cladding in nuclear superheaters has been attributed to concentration of chlorides carried over by wet steam. A task force that investigated the failures points out[17] that failures do not occur in conventional power plants because the steam is dry and appreciably superheated before it reaches stainless-steel surfaces. Also, the steam in conventional power plants contains very little oxygen as compared with a nuclear superheater receiving steam from a boiling-water reactor.

Stress-corrosion cracking of stressed stainless steel has been observed[15] in very dilute chloride solutions in laboratory tests, where specimens were completely immersed and there was no concentration by evaporation. Cracking failures were reported in a 5-ppm chloride solution at 200°F and in a 10-ppm chloride solution at 165°F.

There also appears to be at least one other mechanism whereby chlorides can become concentrated. Savannah River Plant experience[4] has indicated that chlorides concentrate in aluminum corrosion products, apparently by an ion-exchange mechanism.

Alternative Materials

One of the obvious solutions to the problem of stress-corrosion cracking of stainless steels is to use an alternative material. This is not so easy as it may seem at first glance. From an economical and practical standpoint, low-alloy steels or nickel-base alloys are the major alternative. These alloys are not susceptible to chloride stress-corrosion cracking. Steels exhibit caustic cracking, but nickel alloys crack in caustic only at very high temperatures and very high concentrations.

Low-carbon steels have been shown to pit in the same environments that cause chloride stress-corrosion cracking of stainless steel.[18] Pits, more than 0.030 in. deep, were found in carbon-steel tubing of model boilers exposed 5000 hr to boiler water containing 40 to 50 ppm chloride, 6 to 10 ppm sulfite, and 40 to 80 ppm phosphate at *p*H 10.5 to 10.8. Stainless-steel tubes failed by stress-corrosion cracking within 2000 hr of exposure under similar conditions. Carbon steel and low-alloy steels are subject to pitting in high-temperature water containing dissolved oxygen. Pitting can be very severe in crevices under these conditions.[19]

Of the nickel-base alloys, Inconel* appears most promising as an alternative material for stainless steel. Experiments have shown that it possesses the same excellent general corrosion resistance as stainless steel[19,20] and does not exhibit stress-corrosion cracking in high-temperature water containing chlorides.[18–22]

Theoretical Approaches

While the engineers have been busy with immediate solutions to stress-corrosion problems, other scientists have been engaged in long-range fundamental studies of the cracking mechanism—their philosophy being that an understanding of the mechanism should provide clues to means of eliminating the problem. Most of the fundamental studies on stress-corrosion cracking are being conducted on austenitic stainless steels.

The favorite corrodent of the fundamentalist has been a boiling aqueous solution of 42% $MgCl_2$. Although this solution does not approach

*Registered trademark, The International Nickel Company, Inc.

service conditions, it does cause cracking in susceptible alloys within a few hours and is relatively easy to handle. Unfortunately some of the theoretical interpretations based on results obtained in this environment do not always agree with observations of cracking in service, and therein lies the basis for at least some of the disagreement in this field.

There are some general rules on susceptibility to stress corrosion which are fairly well accepted. These are:

1. A pure metal is immune to stress-corrosion cracking.
2. Alloys made from pure metals may be susceptible to cracking.
3. There is no universal corrodent that will cause cracking in all alloys, i.e., the corroding conditions that produce cracking are specific to an alloy or alloy system.
4. Cathodic protection can prevent stress-corrosion cracking and even stop crack propagation if applied while cracking is in progress.
5. One or more minor impurity elements in a metal or alloy can govern its degree of immunity or susceptibility.
6. Changes in structure or homogeneity of an alloy by heat-treatment can influence its immunity or degree of susceptibility.

There are two basic questions to be answered with respect to the mechanism of stress-corrosion cracking in stainless steel: (1) What causes a crack to initiate? (2) What causes a brittle type cracking failure to propagate in an otherwise ductile material? Both aspects have received considerable attention, but the bulk of the research has been concentrated on the more intriguing question of crack propagation. Present theories on the mechanism of cracking will be discussed on a limited scale in the following paragraphs.

Crack Initiation

Hoar and Hines[23] have studied the electrochemical nature of crack initiation. Using loaded wire specimens in boiling 42% $MgCl_2$ solution, they obtained time-potential curves of the type shown in Fig. 7. They note that the curves for stressed and unstressed specimens have the same general shape, until the onset of cracking in the stressed ones. They attribute the initial drop in potential to attack in pores in the oxide film upon immersion. The pores then slowly plug with oxide or hydroxide, and the potential rises. Eventually, hydroxide formation is believed to cease, and, if the pores are not completely healed, attack occurs at the base of the pores, with the potential dropping to a steady state. The potential falls rapidly during the last few minutes before fracture. It then exhibits a rapid upward kick at fracture. Hoar and Hines show that cracking occurs at approximately the same total exposure time, even when there is no applied load during the incubation period prior to fracture; i.e., when unstressed samples are exposed for time A (Fig. 7) and then a tensile load is applied, a slight dip occurs in the potential curve. However, the curve then continues on the same pattern as that for a specimen which had been loaded continuously from the time of immersion.

Miller and Francis[24] observed a similar induction phenomenon on as-received wires exposed to boiling $MgCl_2$ prior to loading. On the other hand, they found that preexposure of annealed stress-free wires did not shorten the time to failure once the stress was applied. Van Rooyen[25] found that, if the load was removed from a stressed specimen at point A on the time-potential curve in Fig. 7, the potential curve started over and essentially repeated the original curve as though there had been no prior exposure. Thus cracking occurred in about twice the time because of the repeat cycle. This suggested that the electrochemical surface reactions could be reversed by removing the applied load. However, experiments by Miller and Francis[24] have failed to duplicate these results.

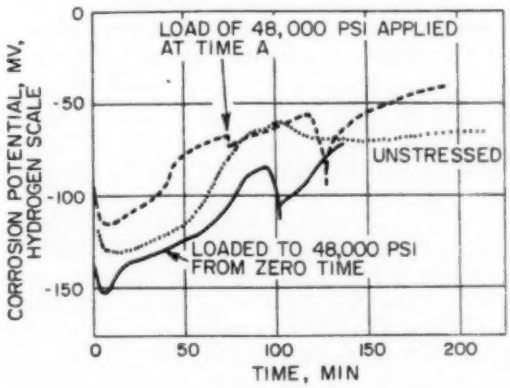

Fig. 7 Potential vs. time curves for 18-8 stainless-steel specimens exposed to boiling magnesium chloride.[23]

Uhlig and Lincoln[26] found that preexposure of unstressed specimens for 3 hr in boiling 42% $MgCl_2$ resulted in a slight decrease in time to cracking when load was applied and that no further effects were observed for preexposures of up to 23 hr. Uhlig, White, and Lincoln[27] found that plastically deformed specimens cracked almost immediately upon entry into the $MgCl_2$ solution. They believe that plastic deformation is a necessary condition for establishing crack sensitivity. They suggest that the induction period observed by Hoar and Hines[23] with elastically deformed specimens is associated with a small amount of creep that always occurs in austenitic stainless steel.

Reed and Paxton,[28] studying single crystals of stainless steel in boiling 42% $MgCl_2$, found that cracks originated from elongated pits that formed when portions of slip lines were attacked by the solution. Leu and Helle[29] suggest that only sharp-edged pits give rise to cracking because they act as notch type stress raisers. At low stresses, only long pits that form at slip bands initiate cracking, whereas, at high stresses, small pits occurring at slip bands or grain boundaries may initiate cracking. Actual initiation of attack is believed to occur when the film is ruptured by applied stress at these locations. Kirk, Beck, and Fontana[30] found that cracking always initiated at the base of a pit in stressed stainless steel exposed to condensing vapors above a 400°F solution containing 875 ppm NaCl.

Uhlig and Lincoln[26] have stated that sizable pits are not necessary to initiate cracking of stainless steel exposed to $MgCl_2$, but such pits are necessary to initiate cracking in NaCl solutions. They believe that the pitting mechanism produces concentrated, low-*p*H $FeCl_2$ within the pit which, like $MgCl_2$, produces immediate cracking.

Coleman, Weinstein, and Rostoker[31] have suggested that stress-corrosion cracking originates from a condition of reduced surface energy brought about by the adsorption of some ion species from the corrosive medium. Electrochemical processes might contribute to failure by removing existing films (at localized areas) that would otherwise prevent adsorption of the critical ion species or, at higher stress levels, might prevent healing of oxide films that are ruptured during loading.

Gulbransen and Copan[32] suggest that stress-corrosion cracking of stainless steels in atmospheres containing chloride ions is related to the formation of submicroscopic platelets of chromium oxide (Cr_2O_3). Their studies, conducted on prestressed specimens at 1100°F in oxygen and water vapor containing 5 ppm chloride, resulted in the growth of thin upright parallel plates of Cr_2O_3 along a definite crystallographic direction. They believe that minute crevices growing downward into the metal surface, as the platelets thrust themselves upward, may lead to a trenching effect, with a concentration of stress at the base of crevices, and eventually to failure. In liquid-phase reactions they conclude that the platelets are dissolved, leaving a narrow trench with high stress concentration.

Crack Propagation

Currently there are two major theories of crack propagation: (1) it is purely electrochemical in nature, and (2) it consists of a two-step process—alternate periods of slow electrochemical attack, followed by rapid mechanical cracking.

Electrochemical Theory. Hoar[33] favors the electrochemical theory of crack propagation, believing that cracks advance by anodic dissolution of strained metal at the crack tip. Graf[34] has also stated that plastic deformation at the tip of a crack makes the metal more reactive. This is based on his work with copper-gold alloys in 2% $FeCl_3$ solution. Uhlig, White, and Lincoln[27] think plastic deformation is a necessary condition for establishing crack sensitivity, but they think that nitrogen is responsible for the corrosion attack. On the basis of their work with low-nitrogen high-purity 18 wt.% chromium–8 wt.% nickel and 20 wt.% chromium–20 wt.% nickel stainless steels,[27,35] they think nitrogen, under conditions of lattice strain, readily diffuses to lattice imperfection sites, such as dislocations. They believe that it precipitates as a nitride, forming a cathodic area that stimulates corrosion of the adjoining alloy, thereby favoring crack propagation. The role of the nickel in the nonsusceptible high-nickel alloy apparently is to inhibit the formation of the cathodic precipitates.

Douglass, Thomas, and Roser[36] also believe that precipitated nitrides increase cracking susceptibility. In electron microscopy studies, they have identified what they believe to be

precipitated nitrides on slip planes. They postulate that, during slip, the effective area of the cathodic nitride precipitates is increased, thereby increasing galvanic corrosion and aiding crack propagation.

Vaughan, Phalen, Peterson, and Boyd[37] believe that the propagation of cracks occurs at anodic paths due to reaction of the stainless steel with corrosion-produced hydrogen. On the basis of electron microscopy studies of cathodically charged specimens, they conclude that, in susceptible alloys, the corrosion hydrogen is picked up by the steel and diffuses readily under an applied load to form stress-oriented transgranular bands of hydrogen-strained ferrite. These bands are highly anodic to the austenitic matrix. Their solution by the corrodent ($MgCl_2$) causes the cracking. In non-susceptible alloys the hydrogen reacts with the steel, but a hydride phase is believed to precipitate immediately. Thus hydrogen does not diffuse to form stress-oriented bands in these alloys.

Copson[38] has also noted the beneficial effect of increasing the nickel content in stainless steels. His results are presented in Fig. 8. They indicate that cracking susceptibility of steels in boiling $MgCl_2$ is low at the zero-nickel level, increases to a maximum at 8 to 10 wt.% nickel, then decreases with increasing nickel beyond that level, until virtual immunity is obtained at about 40 wt.% nickel. Douglass et al.[36] and Swann[39] have found that dislocation stacking-fault energy increases with increasing nickel content. They think this accounts for resistance to stress-corrosion cracking in the high-nickel austenitic alloys (the role of dislocations will be discussed more fully in the next section).

In support of the electrochemical theory of cracking, Logan[40] has recomputed current densities obtained from anodic polarization curves on the basis of the corroding cross-sectional area of the crack and found them to be 5 ma/cm^2. This was sufficient to produce a crack-penetration rate of 0.06 mm/hr, which was the order of magnitude observed in the NaCl-$NaNO_2$ solution with which he was working. Hoar and Hines,[41] making similar calculations, determined a current density of 1.5 amp/cm^2 for advancing crack edges in austenitic stainless steel exposed to boiling $MgCl_2$, which correlated well with crack propagation rates.

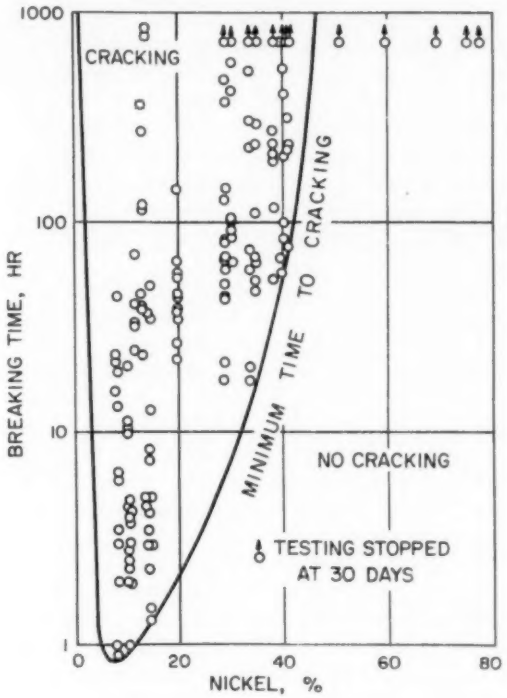

Fig. 8 Breaking time of iron-nickel-chromium wires in boiling 42% magnesium chloride.[38]

Miller and Francis[24] have made electrochemical maps of stressed tubing specimens in boiling $MgCl_2$ which indicated that the appearance of readily visible cracks coincided with the simultaneous appearance of a strongly anodic zone. This has suggested to them an electrochemical mechanism for crack propagation, although the anodic zone could have been the result of, rather than the cause of, the crack.

Electrochemical-Mechanical Theory. The first description of the electrochemical-mechanical theory of propagation of stress-corrosion cracks has been attributed to Keating.[42] Proponents of this theory believe that cracking is a two-stage process—a repeating cycle that consists of a short period of chemical attack which advances the crack very little and which then triggers a sudden mechanical fracture over a long distance (all on a microscopic scale).

Kirk, Beck, and Fontana,[30] with the aid of motion-picture studies, have shown that cracks occur in short bursts. These cracks propagate at rates up to 4 mm/hr in the condensing

vapors above an 875-ppm NaCl solution at 400°F (Uhlig and Lincoln[26] measured propagation rates of 5 to 10 mm/hr in boiling $MgCl_2$, whereas Logan[40] found propagation rates of about 0.06 mm/hr in NaCl-$NaNO_2$ solutions).

Hoar and Hines[23] observed intermittent movement of loaded wire specimens in boiling $MgCl_2$, but they chose to relate this movement to testing procedures rather than to mechanical-fracture bursts.

Nielsen[43] has made sound recordings that revealed periodic noises during crack propagation, suggesting an association with periodic fracture. He also considered the possibility that the sounds were caused by the formation, evolution, or collapse of hydrogen bubbles from the corrosion reaction. Neither van Rooyen[25] nor Miller and Francis[24] have been able to detect sounds during crack propagation in their acoustical experiments.

Forty[44] has postulated that cracks propagate by mechanical fracture in alloys where dislocations line up in slip planes, i.e., in alloys with highly restricted slip. Swann[39] has discussed the role of dislocations at some length in later work. This theory suggests that cracking should occur in alloys with low dislocation stacking-fault energy and not in those with high stacking-fault energy. These conditions are illustrated in the transmission electron micrographs[45] in Fig. 9, which show tangled areas of dislocations (high stacking-fault energy) and parallel lines of dislocations (low stacking-fault energy).

Barnartt, Stickler, and van Rooyen[46] have correlated cracking susceptibility of high-purity iron–16 wt.% chromium–20 wt.% nickel alloys in boiling $MgCl_2$ with dislocation orientation. The alloy itself and the alloy with 1.5 wt.% manganese additions did not crack but exhibited tangled dislocations and hence a high stacking-fault energy and easy cross slip. Additions of 1.5 wt.% molybdenum or 0.5 wt.% titanium to the alloy resulted in rapid stress-corrosion cracking. The highly oriented dislocations indicated a low stacking-fault energy and restricted slip.

On the other hand, Douglass et al.,[36] in presenting their theory of cathodic nitride precipitates on slip planes, believe that low stacking-fault energy is a necessary, but not a sufficient, criterion for stress-corrosion cracking.

Nielsen[43] has proposed that deposition of corrosion products within advancing cracks provides a wedging action that causes a brittle fracture beyond the tip of the crack. Dissolution, in a bromine–anhydrous methanol solution, of stainless steel previously cracked in boiling $MgCl_2$ has revealed fan-shaped corrosion products identified as primarily a spinel oxide, M_3O_4. Pickering, Beck, and Fontana[47] have also proposed a corrosion-product wedging action for stress-corrosion cracking of stainless steel in the condensing vapors of a 2% NaCl–3% HNO_3 solution at 400°F. Pres-

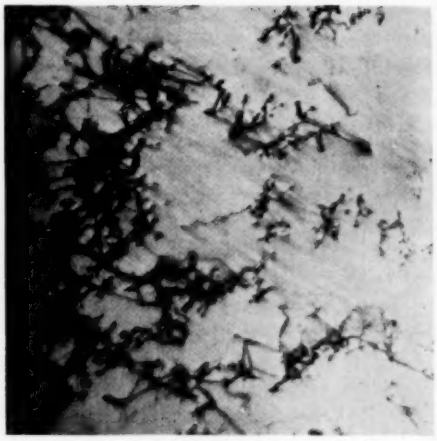

Fe-16Cr-20Ni

1μ

Fe-16Cr-20Ni-1.5Mo

Fig. 9 Transmission electron micrographs of stainless steels deformed 3%, showing dislocation orientation.[45] (Courtesy of *Corrosion* magazine.)

sures in excess of 7000 psi were measured for the wedging action of the corrosion product.

In connection with the electrochemical-mechanical theory of crack propagation, Edeleanu[48] has proposed that the chemical aspects of cracking are due to preferential attack of small quantities of quasi-martensite which form at the tip of the crack, or as a network in the austenite due to straining of the metal. He later stated[49] that the susceptible paths might be strain-induced martensite, but not always, in the light of evidence which indicated that stable austenite alloys also exhibit cracking, and that cracking may occur at temperatures above those where austenite transforms to quasi-martensite.

Summary

Austenitic stainless steels have found widespread use in nuclear reactors because of their excellent general corrosion resistance, ready availability, ease of fabrication, and relatively low cost. Unfortunately they often exhibit stress-corrosion cracking under conditions that promote concentration of chlorides or caustic. These conditions are not unique with nuclear reactors but occur in many industrial applications as well. Nor are they limited to any single reactor type. In fact, it is conceivable that stainless-steel components in sodium-cooled reactors could experience caustic stress-corrosion cracking if moisture were allowed to contact the sodium (such as during shutdown or removal and reinsertion of a component). Laboratory experiments have shown that NaOH or Na/NaOH mixtures can cause cracking in stainless steel at temperatures of interest in sodium-cooled reactors.[50]

Despite this shortcoming, stainless steels are being used extensively in nuclear reactors. The cracking problem is circumvented by careful control of the reactor environment and attention to design features. The latter consists of minimizing applied and residual tensile stresses and avoiding conditions that promote concentration of chlorides and caustic. Careful environmental control has been demonstrated in the operation of the HRE-2 stainless-steel steam generators.[51] Absence of cracking after 3.5 years of operation was attributed to excellent boiler-water treatment, which kept chloride and dissolved oxygen contents low.

Inhibitors have not been widely used because their effectivness in eliminating cracking has not been fully demonstrated. It has been demonstrated that cathodic protection can eliminate cracking in localized areas, but its application on a large scale does not appear feasible because of the complicated geometries involved.

Progress is being made toward defining the mechanism of stress-corrosion cracking, but a complete understanding is not now available. Yet to be resolved are: (1) the mechanism of crack initiation, (2) whether cracks propagate by a two-stage electrochemical-mechanical process or by electrochemical corrosion alone, and (3) whether the electrochemical corrosion is due to highly strained metal, attack at dislocation pileups, cathodic nitride precipitates, anodic hydride precipitates, phase changes in the metal, or some other phenomenon not yet discovered.

References

1. E. G. Bohlmann and G. M. Adamson, Stress-Corrosion Cracking Problems in the Homogeneous Reactor Test, USAEC Report CF-57-1-143, Oak Ridge National Laboratory, Jan. 31, 1957.
2. C. N. Spalaris, Finding a Corrosion-Resistant Cladding for Superheater Fuels, *Nucleonics*, 21(9): 41-49 (September 1963).
3. S. P. Rideout, Stress-Corrosion Cracking of Type 304 Stainless Steel in High-Purity Heavy Water, extended abstracts of papers presented at Second International Congress on Metallic Corrosion, pp. 100-102, NACE (December 1962).
4. E. C. Hoxie, The Nature of Aluminum Corrosion Products Deposited in a Non-Isothermal Hydraulic System, paper presented by L. Costas at Twelfth Annual AEC Corrosion Symposium, Pleasanton, California, May 20–22, 1963.
5. G. E. Marchment, Stress-Corrosion Failure of a High-Pressure Water/Water Cooler in the Dynamic Corrosion Loop at Capenhurst, British Report IGR-TN/CA-974, July 14, 1958.
6. W. E. Berry, O. M. Stewart, and F. W. Fink, Examination of a Nonregenerative Heat Exchanger from the U.S.S. *Nautilus* (SSN-571), USAEC Report BMI-1416, Battelle Memorial Institute, Feb. 19, 1960.
7. E. Landerman, S1W Port Stainless Steel Steam Generator, USAEC Report WAPD-CTA(MPA)-1456, Westinghouse Electric Corp., Bettis Atomic Power Laboratory, Aug. 10, 1956.
8. W. J. Singley, I. H. Welinsky, S. F. Whirl, and H. A. Klein, Stress Corrosion of Stainless Steel and Boiler Water Treatment at Shippingport Atomic Power Station, in *American Power Conference*, Vol. XXI, pp. 748-768, 1959.

9. M. C. Rowland and W. R. Smith, Sr., Precipitation-Hardening Stainless Steels in Water-Cooled Reactors, *Nucl. Eng.*, 7(68): 14-22 (January 1962).
10. E. E. Denhard, Jr., Effect of Composition and Heat Treatment on the Stress-Corrosion Cracking of Austenitic Stainless Steel, *Corrosion*, 16: 359t-369t (1960).
11. R. W. Staehle, F. H. Beck, and M. G. Fontana, Mechanism of Stress Corrosion of Austenitic Stainless Steels in Chloride Waters, *Corrosion*, 15: 373t-381t (July 1959).
12. G. E. Galonian and H. L. Tymchyn, Results of Stress Corrosion Cracking Tests of Retort-Annealed and Resistance-Annealed Type 347 Stainless Steel Tubing, USAEC Report KAPL-M-GEG-10, Knolls Atomic Power Laboratory, Aug. 26, 1957.
13. W. L. Williams, Chloride and Caustic Stress Corrosion of Austenitic Stainless Steel in Hot Water and Steam, *Corrosion*, 13: 539t-545t (August 1957).
14. G. C. Wheeler and E. Howells, Caustic Stress Corrosion of Type 347 Stainless Steel, USAEC Report M-6911, Knolls Atomic Power Laboratory and Babcock & Wilcox Co., Nov. 23, 1960.
15. R. Scharfstein and W. F. Brindley, Chloride Stress-Corrosion Cracking of Austenitic Stainless Steel — Effect of Temperature and pH, *Corrosion*, 14: 588t-592t (December 1958).
16. P. O. Snowden, Inhibition of Stress-Corrosion Cracking of Austenitic Stainless Steel, *Nucl. Eng.*, 6: 409-411 (October 1961).
17. J. C. Griess, J. M. Martin, A. E. Mravca, R. J. Impara, and S. Weems, Bonus Boiling Water Nuclear Superheat Reactor Project. Task Force Report on Chloride Stress Corrosion of Austenitic Stainless Steel, USAEC Report TID-16888, Apr. 13, 1962.
18. J. W. McGrew, Testing Steam Generator Materials for Pressurized Water Reactor Plants, *Corrosion*, 18(1): 27t-32t (January 1962).
19. H. R. Copson and W. E. Berry, Qualifications of Inconel for Nuclear Power Plant Applications, *Corrosion*, 16(2): 79t-85t (February 1960).
20. H. R. Copson and W. E. Berry, Corrosion of Inconel Nickel-Chromium Alloy in Primary Coolants of Pressurized Water Reactors, *Corrosion*, 18(1): 21t-26t (January 1962).
21. D. E. White and E. G. Johnson, Stress-Corrosion Screening Tests of Materials for Steam Generator Tubing in Nuclear Power Plants, *Corrosion*, 16(7): 320t-324t (July 1960).
22. I. C. Mayes and J. McGrew, ANPP Corrosion Program. Final Summary Report. USAEC Report MND-E-2727, Martin Co., Nuclear Division, February 1962.
23. T. P. Hoar and J. G. Hines, The Stress-Corrosion Cracking of Austenitic Stainless Steels, *J. Iron Steel Inst. (London)*, 182: 124-143 (February 1956).
24. J. M. Miller and H. T. Francis, The Mechanism of Stress Corrosion in Stainless Steels. Final Report, May 15, 1959 to May 15, 1960, USAEC Report ARF-2181-12, Armour Research Foundation, Illinois Institute of Technology, September 1962.
25. D. van Rooyen, Qualitative Mechanism of Stress-Corrosion Cracking of Austenitic Stainless Steels, *Corrosion*, 16: 421t-429t (September 1960).
26. H. H. Uhlig and J. Lincoln, Jr., Chemical Factors Affecting Stress Corrosion Cracking of 18-8 Stainless Steels, *J. Electrochem. Soc.*, 105: 325-332 (1958).
27. H. Uhlig, A. White, and J. Lincoln, Jr., Austenitic Cr-Fe-Ni Alloys Resistant to Stress Corrosion Cracking in Magnesium Chloride, *Acta Met.*, 5: 473-475 (1957).
28. R. E. Reed and H. W. Paxton, Stress Corrosion Cracking of Single Crystals of Some Austenitic Stainless Steels, in *First International Congress on Metallic Corrosion*, pp. 301-308, Butterworths, London, 1962.
29. K. W. Leu and J. N. Helle, The Mechanism of Stress Corrosion of Austenitic Stainless Steels in Hot Aqueous Chloride Solutions, *Corrosion*, 14: 249t-253t (May 1958).
30. W. W. Kirk, F. H. Beck, and M. G. Fontana, Stress-Corrosion Cracking of Austenitic Stainless Steels in High Temperature Chloride Waters, in *Physical Metallurgy of Stress Corrosion Fracture*, pp. 227-236, edited by T. N. Rhodin, Interscience Publishers, New York and London, 1959.
31. E. G. Coleman, D. Weinstein, and W. Rostoker, On a Surface Energy Mechanism for Stress-Corrosion Cracking. A Mechanism for Stress-Corrosion Embrittlement, USAEC Report ARF-2152-10, Armour Research Foundation, Illinois Institute of Technology, February 1960.
32. E. A. Gulbransen and T. P. Copan, Effect of Stress and Environment on the Microtopology of the Corrosion Product, in *Physical Metallurgy of Stress Corrosion Fracture*, pp. 155-180, edited by T. N. Rhodin, Interscience Publishers, New York, 1959.
33. T. P. Hoar, Stress-Corrosion Cracking, *Corrosion*, 19(10): 331t-338t (October 1963).
34. L. Graf, Causes of Stress Corrosion in Nonferrous Alloys and Steel, USAEC Translation AEC-tr-5724 [translated from *Werkstoffe Korrosion*, 9: 693-698 (November 1958)].
35. H. H. Uhlig and R. A. White, Some Metallurgical Factors Affecting Stress-Corrosion Cracking of Austenitic Stainless Steels, *Trans. Am. Soc. Metals*, 52: 830-847 (1960).
36. D. L. Douglass, G. Thomas, and W. R. Roser, Stacking Fault Energy, Ordering and Transgranular Stress Corrosion Cracking in Austenitic Alloys, paper presented at the Twelfth Annual AEC Corrosion Symposium, Pleasanton, California, May 20–22, 1963.
37. D. A. Vaughan, D. I. Phalen, C. L. Peterson, and W. K. Boyd, Relationship Between Hydrogen Pickup and Susceptible Paths in Stress-Corrosion

Cracking of Type 304 Stainless Steel, *Corrosion*, 19(9): 315t-325t (September 1963).

38. H. R. Copson, Effect of Nickel Content on the Resistance to Stress-Corrosion Cracking of Iron-Nickel-Chromium Alloys in Chloride Environments, in *First International Congress on Metallic Corrosion*, pp. 328-333, Butterworths, London, 1962.
39. P. R. Swann, Dislocation Structure vs Transgranular Stress-Corrosion Susceptibility in Single Phase Alloys, *Corrosion*, 19(3): 102t-112t (March 1963).
40. H. L. Logan, Studies of Stress-Corrosion Cracking of Austenitic Stainless Steel, *Welding J. (N. Y.)*, 37: 463s-467s (October 1958).
41. T. P. Hoar and J. G. Hines, The Electrochemistry of the Corrosion and the Stress-Corrosion Cracking of 18-8 Chromium-Nickel Steels in Hot Aqueous Magnesium Chloride Solution, in *Proceedings of the Eighth Meeting of the International Committee of Electrochemical Thermodynamics and Kinetics* (C.I.T.C.E.), Madrid, 1956, Butterworths, London.
42. F. H. Keating, *Symposium, Internal Stresses in Metals and Alloys*, London, 1947, pp. 311-331, Institute of Metals, London, 1948.
43. N. A. Nielsen, Symposiun on Physical Metallurgy of Stress-Corrosion Fracture, Pittsburgh, Pennsylvania, April 2–3, 1959.
44. A. J. Forty, The Initiation and Propagation of Cracks in the Stress Corrosion of α-Brass and Similar Alloys, in *Physical Metallurgy of Stress Corrosion Fracture*, pp. 99-115, edited by T. N. Rhodin, Interscience Publishers, New York, 1959.
45. S. Barnartt, General Concepts of Stress Corrosion Cracking, *Corrosion*, 18(9): 322t-330t (September 1962).
46. S. Barnartt, R. Stickler, and D. van Rooyen, Stress-Corrosion Cracking Mechanism in Purified 16% Cr–20% Ni Stainless Steels, *Corrosion Sci.*, 3: 9-16 (January–March 1963).
47. H. W. Pickering, F. H. Beck, and M. G. Fontana, Wedging Action of Solid Corrosion Product During Stress Corrosion of Austenitic Stainless Steels, *Corrosion*, 18(6): 230t-239t (June 1962).
48. C. Edeleanu, Transgranular Stress Corrosion in Chromium-Nickel Stainless Steels, *J. Iron Steel Inst. (London)*, 173: 140-146 (1953).
49. C. Edeleanu, The Phenomena of Stress-Corrosion Cracking in Austenitic Stainless Steels, in *Stress Corrosion Cracking and Embrittlement*, pp. 126-139, edited by William D. Robertson, John Wiley and Sons, Inc., New York, 1956.
50. E. G. Brush, Behavior of Type 347 Stainless Steel in Sodium Hydroxide at Elevated Temperatures, USAEC Report KAPL-M-EGB-22, Knolls Atomic Power Laboratory, July 12, 1956.
51. Oak Ridge National Laboratory, Reactor Chemistry Division Annual Progress Report for Period Ending January 31, 1962, USAEC Report ORNL-3262, May 11, 1962.

Section

I

Reactor Materials

Fuel and Fertile Materials

Unalloyed Uranium

The British[1] have presented results on the creep of uranium under a tensile stress of 350 psi at 550°C under conditions of constant temperature, continuous small thermal cycles, discrete large cycles, and combined continuous small and discrete large cycles. The creep rates under isothermal conditions and discrete cycling were larger than predicted from previous results, but under continuous cycling they agreed well with predictions based on a value of internal stress per mean temperature deviation of 250 psi/°C for a variety of amplitudes and periods of cycle.

Pole figures plotted by the British[2] from uranium sheets rolled under various schedules showed the textures produced, and formability tests showed how these textures affect the deep-drawing properties of the sheets. Hot and warm cross rolling were found to produce a strong texture which was symmetrical about the sheet normal and which showed little directionality, enabling the material to be easily deep drawn.

The crystal structure and irradiation growth of alpha uranium are discussed in a report[3] by National Lead Co. of Ohio.

Atomics International[4] has studied diffusion of Xe^{133} in uranium metal for a number of varying sample conditions with metal of high purity and commercial purity. The following conclusions were reached:

1. A fission-product gas isotope diffuses in uranium under thermal treatment. Realistic diffusion coefficients and activation energies for diffusion have been obtained from the data. The behavior of this isotope may be extended to approximate the behavior of all fission noble gas isotopes. The diffusion coefficients are similar in magnitude to those found for intermetallic diffusion.

2. The microscopic metallurgical condition (i.e., impurities, inclusions, etc.) of the sample material appears to affect the diffusional behavior by influencing the rate and extent of internal precipitation of the gas. The possibility of influencing swelling by control of the metallurgical condition is evident.

The level of gas-atom concentration at which homogeneous nucleation of bubbles takes place appears to be quite low ($<10^{-4}$ at.% burnup). Above this level, most gas atoms will be precipitated internally on being heated to a temperature at which significant diffusion rates are obtained. At this point, diffusional release to the surface is obscured by lack of sensitivity and burst release of gas from ruptured bubbles.

A summary paper[5] giving data on the compatibility of uranium, plutonium, and thorium with aluminum, magnesium, beryllium, ferrous metals, and refractory metals has been issued by the Germans. The experimental techniques and examination of reaction zones are described. The results obtained by the different investigators are analyzed and discussed.

In a compilation[6] covering the December 1961 meeting on preferred orientation at Nuclear Metals, five papers[6a–6e] dealing with uranium textures have been published. (M. S. Farkas)

Alpha-Phase Uranium Alloys

The transformation characteristics (TTT diagrams) for the uranium–10 wt.% molybdenum, uranium–8 wt.% molybdenum, uranium–8 wt.% molybdenum–½ wt.% titanium, uranium–8 wt.% molybdenum–1 wt.% titanium, and uranium–2 wt.% molybdenum–2 wt.% niobium–2 wt.% zirconium–½ wt.% titanium alloys have been developed by investigators at Case Institute of Technology.[7]

Investigators at North Carolina State College[8] have developed an isothermal section at 1800°C for the uranium-carbon-oxygen system. A U(C,O) single-phase area exists in this diagram. The limit of substitutional solid solution of oxygen atoms for carbon atoms in UC is 12.5 at.%, which means that only 25% of the carbon atoms in UC can be replaced by oxygen atoms. The oxygen-saturated UC phase $U(C_{0.75}O_{0.25})$ has a lattice parameter of 4.953 ± 0.001 A. The carbon monoxide partial pressures in equilibrium with this phase were determined for temperatures between 1705 and 1855°C. Cursory tests indicate that $U(C_{0.75}O_{0.25})$ may have significant advantages as a nuclear fuel material, and a comprehensive evaluation of it is in progress. (M. S. Farkas)

Gamma-Phase Uranium Alloys

In creep studies of gamma-phase uranium-molybdenum alloys at Harwell,[9] measurements were made at 625, 675, and 725°C at a stress of 400 psi. Activation energies for creep were determined as follows:

20 at.% molybdenum	28,500 cal/mole
25 at.% molybdenum	34,200 cal/mole
30 at.% molybdenum	37,000 cal/mole

Data obtained for the 20 and 25 at.% molybdenum alloys are shown below. The 20 at.% alloy showed three distinct stages of linear creep at 625°C, which appears to have been the result of grain growth during the test.

Molybdenum, at.%	Temp., °C	Creep rate, hr^{-1}
20	625	9.0×10^{-7} (100 to 600 hr)
		2.1×10^{-6} (700 to 1050 hr)
		2.8×10^{-6} (1100 to 1650 hr)
20	675	5.6×10^{-6} (150 to 1000 hr)
20	725	1.4×10^{-5} (300 to 1100 hr)
25	675	1.1×10^{-6} (100 to 1000 hr)

(A. A. Bauer)

Plutonium

Studies at Hanford[10] indicate that physical damage (micro- and macrocracking) in plutonium decreases with decreasing beta-to-alpha transformation temperatures. A plot of density vs. number of cycles between 180°C (beta phase) and various alpha-transformation temperatures is shown in Fig. I-1.

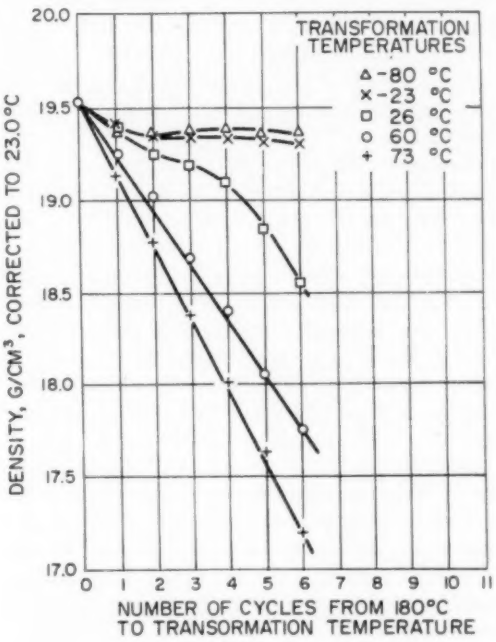

Fig. I-1 Effect of $\beta \rightarrow \alpha$ cycling on the physical damage in plutonium as revealed by room-temperature density measurements.[10]

The surface veining, often observed in unalloyed plutonium, has been identified[11] as bands of columnar grains. These bands form during the first 50% of the beta-to-alpha transformation and are randomly distributed throughout the metal.

According to Los Alamos investigators,[12] alpha plutonium is monoclinic with 16 atoms in the unit cell, which, at 21°C, has the dimensions $a = 6.183$, $b = 4.822$, and $c = 10.963$ A; $\beta = 101.79°$. The space group is $P2_1/m$, and all atoms lie in reflection planes. The atomic-position parameters have been determined to a precision of 0.03 A. Five short and seven long bonds are formed by the seventh plutonium atom, and three short and thirteen long bonds by the eighth atom.

The negative thermal expansion of delta plutonium[13] becomes less negative and finally becomes positive, with increasing amounts of al-

loying additions of aluminum, zinc, zirconium, indium, and cerium. This change in expansion can be correlated with electron concentration, γ. The expansion is zero at a critical value of $\gamma = 4.74$, relative to a value of 4.82 for pure delta plutonium, and it is positive in alloys whose γ is less than 4.74. Several models that can be used to explain the observed behavior are discussed. A new method for estimating the metallic valence of delta plutonium is also described.

Neutron diffraction analyses[14] of plutonium show that its structure at 23°K is essentially the same as the room-temperature structure, except for a reduction in the average number of neighbors from 14 at room temperature to 12.5 at 23°K and a reduction in the gross average plutonium-plutonium interatomic distance from 3.19 A at room temperature to 3.16 A at 23°K. These data indicate that there is no low-temperature allotropic transformation of plutonium.

Recent studies[15] of the plutonium-carbon phase diagram suggest that the solubility limit of PuC on the low-carbon side is about 43 at.% carbon at 610°C and between 43 and 44 at.% carbon at 555°C. The maximum solubility of carbon in PuC was found to be about 48 at.% carbon at 610°C and 47.7 at.% carbon at 555°C. The PuC peritectic horizontal at 1652°C extends from Pu_2C_3 to between 44 and 46 at.% carbon. There are indications that Pu_2C_3 is not completely stoichiometric, but has some solubility for plutonium. Solubility limits on the low-carbon side were found to be 58.5 at.% carbon at 610°C and 59.4 at.% carbon at 555°C.

Several eutectic reactions have been observed in the plutonium-silicon alloy system. A plutonium-rich eutectic occurs between epsilon plutonium and Pu_5Si_3 at about 4 at.% silicon and 590 ± 2°C, a eutectic between PuSi and Pu_2Si_3 occurs at about 54 at.% silicon and 1521 ± 10°C, and a silicon-rich eutectic occurs between $PuSi_2$ and silicon at 83.6 at.% silicon and 1234 ± 5°C. Solubility limits of silicon in delta plutonium are 1 at.% silicon at 450°C and 1.2 at.% silicon at 485°C. Up to 0.6 at.% silicon is soluble in epsilon plutonium at 550°C, and solubility limits of silicon in liquid plutonium at 719 and 832°C are 4.9 and 8.1 at.%, respectively. Pu_5Si_3 has a tetragonal structure with $a = 8.070 \pm 0.005$ A and $c = 5.447 \pm 0.003$ A. The crystal structure of Pu_3Si_2 is tetragonal with $a = 7.483 \pm 0.002$ A and $c = 4.048 \pm 0.002$ A. Calculated density of Pu_3Si_2 is 11.3 g/cm³. Properties of plutonium-silicon compounds are listed below.

Compound	Melting point, °C	Melting reaction	Hardness, DPHN
Pu_5Si_3	1377 ± 10	Peritectic	369 to 484
Pu_3Si_2	1441 ± 10	Peritectic	536 to 661
PuSi	1576 ± 10	Congruent	533 to 710
Pu_2Si_3	1646 ± 10		681 to 856
$PuSi_2$	1638 ± 10		446 to 505

Maximum solubility of plutonium in both gamma and beta lanthanum is about 20 at.% at 835°C, which corresponds to the end of the peritectic isotherm. The solubility decreases to about 8 at.% plutonium at 500°C.[16]

The peritectic point for the liquid + beta praseodymium ⇌ alpha praseodymium reaction in the praseodymium-plutonium system is at 794°C and 31 at.% plutonium. This also corresponds to the maximum solubility of plutonium in both alpha and beta praseodymium. At 770°C, 30 at.% plutonium is soluble in alpha praseodymium.

Investigations of LAMPRE type fuels are continuing, with emphasis on fuel-container compatibility. Molten plutonium-cobalt-cesium alloy fuels containing 3, 5, and 8 g of plutonium/cm³ have been tested for 1000 hr at 700°C in tantalum, tantalum–10 wt.% tungsten, and niobium. Failures were observed in niobium containers with the 5 and 8 g of plutonium/cm³ fuels. No failures occurred in the tantalum-base alloys.

Argonne investigators[17] have determined the tensile properties of a uranium–10 wt.% plutonium–10 wt.% fissium alloy at temperatures up to 700°C. Results are shown in Table I-1. The anomalous variation in strength between 23 and 300°C is believed to be caused by the retention of gamma phase at room temperature. At 300°C, time at temperature was sufficient to transform the gamma to the apparently stronger low-temperature phases.

A report[18] has been issued containing calculations of the X-ray powder pattern and of the angles between planes and directions for alpha plutonium. The calculated powder patterns for copper, nickel, cobalt, iron, chromium, and titanium $K\alpha$ radiations are tabulated. The angles between planes and the angles between di-

Table I-1 TENSILE PROPERTIES OF URANIUM–10 WT.% PLUTONIUM–10 WT.% FIZZIUM ALLOY AT ELEVATED TEMPERATURES[17]

Temp., °C	Tensile strength		Yield strength (0.2% offset)		Modulus of elasticity		Remarks
	psi (±1%)	kg/cm²	psi	kg/cm²	10^6 psi	10^5 kg/cm²	
23.0	33,680*	2,370			12.9	9.1	Less than 0.2% fracture strain; retained γ phase
300.5	47,720	3,350			9.7	6.8	Less than 0.2% fracture strain; transformed from γ phase
501.0	31,840	2,210			7.3	5.1	Less than 0.2% fracture strain; transformed from γ phase
701.5	4,360	310	2,920	205	6.5	4.6	Elongation 9.3%; reduction of area 3.2% in γ phase

*Last digits retained for comparison use only.

rections are listed, and the standard projections are presented. (V. W. Storhok)

Plutonium Compounds

Oak Ridge has reported[19] the preparation of relatively large (−70, +200 mesh) particles of PuO_2 with greater than 90% of theoretical density by air firing at 1200°C. Hanford[20] has prepared PuO_2 by precipitation from molten chloride media, using a sparge of oxygen-chlorine gas mixtures. At 1200°C, European research workers[21] have found 58% conversion of PuO_2 to alpha Pu_2O_3 upon sintering in a dry hydrogen atmosphere (5 mg H_2O/m^3). They have also developed a chemical etch quite suitable for revealing the microstructure of plutonium suboxides.

Both British and Soviet investigators have attempted to oxidize PuO_2. The Russians[22] found compounds of the forms Me_2PuO_4 and Me_6PuO_6 after fusing $PuO_{2.00}$ with NaOH and KOH in the presence of atmospheric oxygen. The conclusion drawn is that PuO_2 was oxidized to PuO_3, which subsequently reacted with the hydroxides to form the plutonates, but this does not imply that PuO_3 is stable, per se. The British[23] substantiate this by concluding that a composition of $PuO_{2.09}$ may be attained upon oxidation, but only by altering the surface of a large sample by adsorption, and that plutonium cannot exist in an oxidation state greater than IV when combined with oxygen alone.

The phase relation between oxygen : plutonium ratios of 1.0 and 1.5 has been tentatively established at Hanford to be (PuO + β Pu_2O_3), with a simple eutectic at $PuO_{1.25}$ (1725°C).[24] A congruent melting temperature of 1825°C has been suggested for PuO. Evidence has been found for the possible existence of a Pu(O,C) face-centered cubic solid solution as a final product following carbon reduction of plutonium dioxide. In connection with the relative stabilities of plutonium oxides, PuO has been shown[12] to be considerably more volatile than β Pu_2O_3.

Workers at Hanford[25] have attempted to densify PuO_2, UO_2–2.5 wt.% PuO_2, and PuO_2–2.5 wt.% UO_2 compositions by arc melting cold-pressed powders under 1 atm of argon. Initial results gave densities in excess of 90% of theoretical; however, the UO_2–2.5 wt.% PuO_2 composition was altered to 4.1 wt.% PuO_2, probably due to mechanical blowing away (presumably by the arc) of the higher melting UO_2 powder. Later results[25] showed that arc melting reduced the plutonium compound to $PuO_{1.77}$, which was subsequently converted to the dioxide at 800°C. Nuclear Materials & Equipment Corporation (NUMEC)[26] found that minor additions of strontium carbonate increased the densities of otherwise identical specimens of sintered PuO_2 from 84 to 93% of theoretical.

A literature survey[27] has been published which includes the irradiation testing results of $(Pu,U)O_2$ mixtures, PuC, and (Pu,U)C solid solutions.

Considerable data on the carbides of plutonium and mixtures of (Pu,U)C have been published, including a discussion of those properties which pertain to a high-temperature gas-cooled reactor system.[28] Strasser[29] has reported his results on preparation and evaluation of specimens in the systems PuC, (Pu,U)C, $(Pu,U)_2C_3$, and carbon-stabilized plutonium monoxide. Hanford's investigations[24] on the

plutonium-carbon system have shown that complex interphase reactions, as yet unidentified, occur in 37 and 39 at.% carbon alloys in the temperature range 500 to 550°C. In the same work, zeta phase has been observed to grow in a nominal 48.2 at.% carbon alloy after 400 days at room temperature. Analysis of the system PuC-TaC shows that melting temperatures decrease quite rapidly with increased plutonium carbide content.[12]

Battelle[30,31] has reported information on the stability of PuN in oxidizing atmospheres, liquid metals, and vacuum, based on experimental and theoretical considerations. Hanford[24] has indicated that PuN is more stable or oxidation resistant than UN at 1600°C in helium for a period of 1 hr. (W. M. Pardue)

Thorium

Investigators at Advanced Technology Laboratories[32] have found zirconium to be the most effective alloying addition in improving the elevated-temperature mechanical properties of thorium–5 and –10 wt.% uranium alloys. Significant improvements were also noted with additions of niobium, molybdenum, carbon, aluminum, and beryllium. Both solid-solution strengthening and dispersion strengthening were encountered. Mechanical properties were found to be sensitive to structure, and structures of optimum properties were obtained by careful control of the arc-melting procedures followed by the proper heat-treatment.

The work-hardening characteristics of Ames thorium[33] have been determined by Vickers and Rockwell E hardness measurements on cold-rolled and cold-swaged specimens. The Vickers work-hardening curves obtained from both types of deformation were found to increase rapidly up to approximately 10% reduction, then remain relatively flat throughout a large intermediate range. Above about 60% reduction, the hardness again increased rapidly. The Rockwell E work-hardening curves of specimens deformed by cold rolling were similar to the Vickers curves in the early and intermediate stages. However, at higher reductions, the hardness did not increase as rapidly as indicated by Vickers measurements. The Vickers hardness curves were in excellent agreement with the results obtained previously at Oak Ridge[33a] and are felt to be more accurate representation of the work hardening of Ames thorium than the Rockwell E curves, especially for specimens of small diameter or thickness. (V. W. Storhok)

Metal-Ceramic Fuels

Dispersion Fuels

Harwell workers[9] have completed mechanical testing of fuel plates with cores of 50 vol.% UO_2 dispersed in a matrix of type 316L stainless steel. The testing was conducted at room temperature, 200, 400, 600, and 700°C on specimens in the hot-rolled and annealed conditions, and in both the longitudinal and transverse directions. The scatter found in the results was attributed to nonuniformities in size, shape, and dispersion of the UO_2 spheres in the stainless-steel matrix. The elongation values increased with increasing temperature from a minimum of 5.5 to 7.0%, whereas the corresponding ultimate-tensile-strength values decreased from 8 to 4 tsi. The annealed plates had greater ductility and lower strength than the hot-rolled plates. Plates tested in the longitudinal direction were slightly stronger and more ductile than those tested in the transverse direction. These differences tended to disappear at the higher temperatures.

The two most common structural defects in dispersion fuel plates of UO_2 in stainless steel are fragmentation and stringering. A method has been reported by Oak Ridge[34] for characterizing the quality of a dispersion by its deviation (due to both types of defects) from a hypothetical ideal model in which the particles are represented by intact, randomly distributed spheres. This method was demonstrated on a variety of stainless-steel spherical UO_2 dispersions and appeared to be reliable and reproducible. Steps have been taken to check the method for equiaxed and irregular-shaped UO_2 dispersions.

Workers at Argonne[35] prepared thoria and thoria-urania compacts containing randomly distributed refractory-metal fibers. Thoria compacts with molybdenum or niobium fibers in quantities as low as 5 wt.% exhibited significantly better resistance to spalling from thermal shock than did thoria alone. The fibers improved the resistance to thermal spalling by suppressing and limiting crack propagation and

by structurally reinforcing the cracked body. Room-temperature thermal conductivity of reinforced thoria was only slightly higher than that of plain thoria, but at 1600°C it was three times greater. The oxidation resistance of molybdenum-reinforced thoria was better than that of any other compact investigated, and improved with increased specimen density. However, because of the presence of microcracks, even the densest specimens were severely attacked after 24 hr in air at 1000°C. Thoria-urania compacts reinforced with molybdenum fibers could be bonded together by conventional brazing techniques. Irradiation of metal-reinforced thoria-urania specimens indicated that molybdenum fibers aided the heat transfer from the fuel, whereas niobium fibers reacted with the fuel and lost their effectiveness. Measured properties were also reported at room and elevated temperature for the fiber-reinforced thoria.[35] (D. L. Stoltz)

Cermet Fuels

Room-temperature mechanical properties measured by Battelle[30] on 50 and 70 vol.% UO_2–tungsten and 60 vol.% UO_2–molybdenum cermets are shown in Table I-2. The cermets were prepared by powder blending and hot isostatic pressing, yielding densities of 94.2 to 97.3% of theoretical. (D. E. Kizer)

Coated-Particle Fuel Materials

Pyrolytic Carbon (PyC) Coatings

PyC coating units are being operated at Oak Ridge to gain experience in the rapid application of laminar coatings deposited at atmospheric pressure.[36] Nine PyC coating runs were made at temperatures of 1400°C and at deposition rates greater than 25 μ/hr. Laminar coatings were obtained in all the runs. Also, Oak Ridge has successfully deposited PyC on Eu_2O_3 at 1400°C.[20] Thermogravimetric tests in vacuum indicated that PyC-coated Eu_2O_3 was stable at 1665°C for a period of at least 1 hr. Powdered mixtures of rare-earth oxide, including Eu_2O_3 and graphite, heated under the same conditions, were incompatible.

Los Alamos plans to use a duplex carbon coating for the UHTREX startup fuel elements.[37] The duplex coating consists of a 30- to 35-μ-thick inner layer of laminar type PyC and a 70- to 75-μ-thick outer layer of columnar PyC. The choice of coating was based on irradiation results reported by Oak Ridge for the duplex type of coating. The good irradiation behavior of a duplex type coating reported by Oak Ridge was confirmed independently at Battelle in irradiation studies of Battelle-prepared particles that have a low-density PyC cushion between the core and outer coating.

The effectiveness of SiC as a barrier to migration of uranium into PyC is being studied at Battelle.[30] On a previous test sample, a low alpha emission of 50-ppm uranium was obtained for UC_2 particles provided with a 5-μ-thick SiC coating and overcoated with PyC by pyrolysis of CH_4 at 1950°C. An additional lot has been prepared by pyrolysis of C_2H_2 and doped with 3 wt.% silicon to determine the effect of the combination on the resistance to radiation damage.

Surface-area measurements were obtained for PyC-coated particles at Battelle.[31] Measure-

Table I-2 ROOM-TEMPERATURE MECHANICAL PROPERTIES OF EXPERIMENTAL TUNGSTEN-UO_2 AND MOLYBDENUM-UO_2 CERMETS[30]

Cermet composition, vol.%	Density, % of theoretical	Modulus of elasticity, 10^6 psi	Poisson's ratio, μ	Compression strength, 1000 psi	Modulus of rupture, 1000 psi	Estimated tensile strength, 1000 psi	Elongation to maximum load, %
Tungsten–50 UO_2	94.5	21.2	0.33	159.8			
	94.6				34.6	33.9	Nil
Tungsten–70 UO_2	96.0	20.5	0.20*	150.4			
	97.3				29.8	29.2	Nil
Molybdenum–60 UO_2	94.3	13.6	0.30*	105.4			
	94.2				68.0	51.0	1

*Value increases with increased strain.

ments were obtained for laminar and columnar type coatings deposited on 200-μ-diameter UC_2 by pyrolysis of C_2H_2 at 1400°C. The laminar coating was found to have a higher surface area in the as-produced condition than did the columnar coating. The measured values were 0.046 and 0.021 m^2/g. Heat-treatment of the two lots in helium at 1250°C for 48 hr did not change the surface area of the coatings. Studies were also started for PyC coatings deposited from C_2H_2 with the known impurity acetone removed. Coatings were prepared at deposition rates of 11, 36, and 57 μ/hr. The crushing strength and hardness were not different from those for coatings prepared from unpurified C_2H_2. Also, composite coatings of 12-μ dense Al_2O_3 overcoated with 103 μ of columnar PyC, and 12-μ dense Al_2O_3 overcoated with 104 μ of laminar PyC were deposited on 80% dense UO_2.[38] Both lots have been submitted for irradiation study.

Oxide Coatings

Battelle has reported additional information for the effect of coating conditions on the quality of BeO coatings deposited on UO_2 by controlled hydrolysis of $BeCl_3$ in a fluidized bed (see Refs. 30, 31, 38, and 39). BeO coatings prepared at 1500°C have a smooth surface and consist of large equiaxed grains, whereas coatings prepared at 1400°C have a rough surface as a result of the growth of elongated grains. It has been established that BeO coatings consisting of equiaxed grains, formed at 1500°C, are insensitive to coating-reactant concentration over a wide range and to variations in the degree of fluidization of the bed particles.[39] At the deposition temperature of 1400°C, the degree of smoothness of the BeO surface was related to the vigor of fluidization, higher gas flow tending to give smooth coatings.[39] Rough coatings are obtained at 1300 and 1350°C, regardless of fluidizing-gas flows. A crushing strength of 865 g was obtained for smooth BeO coating, 60 μ thick, deposited at 1500°C on 127-μ-diameter UO_2.[38] Crushing values of 1200 to 1300 g are normally obtained for similar material prepared at 1400°C.

A combination coating of 12 μ of dense Al_2O_3, 1 μ of PyC, and an outer shell of 52 μ of dense Al_2O_3 was prepared at Battelle to evaluate the effectiveness of the PyC intermediate coating as a crack-stopping layer.[38] The combination coating has passed out-of-pile screening tests and has been submitted for in-pile studies.

(N. D. Veigel)

Irradiation and Evaluation of Coated-Particle Fuels

Oxide-Base Fuel. Recent fission-gas-release data obtained by Oak Ridge[40,41] and Battelle[31,38,39] for coated-particle fuels are summarized in Tables I-3 and I-4.

An 1100°C sweep-capsule irradiation of Al_2O_3-coated UO_2 particles (lot 715A-HT) was completed at Battelle.[39] After an estimated burnup of 12 at.% of the U^{235}, the fission-gas-release fractions were still about 10^{-8}, indicating no coating failure. Data are also now available for Al_2O_3-coated UO_2 specimens irradiated statically at 850°C (Table I-4) at Battelle in capsule BMI-CFP-12. The sweep specimen in this capsule (lot 715A-HT) has shown approximately 1% failure after 6.4 at.% burnup at 815°C. Results for the two static specimens of lot 715A-HT were in agreement with the data for the sweep specimen. Much better performance was found, however, for the other three static specimens, none of which showed any significant amount of coating failure. These materials all had some porosity associated with them, either porous UO_2 cores (lots 733B and 732D) or a porous Al_2O_3 layer in the coating (lot 721C).

The importance of using porous UO_2 fuel particles now appears to be definitely established. It had been shown earlier by Battelle that the catastrophic failure of Al_2O_3 coating at low temperature (100°C) could not be prevented by merely increasing the coating thickness to 60 μ. A porous (80% dense) fuel particle was also required. It was recently demonstrated that a 60-μ Al_2O_3 coating on a large (200 μ), porous UO_2 particle would perform satisfactorily during low-temperature irradiation. This material (lot 771D in Table I-3), having an Al_2O_3-to-UO_2 ratio equivalent to that of lot 715A-HT and not being susceptible to low-temperature failure, should be close to being the optimum in Al_2O_3-coated UO_2 fuel.

A number of mixed or composite coatings on UO_2 particles are also being studied at Battelle. One of these (lot 1039B in Table I-3) is being irradiated in a sweep capsule at 815°C. After 5 at.% burnup the R/B values are still on the order of 10^{-9}. This specimen has a 5-μ Al_2O_3 coating beneath a 118-μ pyrolytic carbon coat-

Table I-3 SUMMARY OF FISSION-GAS-RELEASE DATA FROM COATED-PARTICLE FUELS IN SWEEP-GAS EXPERIMENTS (SEE REFS. 31 AND 38 TO 41)

Lot	Specimen: Fuel	Specimen: Coating*	Matrix	Irradiation capsule	Nominal irrad. temp., °C	Estimated burnup, at.% of heavy metal	R/B: Kr^{85m}, Kr^{87}, and Kr^{89}†	R/B: Xe^{135}	R/B: Xe^{133}
BMI-715A-HT	127-μ UO_2 (98% dense)	42-μ Al_2O_3	Graphite	BMI-CFP-17	1100	11	2×10^{-8}	1×10^{-8}	4×10^{-8}
					1100	12	2×10^{-8}	1×10^{-8}	3×10^{-8}
BMI-771D	200-μ UO_2 (80% dense)	60-μ Al_2O_3	None	BMI-CFP-46	100	0.7	2×10^{-9}	2×10^{-9}	5×10^{-9}
BMI-1039B	200-μ UO_2 (92% dense)	5-μ Al_2O_3 118-μ columnar PyC	None	BMI-CFP-14	815	3	9×10^{-10}	2×10^{-9}	ND‡
					815	4	2×10^{-9}	1×10^{-9}	6×10^{-9}
					815	5	7×10^{-10}	6×10^{-10}	ND‡
NCC-208-2	209-μ $(U,Th)C_2$	120-μ duplex PyC	None	ORNL-B9-11	1120	14.7	9×10^{-7}	4×10^{-7}	2×10^{-6}
NCC-208	200-μ $(U,Th)C_2$	110-μ duplex PyC	Graphite	ORNL-06Z-6	815§	5.2	ND‡	ND‡	ND‡
NCC-207	220-μ UC_2	101-μ columnar PyC	Graphite	ORNL-08-6	400¶	0.3	ND‡	ND‡	ND‡
					390	1.0	2×10^{-6}	3×10^{-6}	2×10^{-5}
					415	1.5	3×10^{-7}	6×10^{-7}	5×10^{-7}
					540	2.0	7×10^{-7}	7×10^{-6}	2×10^{-5}
					580	3.4	1×10^{-5}	2×10^{-5}	4×10^{-5}
					590	4.5	3×10^{-5}	2×10^{-5}	9×10^{-5}
					595	5.8	4×10^{-5}	3×10^{-5}	1×10^{-4}
					595	9.4	4×10^{-5}	3×10^{-5}	1×10^{-4}
BMI-1031C	200-μ UC_2	39-μ porous PyC 69-μ columnar PyC	None	BMI-CFP-44	815	1.7	3×10^{-9}	4×10^{-9}	3×10^{-8}
					815	3.3	3×10^{-9}	3×10^{-9}	7×10^{-9}
					815	4.7	2×10^{-9}	2×10^{-9}	3×10^{-9}
BMI-1043B	200-μ UC_2	66-μ columnar PyC	None	BMI-CFP-43	100	0.01	$<4 \times 10^{-8}$	$<4 \times 10^{-8}$	$<4 \times 10^{-8}$
					100	0.5		5×10^{-4}	1×10^{-3}
BMI-1050A	127-μ UC_2	60-μ columnar PyC	None	BMI-CFP-45	100	0.06	6×10^{-10}	4×10^{-10}	ND‡
					100	0.7	5×10^{-6}	2×10^{-5}	9×10^{-5}
BMI-1048A	127-μ UC_2	60-μ laminar PyC	None	BMI-CFP-42	100	0.01	3×10^{-9}	1×10^{-9}	ND‡
					100	0.7	3×10^{-7}	7×10^{-7}	3×10^{-6}

*Coatings are listed in order of preparation in the case of multiple coatings.

†Data are an average of the release fractions for the three krypton isotopes.

‡ND = none detected in the sample.

§This is the temperature at the surface of the 1.5-in. graphite spheres. The center temperature was approximately 200° higher.

¶These are the temperatures at the surface of the 1.5-in. graphite spheres. The center temperature ranged from about 100° higher at the lower temperatures to about 300° higher at the higher temperatures.

Table I-4 SUMMARY OF STATIC-CAPSULE DATA FOR COATED-PARTICLE FUELS
(SEE REFS. 31, 38, 39, AND 41)

Specimen				Irradiation capsule	Nominal irrad. temp., °C	U^{235} burnup, at.%	Fractional Xe^{133} release, ppm	Uranium removed in leach, %
Lot	Fuel	Coating*	Matrix					
BMI-715A-HT	127-μ UO_2 (98% dense)	42-μ Al_2O_3	Graphite	BMI-CFP-12	850	6.4	13	
BMI-715A-HT	127-μ UO_2 (98% dense)	42-μ Al_2O_3	None	BMI-CFP-12	850	6.4	31	2.5
BMI-733B	127-μ UO_2 (92% dense)	47-μ Al_2O_3	None	BMI-CFP-12	850	6.4	0.45	0.002
BMI-732D	127-μ UO_2 (83% dense)	43-μ Al_2O_3	None	BMI-CFP-12	850	6.4	0.65	0.01
BMI-721C	127-μ UO_2 (98% dense)	8-μ dense Al_2O_3 18-μ porous Al_2O_3 28-μ dense Al_2O_3	None	BMI-CFP-12	850	6.4	0.91	0.009
BMI-735D	127-μ UO_2 (93% dense)	16-μ Al_2O_3 65-μ laminar PyC	None	BMI-CFP-32	850	2.3	0.12	
BMI-997	127-μ UO_2 (93% dense)	31-μ BeO 72-μ laminar PyC	None	BMI-CFP-32	850	2.2	0.13	
BMI-997	127-μ UO_2 (93% dense)	31-μ BeO 72-μ laminar PyC	None	BMI-CFP-13	900	2.7	0.12	
BMI-759A	127-μ UO_2 (93% dense)	18-μ BeO 4-μ laminar PyC 43-μ Al_2O_3	None	BMI-CFP-13	900	2.7	5.7	
BMI-1020B	200-μ UC_2	113-μ columnar PyC	None	BMI-CFP-32	850	2.4	1200	
BMI-1021C	200-μ UC_2	118-μ laminar PyC	None	BMI-CFP-32	850	2.1	60	
BMI-1031C	200-μ UC_2	39-μ porous PyC 69-μ columnar PyC	None	BMI-CFP-32	850	2.3	0.69	
NCC-AD	24-μ UC_2	20-μ laminar PyC 80-μ columnar PyC	None	ORNL-LCP-6	1060–1105	7	ND†	<0.1

*Coatings are listed in the order of preparation in the case of multiple coatings.
†No fission gas was detected when the capsule was punctured.

ing. Other specimens (lots 735D, 997, and 759A in Table I-4) have been irradiated statically at 850 to 900°C to burnups ranging from 2.2 to 2.7 at.% with very little failure occurring. Lots 735D and 997 had Al_2O_3 or BeO coatings overcoated with pyrolytic carbon. The coating on lot 759A consisted of BeO and Al_2O_3 layers separated by a thin layer of pyrolytic carbon. All these materials had relatively porous (92 to 93% dense) UO_2 cores, which may have contributed to their good performance.

As part of the effort to understand the mechanism of low-temperature cracking of oxide coatings during irradiation, Battelle has been studying the stresses induced in ceramics by fission recoils. Two topical reports were issued recently, discussing the results of this work.[42,43] Thin disks of the ceramics (Al_2O_3, BeO, MgO, ZrO_2, SiO_2, SiC, and carbon) were irradiated with one face exposed to recoiling fission fragments. Expansion of the exposed surfaces resulted in curvature of the disks, and measurement of the curvature served as a measure of the expansion. Radiation-expansion coefficients were calculated and used to estimate the tensile and compressive stresses to be expected during fission-fragment irradiation of the interior of spherical ceramic coatings. The calculated stresses were of sufficient magnitude that they could be expected to contribute to low-temperature cracking of the coatings. In the case of Al_2O_3, expansion normal to the exposed surface was also studied, and the results indicated that the expansion was not isotropic but that the stresses were preferentially relieved by expansion normal to the free surface.[43]

Carbide-Base Fuel. Elevated-temperature sweep-capsule irradiations of carbide fuel particles that have duplex pyrolytic carbon coatings have continued at Oak Ridge.[40,41] One specimen reached 14.7 at.% burnup at 1120°C, with the fission-gas-release fractions being 10^{-7} to 10^{-6} (Table I-3). Only 0.01% of the coatings are estimated to have failed.[40] No detectable fission-gas release ($R/B < 10^{-10}$) was found for a graphite-matrix specimen of similar duplex-coated particles after 5.2 at.% burnup at a specimen surface temperature that was gradually increased from 620 to 815°C. A third specimen of the duplex type was irradiated statically in the LITR to an estimated burnup of 7 at.% at a temperature that ranged from 1060°C to 1105°C, with essentially no failure occurring. Puncture of the capsule gave no fission gas, and less than 0.1% of the uranium was leached from the particles. All these specimens were supplied by National Carbon.

A specimen of duplex pyrolytic carbon-coated particles is also being irradiated at Battelle in a sweep capsule (lot 1031C in Table I-3).[31,38,39] After 4.7 at.% burnup at 815°C, no failure has yet occurred. The superior performance of this type of coating was also shown in static capsule experiments (Table I-4). After 2.3 at.% burnup at 850°C, the Xe^{133} release from lot 1031C was only 0.69 ppm; whereas specimens having monolithic laminar and columnar pyrolytic carbon coatings of comparable thicknesses (lots 1021C and 1020B) released 60 and 1200 ppm, respectively, after equivalent irradiations at the same temperature. The laminar coating, although worse than the duplex coating, did perform better than the columnar specimen.

A graphite-matrix specimen of columnar pyrolytic carbon-coated UC_2 particles (lot NCC-207) was also evaluated in a sweep capsule at Oak Ridge.[41] The surface temperature of this specimen was gradually increased from 400 to 595°C during the irradiation to 9.4 at.% burnup. Coating failure progressed during the first half of the irradiation, but none occurred during the last half. Approximately 1% of the coatings were estimated to have failed.[41]

Additional thin (approximately 60 μ) monolithic coatings of pyrolytic carbon were studied in-pile at ambient temperature at Battelle (Table I-3). One of these (lot 1043B) was prepared from methane at 1400°C, and it failed completely in a few hours. Its performance was no better than that of coatings deposited from acetylene at the same temperature. Comparison of lots 1050A and 1048A showed that the latter was much superior, even though they both had the same physical dimensions. Lot 1048A had a laminar type coating deposited from benzene, and lot 1050A had a columnar coating deposited from acetylene. It is not yet certain whether the coating structure or the hydrocarbon used is the major factor influencing the performance, although it is believed to be the coating structure.

Some very interesting results of postirradiation metallographic examinations of pyrolytic carbon-coated UC_2 particles were recently reported by Oak Ridge.[40] These are reproduced in Figs. I-2 to I-4. Figure I-2 shows a particle with a laminar pyrolytic carbon coating prior

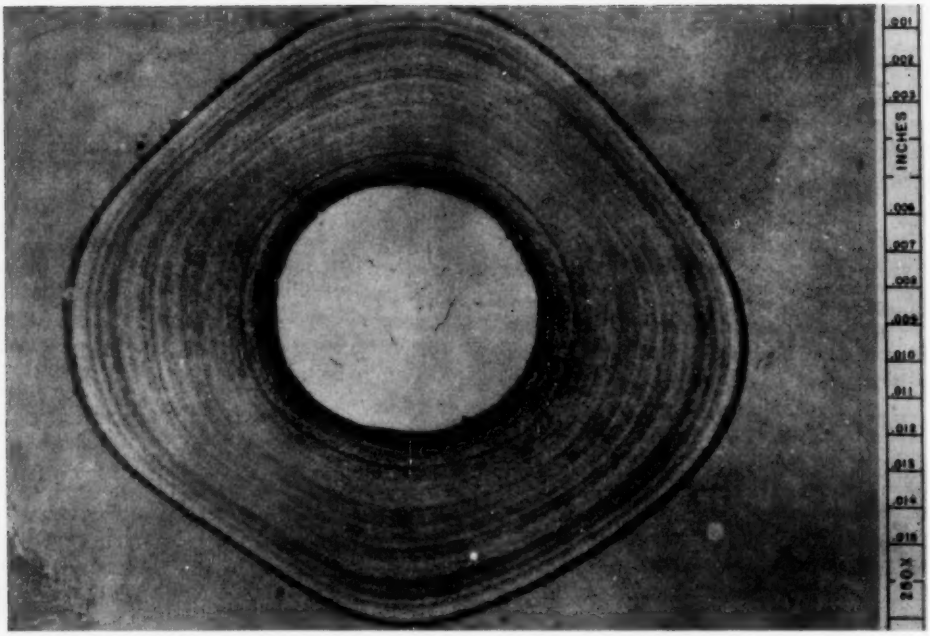

(*a*)

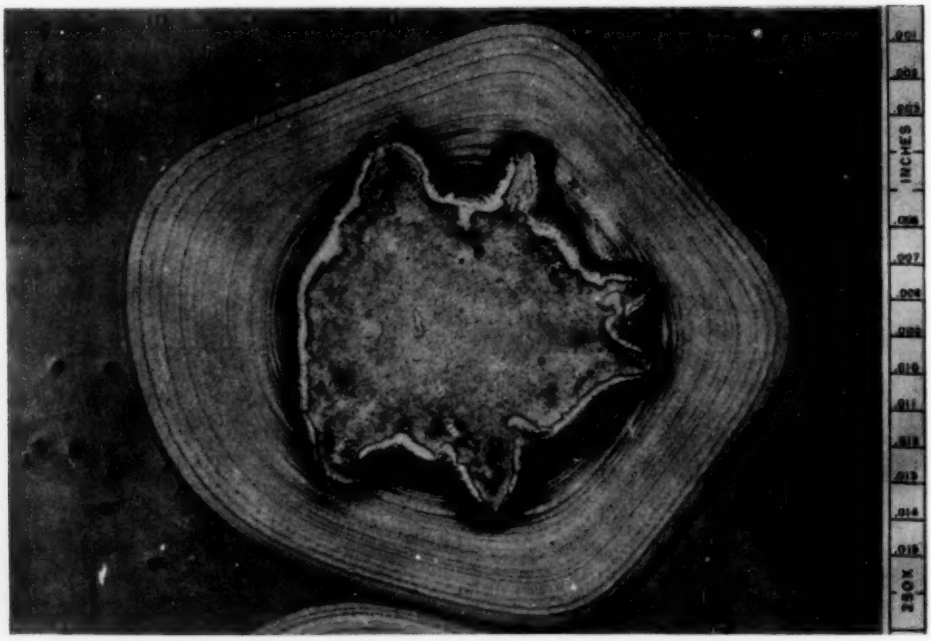

(*b*)

Fig. I-2 Sectioned, laminar type pyrolytic carbon-coated uranium carbide particles; (*a*) unirradiated, (*b*) irradiated to 15 at.% uranium burnup at 815 to 980°C.[40]

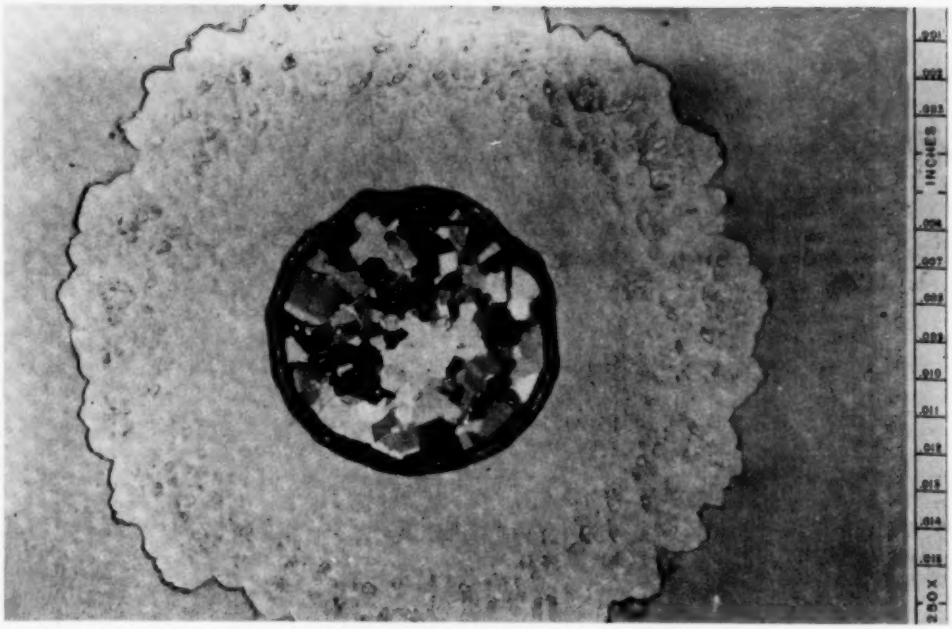

(*a*)

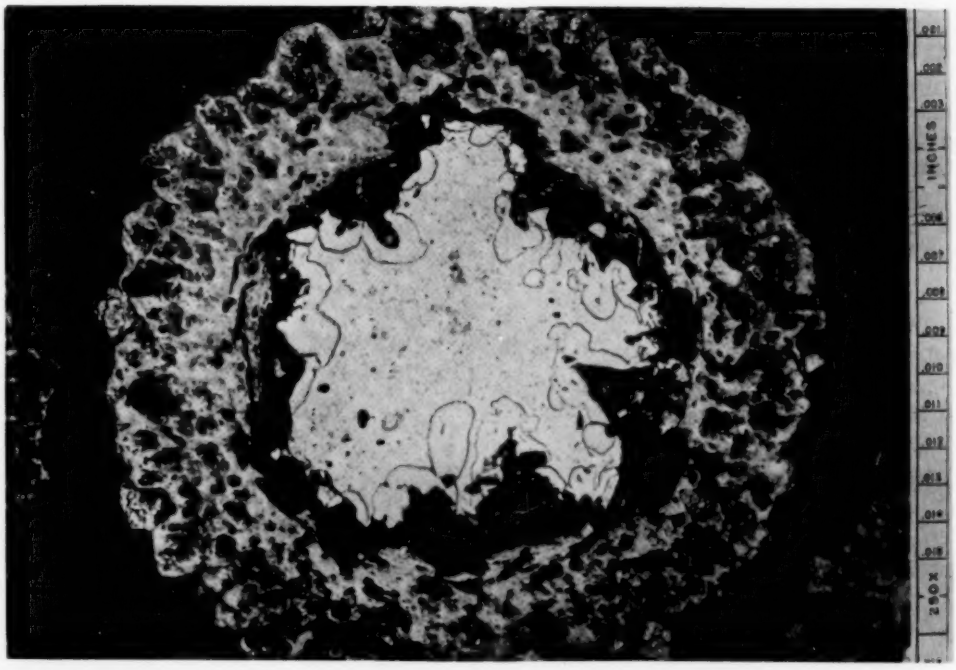

(*b*)

Fig. I-3 Sectioned, columnar type pyrolytic carbon-coated uranium carbide particles; (*a*) unirradiated, (*b*) irradiated to 12 at.% uranium burnup at 815 to 900°C.[40]

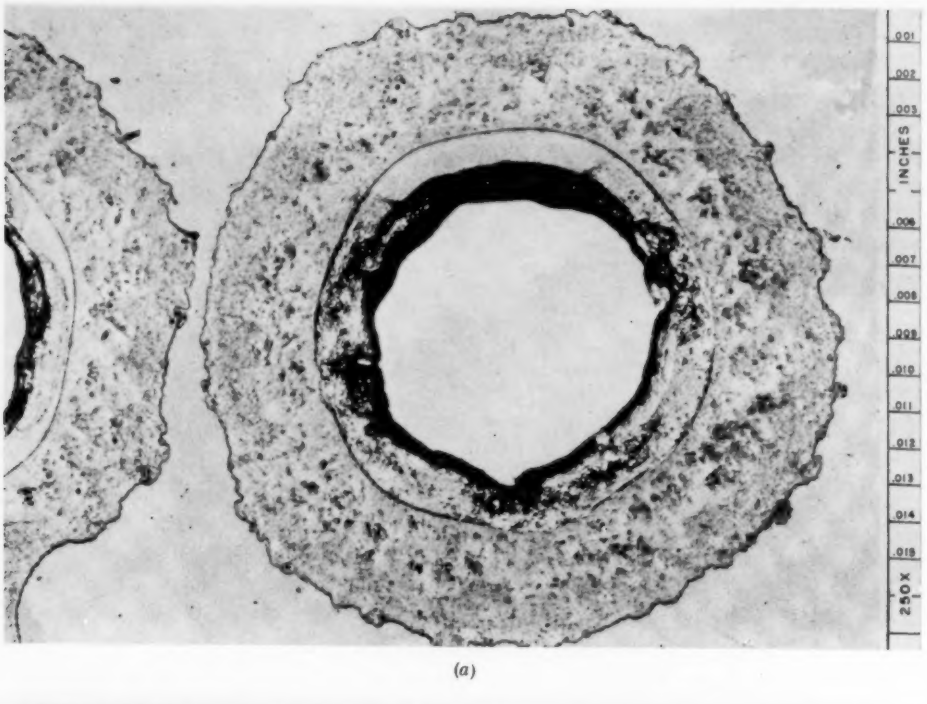

(*a*)

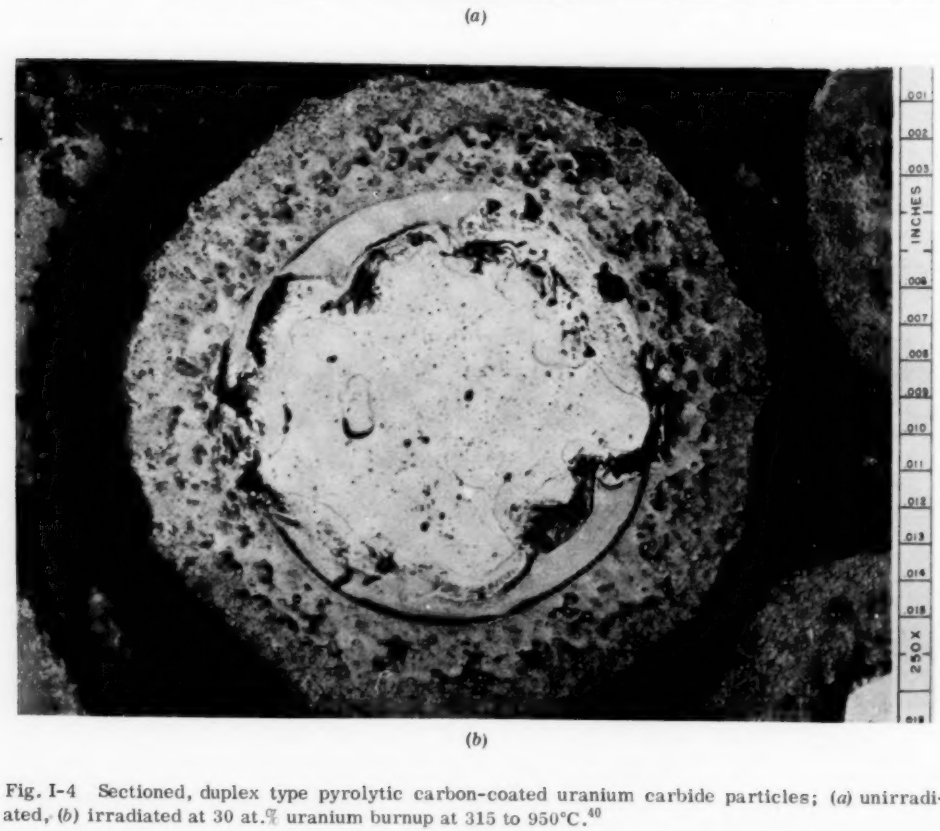

(*b*)

Fig. I-4 Sectioned, duplex type pyrolytic carbon-coated uranium carbide particles; (*a*) unirradiated, (*b*) irradiated at 30 at.% uranium burnup at 315 to 950°C.[40]

to irradiation and another particle of the same type after irradiation to 15 at.% burnup at 815 to 980°C. A reaction zone with protrusions into the coating is evident at the interface between the core and the coating after irradiation. In Fig. I-3, a similar reaction zone is apparent in the columnar type coated particles after irradiation to 12 at.% burnup at 815 to 900°C. The voids apparent in the columnar coating after irradiation are not due to irradiation effects but are due to the severe etching required to delineate the microstructure of the fuel particle. Typical duplex type coated UC_2 particles are shown in Fig. I-4 before and after irradiation to 30 at.% burnup at 315 to 950°C. The reaction zone appeared in many cases to have completely penetrated the inner laminar layer.

(C. W. Townley)

Graphite Matrix Studies

Only persons intimately involved with the problems of dispersing coated-particle fuels in graphite fully appreciate that selected process conditions are essential to avoid damage of the impermeable coatings of the dispersed fuel particles. The effects of two different process schemes on the coating integrity of dispersed fuel are discussed below.

Oak Ridge[41] noted the damage sustained by pyrolytic carbon-coated carbide particles randomly dispersed in a graphite mix, uniisostatically molded, and conventionally baked. The principal objective of the work was to determine the maximum concentration of coated particles which could be incorporated in a graphite matrix under various cold-forming pressures without causing more than some minimum amount of damage to the particle coatings. Fuel loadings ranging from approximately 6 to 23 vol.% of coated particles were used, and forming pressures ranged from 3000 to 35,000 psi. The baked specimens were subjected to acid electrolysis, and the coating damage was assessed by the uranium concentration in the leach solution. The coated particles tested were normal uranium carbide spheroids, with an average diameter of 176 μ, coated with a laminar layer averaging 98 μ in thickness. The uranium content of the coated particles was 44.10 wt.%, and the leachable uranium in the as-received material corresponded to 4.62×10^{-4} wt.% of the contained uranium.

Body preparation consisted of blending the coated particles, graphite filler, and furan resin in benzene. After gentle mixing until a slightly damp state was reached, the material was passed through an 18-mesh screen. The resulting granules were dried overnight at 45°C to remove the remainder of the benzene.

Initial forming of the specimens was accomplished by placing a weighed charge in a cylindrical die and lightly pressing at 100 psi. The pellets were then enclosed in a rubber sheath, evacuated, and warm molded isostatically in an autoclave containing water at 100°C and 1200 psi. Next, the sheathed pellets were isostatically pressed in oil at room temperature to pressures of 3, 6, 9, 12, 15, 20, 25, and 35 ksi. (For the body with the highest fuel concentration, the maximum pressure used was 12 ksi.) All specimens were baked on a 24-hr schedule to 1000°C in a hydrogen atmosphere. The results of the experiments are given in Table I-5 where it is seen, as one would expect, that

Table I-5 EFFECT OF FORMING PRESSURE AND FUEL LOADING ON DAMAGE TO PYROLYTIC CARBON-COATED PARTICLES DURING FABRICATION IN GRAPHITE MATRICES[41]

Forming pressure, psi	Coated-particle concentration, vol.%	Coated particles damaged,* %
3,000	5.8	0.01
	10.5	0.005
	14.8	0.01
	18.8	0.04
6,000	6.3	0.01
	11.7	0.02
	15.7	0.025
	20.8	0.01
9,000	6.9	0.01
	12.0	0.01
	16.4	0.015
	22.3	0.14
12,000	7.0	0.02
	12.7	0.02
	17.7	0.45
	23.1	0.15
15,000	7.4	0.06
	13.0	0.13
	18.5	0.225
20,000	7.8	0.14
	13.5	0.06
	19.2	0.33
25,000	7.8	0.06
	13.6	0.18
	19.7	0.58
35,000	8.1	0.06
	13.8	0.50
	19.8	1.28

*Based on uranium content of acid electrolysis solution.

the coating damage increases with forming pressure and fuel loading. The data indicate that, if, in view of the fission-product-retention requirement, for example, the fraction of coatings damaged must be limited to the order of 10^{-4}, then the limiting forming pressures for 7 vol.% loadings would be about 12,000 psi. A forming pressure of 9000 psi would be suitable, in this case, for loadings of 13 and 16 vol.%, respectively, and 6000 psi could be used for loadings as high as 21 vol.%.

Table I-6 SUMMARY OF PROCESS CONDITIONS AND NOMINAL PROPERTIES OF FUELED CYLINDERS PREPARED FROM PELLETIZED COATED-PARTICLE FUEL[31]

	Set 1	Set 2	Set 3
Baking conditions			
Temperature at which pressure was applied, °C	250	250	250
Maximum pressure, psi	5000	5000	5000
Unfueled matrix end disks incorporated	Yes	Yes	Yes
Density			
Composite, g/cm^3	1.83	1.91	1.93
Matrix (calculated), g/cm^3	1.74	1.73	1.62
Xe^{133} release during heating after neutron activation for 1 hr			
Maximum temperature, °C	1150	1150	1150
Release, ppm	0.18	0.095	0.09*
Tensile strength,† psi	2070	2090	1240
Fuel loading			
UC_2, wt.%	7.79	14.1	21.7
1020B, vol.%	12.5	23.5	36.7
UC_2, g/cm^3 of specimen	0.143	0.269	0.420

*Value obtained since publication of reference report.

†Tensile strength measured by diametral loading of 0.25-in.-diameter by 0.2-in.-long cylinders.

Battelle[31] has reported fuel dispersion and matrix process conditions that permitted incorporation of up to 37 vol.% coated-particle fuel with negligible evidence of fuel-particle damage. The fuel was 150- to 250-μ-diameter UO_2 coated with 113 μ of pyrolytic carbon. Fuel dispersion was accomplished by pelletizing, coating each individual fuel particle, with graphite matrix. Such pelletized material was then consolidated and baked by hot-pressing procedures similar to those which have been reported extensively by General Atomic. The resulting fuel compacts exhibited less than 1-ppm Xe^{133} release in postneutron activation tests, indicating negligible damage to the dispersed fuel. In addition, such fuel dispersions have idealized (approaching equidistant) fuel dispersion, rather than random spacing. Table I-6 presents process and nominal property data for such fueled graphite cylinders.

General Atomic[44] is investigating the feasibility of producing graphite-matrix fuel dispersions of superior properties by hot working such composites. Preliminary data have been reported on experiments to establish hot-work conditions that would not adversely affect dispersed carbide particles. The essential point is to obtain appreciable hot-working strain while holding the temperature below the fuel carbide-graphite eutectic temperature. In initial experiments, bodies of matrix graphite containing approximately 9 vol.% of UC-ZrC particles were prepared by General Atomic's hot-pressing technique. The particles were approximately 400 μ in diameter and were coated with pyrolytic graphite. Microstructures (at 150×) before and after deformation of these fueled specimens at 2550°C to a strain of 35% indicated that particle coatings were deformed but usually without rupture. Microstructural examination of other specimens containing 20 vol.% carbide particles and hot worked at about 2400°C to approximately 30% strain indicated some degree of fuel-particle disintegration. Preferred process conditions are being sought in the continuing study. (M. C. Brockway)

Uranium Oxides

Properties and Behavior of Uranium Oxide Fuels

Bettis[45] has reported studies of electrical conductivity and thermoelectric power with nearly stoichiometric UO_2 at temperatures from 25 to 1100°C. Below 800°C, UO_2 was found to be a p type extrinsic semiconductor, with the extrinsic conductivity attributed mainly to minor deviations from stoichiometry. In the extrinsic range, carrier mobility increases exponentially with temperature with an activation energy of 0.13 ev. Above 800°C, conduction is intrinsic with an energy gap of 1.9 ev. In other studies the French[46] have observed that the electrical conductivity of sintered UO_2 decreases with decreasing porosity and almost disappears at densities greater than 95% of theoretical. This effect is thought to be connected with gas adsorption on the specimens.

Results from Chalk River[47] show that, at low temperatures, the thermal conductivity of UO_2 under irradiation is lower than that of unirradiated material. This effect seems to be confined to temperatures below about 700°C. Natural UO_2 has exhibited this effect for exposures up to 2.8×10^{20} neutrons/cm^2, with the thermal conductivity approaching a minimum limit of about 0.035 watt/(cm)(°C). Studies at Hanford[12] indicate that the reduction in thermal conductivity caused by irradiations up to 2×10^{19} fissions/cm^3 recovers by 90% after annealing at 900°C. Annealing at 1200°C produces 100% recovery.

Infrared absorption data from Hanford[25] for single-crystal UO_2 between wavelengths of 3 and 13 μ showed two strong absorption bands at 5.5 and 10 μ. These bands seem to be independent of oxygen-to-uranium ratio.

UO_2 did not react appreciably with molten stainless steel (type 304) after a 90-min exposure at 1600°C.[25] (R. H. Barnes)

Preparation of Uranium Oxide Fuel Bodies

French workers[48] have completed a second year of UO_2 extrusion studies to prepare rods of UO_2. In a separate study[49] at the same site, UO_2, 5.5% enriched, was fabricated into fuel rods by extrusion and isostatic pressing. An average density of 10.70 g/cm^3 was achieved after sintering at 1670°C for 6 hr in a cracked ammonia atmosphere. The final UO_2 rod was 0.48 in. in diameter and 6 in. long.

From results of vibratory compaction studies at Combustion Engineering,[50] it has been tentatively concluded that a UO_2 compaction density of 89% of theoretical is the best to be expected inside ½-in.-diameter 15-mil-wall stainless-steel tubes with present production methods, utilizing sized, fused UO_2 as received from the vendor. Densification and compaction of 1000 g of this material into a 3-ft-long fuel rod can be achieved in 6 min. Up to 37 rods have been compacted simultaneously, using a high-impact vibrator. Densities between 84 and 87% of theoretical were obtained on individual rods from a 37-rod group.

Pneumatic impaction of UO_2 at Hanford[24] has demonstrated that any one of eight different types of UO_2, varying from ceramic-grade powder to pulverized fused UO_2, can be impacted to densities greater than 98% of theoretical. A minimum wall thickness of 0.050 in. for a 4-in.-diameter type 310 stainless-steel can containing 17 lb of UO_2 is sufficient to prevent can rupture during impaction at 1200°C and 230,000 psi. The high-density material thus produced is used as starting stock for further processing into fuel elements. (D. E. Rhodes)

Uranium Carbides, Nitrides, and Sulfides

Properties

Yamamoto, Watanabe, and Sano have obtained data[51] which show that the stability of UC_2 increases with temperature relative to the stability of the refractory solid-solution carbides. The maximum amount of UC that can be added to refractory carbide-graphite mixtures without forming UC_2 decreases with increasing temperature, as follows.

	Maximum addition of UC, mole %	
Temp., °C	To ZrC + C	To NbC + C
1600	49	46
1800	32	45
2000	28	37

General Atomic[52] has tested uranium–5 wt.% carbon alloys in contact with various metals for

24 hr at 1800°C. Iridium reacted with the UC and melted and flowed away from the interface, leaving a void. Rhenium reacted superficially with the UC, producing a very thin layer on the surface of the metal. A light phase containing a dark precipitate formed to an appreciable depth on the surface of tungsten–26 wt.% rhenium alloy in contact with the UC.

Uranium dicarbide and uranium sesquicarbide are reduced to uranium monocarbide by hydrogen at temperatures above 1800°C, according to Atomics International.[53]

Levinson calculated the heat capacity of uranium dicarbide from data obtained up to 2300°C.[54] The heat capacity at 1211°C was 0.091 cal/(g)(°C). The heat capacity at 2308°C was 0.127 cal/(g)(°C). A heat of transformation of 11.0 cal/g was measured at a temperature of 1770°C.

Grossman[55] has obtained measurements of the thermal conductivity, electrical resistivity, the total hemispherical emittance, and the normal spectral emittance of uranium monocarbide. The thermal conductivity was found to be constant at 0.057 cal/(sec)(cm)(°C) from 1200 to 2050°K. The resistivity was found to obey the relation, $20.4 + 114.8\ T \times 10^{-3}$ μohm-cm, from 1200 to 2050°K.

The Radiation Effects Information Center has prepared a review[27] of the available data on the performance of uranium carbides, uranium nitride, and uranium silicides under nuclear radiation.

Strasser, Taylor, and Anderson[56] have completed two irradiations of slightly hypostoichiometric UC at average maximum fuel temperatures of 760°C and burnups up to 16,400 Mwd/metric ton. Surface temperatures were lower than 760°C. One specimen was clad with niobium, and one was clad with stainless steel. Each specimen consisted of several pellets of UC. The niobium did not react with the UC during the irradiation that lasted 2800 hr at a temperature of 430°C. The stainless steel did show a slight reaction with the UC after 2800 hr at 490°C. The fuel itself showed a volume change of 1.4%, and 0.4% of the fission gases were released.

British investigators[57] have examined some sintered pellets of hypostoichiometric UC, some sintered pellets of UC–10 wt.% Fe_2U, and some cast pins of UC–10 wt.% PuC after irradiations to burnups ranging up to 16,500 Mwd/metric ton at central temperatures ranging up to 1010°C. The specimens were clad in stainless steel. The fission-gas release could all be attributed to recoils, the microstructures were unchanged, no dimensional changes were observed, and the fuel-sheath compatibility was good.

Particles of UC_2 consisting of one or two grains of cubic UC_2, but containing numerous platelets of tetragonal UC_2, were irradiated by General Atomic.[58] The release of fission products was then studied during annealing at temperatures from 1000 to 1800°C.[9] Typical data are shown in Table I-7.

Dell and Allbutt have prepared a review[59] of data in the literature through 1962 with regard to the chemical and physical properties of the nitrides and sulfides of uranium, thorium, and plutonium.

Representative data from French studies (under contract to the Dragon Project) of thorium-uranium-carbon alloys, primarily in the region near thorium dicarbides,[60] are as follows. Thorium dicarbide has a transformation temperature below 1600°C. Thorium sesquicarbide does not exist at 1600°C. The thermal expansion coefficient of thorium dicarbide is 10.8 to 11.0×10^{-6} from 20 to 1200°C. A volume increase of 4.8% between 1240 and 1290°C suggests that this is the transformation temperature for thorium dicarbide. The thermal conductivity of thorium dicarbide is 0.05 cal/(cm)(sec)(°C); that of thorium monocarbide is 0.2 cal/(cm)(sec)(°C) from 200 to 400°C.

Battelle workers have found[61] that uranium mononitride of better than 95% of theoretical density can be prepared by hot pressing at about 1500°C under a pressure of 10,000 psi. It has a thermal expansion coefficient of about 9.3×10^{-6} from 20 to 1000°C and a thermal conductivity of about 0.06 cal/(cm)(sec)(°C) at

Table I-7 FRACTIONAL RELEASE OF FISSION PRODUCTS FROM UC_2 PARTICLES DURING POSTIRRADIATION ANNEALING[58]

Temp., °C	Time, hr	Fractional release of			
		Xe^{133}	Ba^{140}	Te^{132}	I^{131}
1000	72	0.016	0.007	0.0010	0.0012
1200	72	0.036	0.020	0.0084	0.0071
1300	66	0.058	0.037	0.0079	0.0071
1400	68	0.075	0.091	0.057	0.020
1550	74	0.086	0.037	0.113	0.019
1700	71	0.123	0.055	0.183	0.044
1800	48	0.27	0.20	0.12	0.062

1000°C. It has a resistivity of about 200 μohm-cm at 600°C. Its dynamic modulus of elasticity is about 31×10^6 psi, and its hardness is 500 to 600 kg/mm^2 at 20°C and 80 kg/mm^2 at 1200°C. (W. Chubb)

Fuel-Water Reactions

In experiments by Argonne[62] on the reaction of aluminum-uranium alloys with water, small samples of aluminum-uranium (enriched) alloy plates submerged in room-temperature water were subjected to severe nuclear transients in the Transient Reactor Test facility (TREAT) to determine the extent of metal-water reaction and to observe the physical changes that occurred. One of the two types of specimens tested was an aluminum-clad 77 wt.% aluminum–23 wt.% uranium (fully enriched) plate cut from a standard SPERT-ID plate. Both cladding and core material were 20 mils thick. These plates had nominal dimensions of 0.06 by 0.5 by 1.4 in. The edges of these plates were not clad. The second type of specimen was a plate with the dimensions of 0.2 by 0.5 by 0.5 in. This material was unclad SL-1 core material (81 wt.% aluminum–17 wt.% uranium, fully enriched, –2 wt.% nickel). Samples of each of these materials were placed in high-pressure autoclaves and submerged in distilled water with a slight overpressure of helium. They were subjected to TREAT transients that imparted energies of 174 to 1023 cal/g of plate (both cladding and core) in periods of from 42 to 112 msec. Heating of the fuel specimens from 25°C to as high as 2480°C (the vaporization temperature of aluminum) was achieved in times as short as 0.4 sec.

The extent of reaction, which resulted from the meltdown of the plates in water, was determined by measuring the hydrogen evolved. A summary of the results is given in Fig. I-5. Three regions of reaction occurred as the nuclear energy input was increased. In the first region, the extent of reaction increased from negligible amounts (<0.1%) at an energy input of 174 cal/g to 7.2% at 530 cal/g. At energies higher than 530 cal/g, the extent of reaction increased markedly for both types of specimens tested. The unclad plates reacted to a greater extent than the clad plates in the second region, with as much as 22.2% of an unclad plate having reacted at 740 cal/g. The differences in extent of reaction were probably due

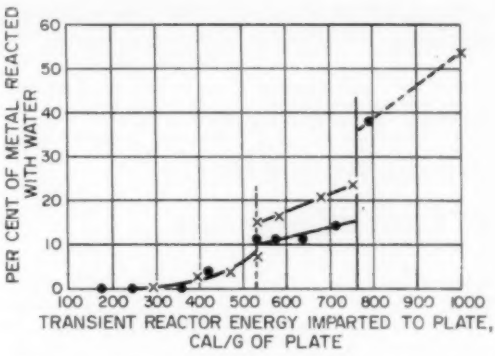

Fig. I-5 Extent of metal-water reaction for uranium-aluminum fuel plates in 25°C water.[62] ×, unclad plates (0.2 by 0.5 by 0.5 in.); •, clad plates (0.06 by 0.5 by 1.4 in.).

to the effect of cladding and geometry. Above 740 cal/g, a third region of very extensive reaction (>35%) was found.

The threshold for breakup into particles occurred between energy inputs of 361 and 430 cal/g. The average equivalent diameter of the particles in the most energetic transient conducted with the clad plate material was 18.6 mils.

Similar experiments[63] were performed in which the specimens were submerged in water at a temperature of 285°C during exposure to a neutron pulse. The SPERT-ID plates were subjected to nuclear energy inputs of 390 and 570 cal/g. The SL-1 specimens received energy inputs of 350 and 500 cal/g. At the inputs of lower energy, the extent of reaction was 0.35% and 0.24% for SPERT-ID and SL-1 samples, respectively. At the higher energy inputs, 89% of the SPERT-ID sample and 76% of the SL-1 sample reacted. The extent of the reactions at the higher energy inputs was considerably greater than the corresponding runs as reported above, which were carried out in room-temperature water. The higher rates were suggested as being attributable to not only the higher initial autoclave pressures but also to possibly smaller heat losses from the specimens during heating.

Argonne[64] has also reported a brief study of the vapor-phase burning of unfueled aluminum in liquid water. Samples of aluminum ranging in weight from 150 to 1000 mg were levitated, heated, ignited in air, and dropped into room-temperature water. The pellet diameters decreased at the rate of 0.16 mm/sec, which

corresponds to a consumption rate of 1.0 g of aluminum/(cm^2)(min). (A. W. Lemmon, Jr.)

Basic Studies of Irradiation Effects in Fuel Materials

Metals

The results obtained at Argonne[65] from an investigation of swelling of uranium upon post-irradiation annealing show that pronounced swelling at about 600°C accompanies recrystallization of the specimens. Microstructures exhibiting large bubbles at grain boundaries are interpreted to show that fission gases are swept to grain boundaries by the recrystallization and grain-growth process. Alternatively, since grain boundaries act as vacancy sources, it is possible that gas-filled bubbles with a detectable size are able to nucleate and grow only at grain boundaries. It is also reported that substantially less swelling is observed when specimens are heated in the beta phase than when specimens undergo recrystallization in the alpha phase. The cause (or causes) of an observed uniform distribution of small bubbles in the beta-treated material is the subject of further analysis.

A bibliography of radiation effects on solid uranium-based nuclear fuel materials has been prepared by Uhlmann[66] of Sweden. The bibliography includes abstracts of 50 references covering a wide variety of topics. Included are articles on uranium and uranium alloys; carbides, oxides, and nitrides; and dispersions and coated-particle fuels. Fission-gas-release studies are also covered.

Ceramics

At Harwell[9] studies of the ejection of uranium by fission fragments led to the following conclusions: (1) when atoms ejected from the surface of uranium metal by escaping fission fragments are collected on a foil, the amount of collected material reaches a saturation value because reejection takes place, (2) calculations indicate that reejection may be caused by bombardment of the collector by fission fragments escaping from the surface of the uranium emitter, and (3) the number of uranium atoms ejected from the surface of uranium by an average fission fragment escaping from the surface is about 2000, and this number is not materially affected by an oxide layer.

Mathematical analysis[9] of the difference in nature between fission-fragment tracks in vacuum-deposited films of UO_2 with a 30 A grain size, in larger-grain-size UO_2, and in single crystals has shown that a phenomenological reflection coefficient of 0.3 to 0.5 for energy incident at a grain boundary can account for the experimental results. Theoretical considerations show that the furrows in vacuum-deposited films are formed by explosive evaporation; i.e., the heating produced by the passage of a fragment creates a high local pressure, sufficient to eject the surrounding material in the form of particles.

Vapor-grown single crystals of nearly stoichiometric UO_2 have been thinned for transmission electron microscopy by Blank and Amelinckx.[67] The as-grown crystals show a dense pattern of precipitates and may contain loops due to quenched-in vacancies, but contain hardly any dislocations. Two models for the production of loops are proposed. Dislocation networks (small-angle boundaries) are produced on annealing the crystals. Irregular patterns of dislocations arise when sufficiently thick parts of the crystal foils are treated with heat shocks in the microscope by suddenly increasing the beam current. After exposure to 10^{15} neutrons/cm^2, the crystal foils show fission tracks, short segments of straight dislocation lines, and black dots, which are partly distributed at random and partly aligned on fission tracks. Interaction between fission tracks and dislocations has been observed. The conditions for contrast production on fission tracks have been investigated. The experimental findings can be explained by a model of a displacement field around the fission tracks.

A study of fission-gas release from lightly irradiated sintered UO_2, reported by Saclay,[68] reveals considerable influence of the atmosphere in which the compacts were stored and treated and of their surface condition and specific surface area. Effective diffusion coefficients (D') were estimated at 1400°C for various grades of UO_2, including monocrystalline pieces for which $D'_{mean} = 6.9 \times 10^{-14}$/sec. True diffusion coefficients are reported for specimens where the surface area could be measured.

The methods by which deviations from normal diffusion kinetics can be detected in both in-pile and out-of-pile fission-gas-emission experiments have been summarized and discussed by Harwell workers.[69] It is suggested that the observed effects in both the in-pile and out-of-pile experiments can be interpreted in terms of a combination of "knockout" and "pore diffusion" mechanisms. For example, in pore diffusion, bursts are believed to occur on heating from a lower to a higher temperature as a result of high-temperature release of some of the xenon accumulated at imperfections. At each temperature an equilibrium is set up in which the rate of loss of Xe^{133} from the imperfection is made up by normal diffusion into the imperfection from the surrounding UO_2. On cooling, the normal bulk-diffusion mechanism is frozen out, and the observed release arises from the residual Xe^{133} in those imperfections having a low energy of activation.

At Bettis[70] zirconia-urania solid-solution high-density plates, fabricated from ZrO_2 and slightly enriched UO_2 powders, were irradiated with neutrons, and the amount of Xe^{133} released was measured as a function of temperature. Assuming a diffusion mechanism based on a model of a flat plate containing a uniform distribution of fission gas, diffusion coefficients were calculated for the 700 to 1250°C temperature range.

The diffusion coefficient for Xe^{133} in slightly irradiated (1×10^{16} fissions/cm^3), single-phase tetragonal ZrO_2–26 wt.% UO_2 plates can be represented by the equation

$$D = 15 \exp(-92{,}275/RT)$$

(F. A. Rough)

References

1. W. S. Blackburn, Creep of Uranium at 550°C Under a Tensile Stress of 350 PSI, British Report TNPG-401, June 1963.
2. M. J. C. Hill, Textures in Rolled Uranium Sheet, British Report AWRE-O-21/63, May 1963.
3. P. R. Morris, Irradiation Growth in Natural Uranium Fuels, USAEC Report NLCO-876, National Lead Co. of Ohio, April 1963.
4. J. W. Savage, Diffusion of Fission Gas in Uranium, USAEC Report NAA-SR-6761, Atomics International, Aug. 15, 1963.
5. Heinz-Eberhard Roellig, Compatibility of Fissionable Materials with Construction Materials. Part I. Compatibility of Metallic Fissionable Materials with Cladding Materials, German Report ZFK-WF-13, March 1962.
6. Nuclear Metals, Inc., Papers Presented at the X-Ray Preferred Orientation Meeting held at Nuclear Metals, Inc., West Concord, Mass., December 7–8, 1961, USAEC Report NMI-4992, May 9, 1963.
   a. Anisotropic Growth vs. Preferred Orientation in Unrestrained Uranium, E. F. Sturcken, B. G. LeFevre, and W. R. McDonnell.
   b. A Note on Residual Textures in Beta-Treated Uranium, L. Robins.
   c. Axial Textures in As-Extruded Uranium Tubes — Mark VB Production, L. Robins.
   d. Irradiation Growth in Alpha-Uranium Single Crystals, P. R. Morris.
   e. Texture Induced During Beta Treatment of Uranium, R. B. Russell.
7. P. E. Repas, R. H. Goodenow, and R. F. Hehemann, An Investigation of Transformation Characteristics of Three Uranium Base Alloys. Final Report, Report AMRA-CR-63-02/1 (F), Case Institute of Technology, January 1963.
8. R. F. Stoops and J. V. Hamme, Uranium Interstitial Phases, Progress Report, May 1963, USAEC Report NCSC-2663-12, North Carolina State College, May 1963.
9. Metallurgy Division, Atomic Energy Research Establishment. (Unpublished)
10. Hanford Atomic Products Operation, Metallurgy Research Operation Quarterly Progress Report, January–March 1963, USAEC Report HW-77052, Apr. 15, 1963.
11. Hanford Atomic Products Operation, Reactor and Fuels Laboratory Monthly Report, July 1963, USAEC Report HW-78420A, Aug. 15, 1963. (Classified)
12. W. H. Zachariasen and F. H. Ellinger, The Crystal Structure of Alpha Plutonium Metal, *Acta Cryst.*, 16(8): 777-783 (Aug. 10, 1963).
13. K. A. Gschneider, Jr., R. O. Elliott, and J. T. Waber, Influence of Alloying on the Negative Thermal Expansion of Delta Plutonium, *Acta Met.*, 11(8): 947-955 (August 1963).
14. R. B. Roof, Jr., A Neutron Diffraction Examination of Alpha Plutonium at 23°K, USAEC Report LA-2912, Los Alamos Scientific Laboratory, May 1963.
15. J. A. Leary, W. J. Maraman, W. N. Miner, and F. W. Schonfeld, Quarterly Status Report on Solid Plutonium Fuels Program for Period Up to June 30, 1963, USAEC Report LAMS-2949, Los Alamos Scientific Laboratory, July 1963.
16. Los Alamos Scientific Laboratory, Quarterly Status Report on LAMPRE Program for Period Ending May 20, 1963, USAEC Report LAMS-2915, June 1963.

17. Argonne National Laboratory, Reactor Development Program Progress Report, April 1963, USAEC Report ANL-6717, May 15, 1963.
18. A. F. Berndt and L. T. Lloyd, Tabulations of Calculated Crystallographic Data for Alpha Plutonium, USAEC Report ANL-6676, Argonne National Laboratory, June 1963.
19. Oak Ridge National Laboratory Status and Progress Report, June 1963, USAEC Report ORNL-3477, July 11, 1963.
20. Hanford Atomic Products Operation, July 1963. (Unpublished)
21. Société Belge pour l'Industrie Nucléaire, Use of Plutonium as a Fuel in Nuclear Reactors. Quarterly Progress Report, October 1–December 31, 1961, USAEC-Euratom Report EURAEC-227, Jan. 18, 1962.
22. Ye. Ye. Zastenker et al., Oxidation of Plutonium Dioxide with Atmospheric Oxygen, *Radiokhimiya*, 5(1): 141 (1963).
23. E. E. Jackson and M. H. Rand, The Oxidation Behaviour of Plutonium Dioxide and Solid Solutions Containing Plutonium Dioxide, British Report AERE-R-3636, June 1963.
24. Hanford Atomic Products Operation, Ceramics Research and Development Operation Quarterly Report, January–March 1963, USAEC Report HW-76301, Aug. 23, 1963.
25. F. W. Albaugh, Hanford Atomic Products Operation, Reactor and Fuels Laboratory Monthly Report, June 1963, USAEC Report HW-78052A, July 15, 1963. (Classified)
26. Nuclear Materials & Equipment Corp., June 10, 1963. (Unpublished)
27. J. B. Melehan, V. W. Storhok, R. J. Burian, and M. Kangilaski, The Effects of Nuclear Radiation on Ceramic Reactor-Fuel Materials, Report REIC-27, Battelle Memorial Institute, Radiation Effects Information Center, June 30, 1963.
28. S. Langer, Plutonium Carbide Fuels for HTGR's, *Nucleonics*, 21(9): 73 (September 1963).
29. A. Strasser and D. Stahl, Carbide Fuel Development, Progress Report, October 1, 1962–March 31, 1963, USAEC Report UNC-5056, United Nuclear Corporation, May 1, 1963.
30. R. W. Dayton and R. F. Dickerson, Progress Relating to Civilian Applications During May 1963, USAEC Report BMI-1632(Del.), Battelle Memorial Institute, June 1, 1963.
31. R. W. Dayton and R. F. Dickerson, Progress Relating to Civilian Applications During June 1963, USAEC Report BMI-1639(Del.), Battelle Memorial Institute, July 1, 1963.
32. R. H. Cole and L. E. Wilkinson, Development of High-Strength Ternary and Quaternary Thorium-Uranium Base Alloys, Report ATL-A-128, Advanced Technology Laboratories, Nov. 1, 1962.
33. D. E. Williams and W. L. Larsen, The Work Hardening of Ames Thorium, USAEC Report IS-576, Ames Laboratory, July 1963.
a. D. E. Hamby, Interim Report on Metallurgy of Thorium and Thorium Alloys, ORNL-1090, p. 24, 1951.
34. J. H. Cherubini and S. Peterson, A Technique for the Quantitative Characterization of Dispersions, USAEC Report ORNL-TM-446, Oak Ridge National Laboratory, Feb. 28, 1963.
35. Y. Baskin and J. H. Handwerk, Thoria and Thoria-Urania Reinforced by Metal Fibers, USAEC Report ANL-6529, Argonne National Laboratory, June 1962.
36. Oak Ridge National Laboratory Status and Progress Report, July 1963, USAEC Report ORNL-3491, Aug. 8, 1963.
37. Los Alamos Scientific Laboratory, Quarterly Status Report on Ultra High Temperature Reactor Experiment (UHTREX) for Period Ending June 20, 1963, USAEC Report LAMS-2933, July 23, 1963.
38. R. W. Dayton and R. F. Dickerson, Progress Relating to Civilian Applications During July 1963, USAEC Report BMI-1642(Del.), Battelle Memorial Institute, Aug. 1, 1963.
39. Battelle Memorial Institute, Progress Relating to Civilian Applications During August 1963, USAEC Report BMI-1644, Sept. 1, 1963. (Classified)
40. Oak Ridge National Laboratory, Gas-Cooled Reactor Program Semiannual Progress Report for Period Ending March 31, 1963, USAEC Report ORNL-3445, July 23, 1963.
41. Oak Ridge National Laboratory, June 28, 1963. (Unpublished)
42. T. S. Elleman, R. B. Price, and D. N. Sunderman, Fission-Fragment-Induced Stresses in Ceramic Materials, USAEC Report BMI-1635, Battelle Memorial Institute, June 4, 1963.
43. T. S. Elleman, R. B. Price, and D. N. Sunderman, Fission-Fragment-Induced Expansion in Single-Crystal Alpha Alumina, USAEC Report BMI-1646, Battelle Memorial Institute, Sept. 4, 1963.
44. W. V. Goeddel and L. R. Zumwalt (Eds.), Coated-Particle-Fuels Research at General Atomic from November 1, 1962–May 31, 1963, USAEC Report GA-4260, General Atomic Division, General Dynamics Corp., June 3, 1963.
45. R. A. Wolfe, The Electrical Conductivity and Thermoelectric Power of Uranium Dioxide, USAEC Report WAPD-270, Westinghouse Electric Corp., Bettis Atomic Power Laboratory, Apr. 1, 1963.
46. B. Raz and H. Schmidt, A Remark on the Anomaly of Electric Resistance of UO_2, *J. Nucl. Mater.*, 8: 265 (March–April 1963).
47. R. C. Hawkings and J. A. L. Robertson, The Thermal Conductivity of UO_2 Under Irradiation: Some Early Results, Canadian Report CRDC-1143, March 1963.
48. R. Hauser, Uranium Oxide Extrusion. Final Report (2nd Year), USAEC-Euratom Report

EURAEC-368, Campagnie Industrielle des Combustibles Atomiques Frittes, March 1963.

49. J. Mercier, Extrusion of UO_2 Enriched to 5.5% for Irradiation Test in VBWR Reactor of Vallecitos—Draft of Final Report, USAEC-Euratom Report EURAEC-399, Compagnie Industrielle des Combustibles Atomiques Frittes, Aug. 20, 1963.
50. B. E. Murtha and W. P. Chernock, The Development and Testing of UO_2 Fuel Systems for Water Reactor Applications. Quarterly Progress Report for Period Ending March 31, 1963, USAEC Report CEND-178, Combustion Engineering Inc., April 1963.
51. Y. Yamamoto, K. Watanabe, and T. Sano, Study of the Preparation of (U, Zr)C and (U, Nb)C as Reactor Fuels, Preprint, International Conference on Atomic Energy, Czechoslovakia, July 1963.
52. L. Yang, A. F. Weinberg, F. D. Carpenter, R. G. Hudson, C. W. Savery, D. E. Johnson, and J. Lindgren, Quarterly Progress Report for Period Ending November 30, 1962, Investigations of Carbides as Cathodes for Thermionic Space Reactors, Reactors, Report GA-3866, General Atomic Division, General Dynamics Corp., May 20, 1963.
53. W. G. Smiley and W. D. Turner, Decarburization of Cast Uranium Carbide by Heating in Hydrogen, USAEC Report NAA-SR-7921, Atomics International, Aug. 15, 1963.
54. L. S. Levinson, Heat Content of UC_2 from 1484 to 2581°K, *J. Chem. Phys.*, 38: 2105-2106 (May 1963).
55. L. N. Grossman, High Temperature Thermophysical Properties of Uranium Monocarbide, *J. Am. Ceram. Soc.*, 46: 264-267 (June 1963).
56. A. Strasser, K. Taylor, and J. Anderson, Carbide Fuel Development, Phase IV Report, September 15, 1961–September 30, 1962, USAEC Report UNC-5055, United Nuclear Corporation, Mar. 31, 1963.
57. B. T. Bradbury, J. E. Cole, B. R. T. Frost, and J. D. B. Lambert, Post Irradiation Examination of Stainless Steel Clad UC, UC-UFe_2, and PuC-UC Fuel Pellets, British Report AERE-R-4323, May 1963.
58. L. R. Zumwalt, P. E. Gethard, and E. E. Anderson, Fission-Product Release from "Single Crystal" UC_2 Particles, USAEC Report GA-4267, General Atomic Division, General Dynamics Corp., June 5, 1963.
59. R. M. Dell and M. Allbutt, The Nitrides and Sulphides of Uranium, Thorium, and Plutonium: A Review of Present Knowledge, British Report AERE-R-4253, March 1963.
60. M. Marchal and A. Accary, A Basic Study of the Thorium-Uranium-Carbon System, Dragon Project Report-133, January 1963.
61. E. O. Speidel and D. L. Keller, Fabrication and Properties of Hot-Pressed Uranium Mononitride, USAEC Report BMI-1633, Battelle Memorial Institute, May 30, 1963.
62. R. O. Ivins, A Study of the Reaction of Aluminum-Uranium Alloy Fuel Plates with Water Initiated by a Destructive Reactor Transient, USAEC Report CONF-39-70, Argonne National Laboratory, February 1963.
63. Argonne National Laboratory, Reactor Development Program Progress Report, May 1963, USAEC Report ANL-6739, June 15, 1963.
64. Argonne National Laboratory, Reactor Development Program Progress Report, August 1963, USAEC Report ANL-6780, Sept. 15, 1963.
65. Argonne National Laboratory, Metallurgy Division Annual Report for 1962, USAEC Report ANL-6677, October 1963.
66. W. Uhlmann, Radiation Effects on Solid, Uranium Based Nuclear Fuel Materials, a Bibliography, Swedish Report VDIT-16(3.2), May 1963.
67. H. Blank and S. Amelinckx, Some Preliminary Results on Defects in Irradiated UO_2 Single Crystals as Revealed by Transmission Electron Microscopy, *J. Appl. Phys.*, 34(8): 2200-2209 (1963).
68. J. L. Berry, R. Darras, H. Chevilliard, and T. Gerevini, Contribution on the Investigation of the Escape of Fission Gas from Irradiated Sintered Uranium Oxide (in French), *J. Nucl. Mater.*, 8: 102-115 (January–February 1963).
69. D. Davies and G. Long, Abnormal Kinetics in the Release of Inert Gases from Uranium Dioxide, British Report AERE-M-969, May 1963.
70. J. C. Clayton, The Evolution of Xenon-133 from Slightly Irradiated Zirconia-Urania Plates, USAEC Report WAPD-TM-313, Westinghouse Electric Corp., Bettis Atomic Power Laboratory, August 1963.

Section

II

Reactor Materials

Moderator Materials

Graphite

Irradiation of graphite at liquid-nitrogen temperature produced no apparent change in its modulus of elasticity.[1] However, when the irradiated specimens were pulse annealed, the British investigators observed an anomalous increase in Young's modulus in the temperature range 200 to 300°K. The magnitude of this increase was dependent on the dose the sample had received, varying as the square of the initial resistance change. Samples with the highest irradiation dose began their anomalous rise in modulus at the lowest annealing temperature, and the value showed a plateau as the temperature was further increased. The peak was associated with the formation of diinterstitials, and the plateau of the higher dose specimens was attributed to the formation of larger complex groups. Thus Young's modulus may well be a useful property for the study of complex interstitial-group formation in the graphite lattice.

Flux-level effects on high-flux neutron-irradiation damage in graphite were interpreted by Harwell workers[2] in terms of the results of transmission electron microscopy, which reveals resolvable interstitial clusters. These clusters are shown to be most naturally accounted for by a homogeneous nucleation model.

A state-of-the-art report issued by the Radiation Effects Information Center at Battelle[3] for the period 1962-1963 contains extensive summary data on the effects of neutron irradiation on graphite.

A study at Lockheed[4] of the oxidation resistance of several types of carbon and graphite is particularly interesting because it includes such a diversity of carbon structures as porous carbon, AGOT graphite, glassy carbon, and pyrolytic graphite. The oxidation rates of the materials were generally controlled by two mechanisms, depending on the temperature: (1) the chemical reactivity at temperatures from 900 to 2200°F and (2) the gas diffusion from 2200°F to the sublimation temperature.

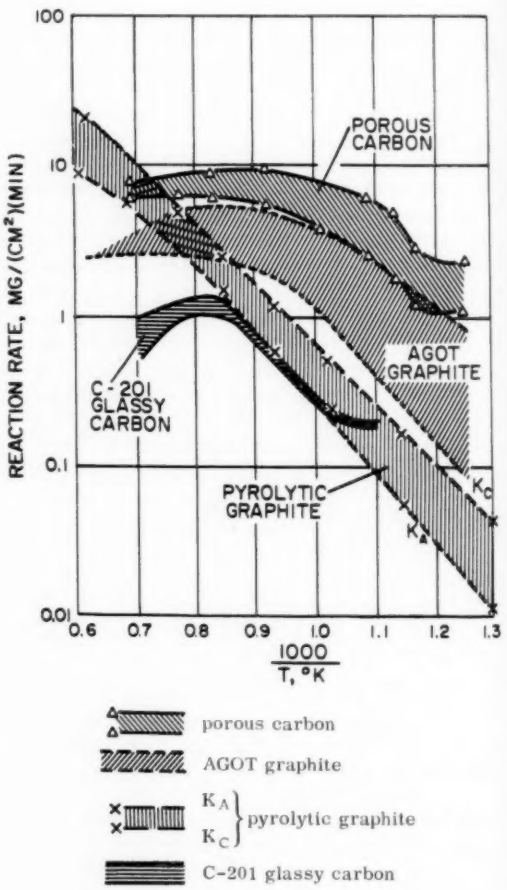

Fig. II-1 Oxidation rates for various types of graphite and carbon in air at 1 atm.[4]

The oxidation rates depended on porosity or the degree of basal-plane exposure in the low-temperature region (900 to 2200°F) and were not a function of the degree of crystallization. Figure II-1 shows the reaction-rate constants at 1 atm of air pressure. As can be seen, the superiority of glassy carbon is more pronounced at the higher temperatures.

In a compilation and analysis of property data on pyrolytic graphite prepared by Lockheed,[5] the origin and nature of the physical, thermal, and mechanical anisotropies are examined. The profound effects of process variables such as substrate characteristics, deposition temperature, gas pressure, and annealing temperature on material properties are analyzed in relation to the microstructural variations produced. The advantages, as well as the limitations, imposed upon the design of components by the anisotropic nature of pyrolytic graphite are discussed, principally in regard to thermal stresses, with a view toward aiding the designer in exploiting the unique characteristics of pyrolytic graphite. An account is also given of the reaction mechanisms involved in the oxidation of the subject material. The conflicting viewpoints and experimental evidence supporting either the reaction-controlled or the diffusion-controlled rate-of-oxidation theories in the high-temperature region are summarized. (M. C. Brockway)

Beryllium Metal and Alloys

Beryllium Wire

Workers at Franklin Institute[6] produced wires from vacuum-cast and extruded Pechiney SR beryllium, with a grain size of 30 to 40 μ after a heat-treatment at 800°C for 30 min and with a grain size of 5 to 10 μ after 2 hr at 600°C. The former could be bent cold around a $^3/_{16}$-in. radius 45°; the latter, 180°. In a tensile test, the latter specimen exhibited 9.7% elongation with no necking, 65,600-psi yield strength, and 96,500-psi ultimate strength.

A high-purity zone-refined single crystal of beryllium was drawn into fine wire at Brush Beryllium.[7,8] (Zone-refined crystals of both thermally and electrolytically reduced beryllium were converted to polycrystalline aggregates by a combination of deformation and heat-treatment.) Pronounced inflections or steps were found in the stress-strain diagrams from tensile tests of this wire. The inflections suggested that the strengthening sequence proceeds by unique stages that are separated by pauses for structural adjustments. The structural adjustments probably would be changes in the subgrain (or "cell") configuration, or recovery thereof, thus decreasing the effective grain size while restoring the capacity for subsequent work hardening. The wire fabricated from zone-refined beryllium had about the same as-drawn ductility at room temperature as did commercially pure wire.

Beryllium wire with a minimum diameter of less than 1.5 mils was fabricated by conventional warm-drawing techniques.[9] Typical tensile data for wires fabricated with various reductions are shown in Table II-1. The investigators suggest that the wide spread of values obtained on the smallest size may indicate a plateau in the strength, regardless of size.

Table II-1 STRENGTH OF WARM-DRAWN BERYLLIUM WIRE[9]

Wire diameter, in.	Reduction ratio, from last anneal	Strength		Elongation, %
		Tensile, 1000 psi	Yield, 1000 psi	
0.0036	295 : 1	182	143	2.3
0.00281	486 : 1	184	142	1.9
0.001578	1540 : 1	138 to 200	122 to 186	0.2 to 0.7

Fabrication of Beryllium

Passmore[10] made diffusion-bonded joints in beryllium with strengths equal to those of the base metal (about 40,000 psi for hot-pressed and 60,000 psi for extruded beryllium), with little plastic deformation and no observable grain growth across the interface. He suggests that this indicates that the bonding mechanism involves atomic contact across the interface, probably facilitated by the occurrence of some localized plastic deformation and surface diffusion.

Hanks and Keil[11] patented a process for brazing beryllium metal parts by coating the beryllium parts with a silver-aluminum (65 to 75 wt.% silver) alloy, using a 50-50 lithium fluoride – lithium chloride flux, and heating the

coated joint to a temperature of about 700°C for about 10 min.

Correlative fluid extrusions performed on sintered polycrystalline tungsten and beryllium and on a single crystal of beryllium[12] gave indications that crack-free fluid-to-fluid extrusions should be possible for all materials. Additional modes of deformation apparently are activated at higher pressure levels.

Mechanical Properties of Beryllium

Tensile tests on hot-pressed Brush and Pechiney beryllium were made by Lockheed[13] from room temperature to 400°C. Elongation of the Brush material rose gradually with increasing temperature, so that there does not appear to be a particular temperature that could be identified as a ductile-to-brittle transition temperature. On the other hand, the elongation for the Pechiney samples increased rapidly after reaching a temperature that varied among three samples from 200 to over 300°C. In two cases the elongation decreased at 400°C, and in the others it increased with a wide scatter. For the latter, it is believed that 400°C represents a ductile-to-brittle transition temperature. Strengths of the Brush beryllium were slightly higher than those of the Pechiney. Overall, the higher purity Pechiney material did not appear to offer any advantages over the Brush QMV material in the temperature regions investigated.

Rabenstein[14] reported on a program designed to evaluate the conventional and rapid-rate tensile properties and the short-time high-stress creep properties of beryllium sheet and block. Test temperatures ranged from room temperature to 1500°F, and the data are presented in graphical form suitable for design use. At temperatures above about 900°F, time-dependent strain becomes a factor, and the design must be based on creep strength.

Table II-2 shows preliminary creep data for Brush Beryllium's Instrument Grade beryllium, I-400.[15] A photograph of a turbine wheel for the auxiliary power unit of a missile forged (?) of I-400 beryllium appeared in *American Metal Market*.[16] Other applications under study are blades, buckets, and shafts for jet engines.

Morrow and Moore[17] found that optimum mechanical properties at 600°C of beryllium-iron alloys were obtained in alloys containing 0.15 wt.% iron. The tensile properties of overaged iron alloys which contained 0.04 to 0.40 wt.% iron were independent of aging and cooling rate from 600°C, so long as strain rates of 2.7×10^{-2}/min or over were employed. At slower strain rates the properties were affected by the cooling rate. No grain growth occurred during overaging, but generally grain growth occurred after solutionizing for more than 10 min at temperatures approximately 25°C above the solvus. Grain growth decreased the maximum ductility that could be obtained by subsequent overaging. In an alloy containing 0.4 wt.% iron, the elongation at fracture in 600°C tensile tests was raised from less than 1% to more than 40% by overaging, whereas the limit of proportionality fell from ~26,000 to ~20,000 psi. The ultimate tensile strength, however, was higher after overaging (36,000 vs. 28,000 psi), due to the change in fracture mode from brittle cleavage to a ductile, fibrous mode of failure. The aging process is completed in about 200 hr at 600°C or about 2 hr at 800°C.

Table II-2 CREEP DATA FOR INSTRUMENT GRADE BERYLLIUM,[15] I-400

Stress, 1000 psi	Time at 1000°F, hr	Minimum creep rate, %/hr
19.9	6.5	0.042
12.8	118.5	0.0011
15.2	4.8	0.0123
12	64.5	0.00092
10.52	105	

Physical Metallurgy of Beryllium

A room-temperature tensile test by Franklin Institute[18] on a single crystal of beryllium–5 wt.% copper alloy whose *c* axis was within 1° of being perpendicular to the tensile axis gave these results:

Critical resolved shear stress $(10\bar{1}0)$, psi	11,300
Elongation, %	36.8
Shear strain, %	72.5
Resolved shear stress at fracture $(10\bar{1}0)$, psi	24,000

The crystal deformed entirely by duplex glide and exhibited a knife-edge fracture. The increase in the critical resolved shear stress for prism glide resulting from the addition of 5 wt.% copper is much less marked than the corresponding increase for basal glide (from 9000 to 11,300 psi for prism glide; from 400 to 7800

psi for basal glide). These results emphasize the insensitivity of prism glide to impurity content.

Tensile tests on specimens cut from a 12-pass zone-refined crystal made from distilled beryllium indicated that additional zone refining did not significantly lower the critical resolved shear stress.[19] The low-temperature resistivity values of a sample from a 6-pass distilled crystal, compared with those from the 12-pass distilled crystal, showed that the overall purity was not improved significantly by the last 6 passes. It is possible that a buildup of copper and nickel, which concentrate at the starting end of the bar, was the cause of this behavior. A significant difference between the two crystals was found in glide capacity and fracture characteristics. The 6-pass crystal showed a glide strain of 91% before failure in the gauge length by brittle cleavage. The 12-pass crystal showed a glide strain of 150%, and fracture occurred prematurely outside the gauge length; the fracture was not simple cleavage. Greater resistance to basal cleavage also was noted for the 12-pass crystal.

Mechanical property studies of zone-refined single crystals of beryllium by Nuclear Metals investigators[20] showed that the critical resolved shear stress at room temperature for basal and prismatic slip decreased in a regular manner with decreasing impurity content. Absolute decreases in critical stress were approximately equal for both kinds of stress after equivalent purification. Large increases in basal-plane ductility at room temperature, accompanied by decreases in the rate of work hardening, were produced by purification. Extensive ductility was observed in a purified crystal at temperatures as low as $-196°C$, whereas at 425°C brittle failure by basal cleavage was eliminated. Purification also eliminated the brittle behavior following prismatic slip that is observed in commercial-purity crystals.

Slip in directions out of the basal plane in thin films of beryllium was reported to have been observed at room temperature by Walters et al.[21] They observed the movement of dislocations with a $\frac{1}{3}\langle\bar{1}\,1\,2\,3\rangle$ Burger's vector. It is thought that these movements may not take place in bulk material at room temperature if the critical resolved shear stress is high, in which case twinning will be the more favorable deformation mode. However, if increased purification lowers the stress required to cause deformation by the $\langle\bar{1}\,1\,2\,3\rangle$ slip mode, then slip instead of twinning may become favorable, and in improvement in the room-temperature ductility of beryllium might result.

Scott[22] described a number of electron-microscopy techniques for studying problems associated with the plastic behavior of beryllium. He suggests that observations made on the stacking-fault energy of beryllium may be particularly relevant to the question of matrix ductility (in a beryllium–0.15 wt.% iron alloy). Quenching the alloy from 920°C resulted in lower values of stacking-fault energy than quenching from 800°C, and the material quenched from 920°C was more brittle in the temperature range 300 to 600°C.

McKay and Hill[23] measured the lattice parameter of 99.9% pure beryllium. The values they found at 20.5°C are: $a_0 = 2.2858 \pm 0.0002$ and $c_0 = 0.0003$ A. The measured hardness of the distilled crystals ranged from 64 to 190 DPN, varying with the angle between the long diagonal of the indenter and the $\langle 1\,1\,\bar{2}\,0\rangle$ direction. Purification above approximately 99% did not significantly affect the hardness.

The Physicotechnical Institute, Ukranian Academy of Sciences, studied the solubility of titanium, zirconium, yttrium, and nickel in vacuum-distilled beryllium, vacuum-deposited beryllium foils, and binary beryllium alloys with 1.5 wt.% nickel or 1 wt.% titanium, zirconium, or yttrium, cast in a vacuum of 2×10^{-6} mm Hg. The specimens contained 0.013 to 0.015 wt.% metallic impurities (0.42 wt.% in the foils), 0.01 to 0.3 wt.% carbon, and 0.03 to 0.07 wt.% BeO. It was found that titanium, zirconium, and yttrium have no effect on the lattice parameters of beryllium, which indicates that none of these elements has any significant solubility. At room temperature, only nickel dissolves in beryllium to any appreciable extent. The solubility of nickel increases with increasing temperature, and at about 300°C it is approximately 1.5 wt.%. The temperature dependence of lattice parameters a and c and the ratio c/a, taken at 20 to 900°C in a vacuum of 3×10^{-5} mm Hg for beryllium and in air for beryllium and the beryllium-nickel alloy, shows a considerable effect from oxygen absorbed by beryllium at high temperatures.[24] The difference in value of the c parameter for pure beryllium determined in vacuum and in air reaches 0.5 kX at 900°C. Nickel appears to reduce the solubility limit for oxygen in beryllium. It is assumed that the

solubility limit for oxygen and nitrogen in distilled beryllium[25] is 2 to 3 wt.% at 900°C and is probably higher at 1200 to 1250°C. Rapid cooling from 900 to 20°C does not prevent decomposition of the solid solution of oxygen and nitrogen in beryllium. The combined effect of nickel and dissolved gases on the structure of beryllium is complex, but it appears that the solid solubility of nickel in beryllium is less in metal saturated with oxygen than in high-purity beryllium.[26]

From studies at Nuclear Metals of thinned beryllium alloy films by electron-microdiffraction techniques and by extended heat-treatments, it was determined that the solubility of iron is approximately 0.1 wt.% at 650°C, and that 700°C is close to the solid solubility limit for 0.25 wt.% iron in beryllium.[27]

Corrosion and Irradiation Properties of Beryllium

A fuel-element sheath made of beryllium containing a large amount of uranium impurity will be serviceable if it is coated with at least a 15-μ-thick deposit of beryllium containing less than 0.5 ppm uranium, according to a British patent.[28] The coating preferably is applied by a vacuum deposition process.

A limited number of tests were run at Oak Ridge[29] on the oxidation of beryllium in 200 mm Hg pressure of $C^{14}O_2$ at temperatures between 593 and 815°C for times up to 500 hr. The reaction products were BeO and Be_2C. The beryllium specimens increased in carbon content during exposure to the CO_2. The carbon remained associated with the surface reaction product and did not diffuse into the beryllium. Corrosion proceeded preferentially along the longitudinal axis of the material.

Antill and Tyzack[30] report that neither the rate of film growth nor the ultimate film thickness on beryllium oxidized in CO_2 at 300 psi for any one temperature and batch of material is influenced by water-vapor content of the CO_2. The film on vacuum-hot-pressed and double-extruded commercial-purity beryllium reaches approximately 1000 A on heating at 600°C for about 2000 min. Under the same conditions, the rate of film growth on a beryllium – 0.9 wt.% calcium tube is appreciably slower initially, but reaches the same film thickness as commercial-purity beryllium after about 1000 min, and increases to approximately 1400 A after 2000 min.

The results of corrosion tests of beryllium and beryllium-nickel alloys in water at 325°C, shown in Table II-3, indicate the superior performance of the beryllium-nickel alloys. The 1 and 5 wt.% nickel alloys resisted saturated steam at 325°C also, showing weight gains, at 14 days, of 20 and 17 mg/dm^2, respectively.[31]

Table II-3 CORROSION OF BERYLLIUM IN WATER[31] AT 325°C

Material	Test time	Weight gain, mg/cm^2
Be; arc melted, forged, rolled	12 hr	Completely oxidized
Be–0.5 Ni; arc melted, forged, rolled	14 days	15
Be–1.0 Ni; arc melted, forged, rolled	14 days	11
Be–5.0 Ni; arc melted, forged, rolled	14 days	25

Evidence was gathered in a British laboratory[32] which seems to controvert the hypothesis that catastrophic oxidation of beryllium results from preferential attack on carbide inclusions. Beryllium, in which the carbon had been isotopically labeled with C^{14}, was partially oxidized at 700°C. Analysis showed that the carbon was not oxidized preferentially but that its oxidation had proceeded to the same depth as that of the beryllium.

Raine and Robinson[33] found that beryllium alloys containing 0.08 wt.% or more of calcium showed outstanding resistance to corrosion at temperatures up to 700°C in both wet and dry CO_2 at a pressure of 21.5 atm. The corrosion resistance of the alloys decreases with a decrease in the CO_2 pressure and increases with an increase in the amount of calcium added. Variations in the moisture content of the CO_2 from 30 to 300 ppm by weight had no effect on the corrosion resistance of the alloys, whereas increasing the corrosion test temperature from 600 to 700°C had a negligible effect on the corrosion rate after the first 1500 hr. The addition of calcium in amounts up to 0.72 wt.% (and probably higher) had a negligible effect on high-temperature ductility.

A hypothesis was advanced by both the AEC and NASA which stated in effect that beryllium could not be used in space structures or equipment inhabited by humans because neutrons can be produced in beryllium by space radiations,

including solar-flare protons, Van Allen protons, and electrons from the new bomb-produced artificial radiation belt. If produced in sufficient quantity, these neutrons would be very dangerous. The space protons will produce neutrons in magnesium, aluminum, titanium, iron, or in any other material, as well as in beryllium. Only beryllium will produce neutrons from electrons in the artificial radiation belt. R. A. Glass of Lockheed[34] has calculated that the maximum neutron dose that could be received from beryllium by a man in close proximity to a beryllium wall at the heart of the artificial radiation belt is 0.2 mrem/hr. The weekly tolerance for a radiation worker is 100 mrem. Therefore, since 500 hr would be required to accumulate the weekly tolerance of 100 mrem, a man could stay indefinitely in the flux emanating from the beryllium. Dr. Glass had not completed work on the other half of the problem, but the results of a preliminary calculation showed that neutron production from space electrons will not be important.

Chute[35] found that the nucleation and growth of helium bubbles in irradiated beryllium metal depends to a large extent on the material history as well as on temperature and dose. Direct hot-extruded Pechiney powder annealed for 1 hr at 800°C, and air cooled before irradiation, showed significantly less bubble formation than any other type of beryllium for the same temperature and dose. This resulted in superior high-temperature mechanical properties. Addition of oxide by preoxidizing the powder before extrusion, which markedly improves the corrosion resistance of this material, did not appear to affect the bubble distribution.

The Canadians[36] noted the following observations after tensile-testing Brush warm-extruded beryllium that had been irradiated at Oak Ridge:

1. Brush S-200-B beryllium, warm extruded and heat-treated by slow cooling for 2 hr at 800°C:
   (*a*) Retains its excellent mechanical properties over the temperature range 200 to 500°C after prolonged heating at 430°C
   (*b*) Retains its excellent mechanical properties over the above temperature range after irradiation to $\leq 1.5 \times 10^{19}$ neutrons/cm^2 ($E > 1.0$ Mev) at temperatures of 200 to 300°C
   (*c*) Suffers a significant loss of ductility over the temperature range 200 to 500°C after irradiation to 10^{21} neutrons/cm^2 ($E > 1.0$ Mev) at 430°C
   (*d*) Appears to have no ductility at testing temperatures ≤200°C after irradiation to 10^{21} neutrons/cm^2 ($E > 1.0$ Mev)
2. Brush N-50-B beryllium, warm extruded and heat-treated by slow cooling after 2 hr at 800°C:
   (*a*) Retains its excellent mechanical properties over the temperature range 200 to 500°C after prolonged heating at 350°C
   (*b*) Retains much of its ductility over the above temperature range after irradiation up to 4×10^{19} neutrons/cm^2 ($E > 1.0$ Mev) at temperatures of 250 to 350°C

(W. Hodge)

Beryllium Oxide

Specimens of BeO irradiated by General Electric[37,38] at 700 to 900°C to dosages up to 1.8×10^{21} neutrons/cm^2 (≥1 Mev) showed volume expansions ranging from 0.75 to 2.0%. Expansions on the order of 1% were exhibited by specimens irradiated at 800 to 1000°C to 10^{21} neutrons/cm^2 (≥1 Mev). A general trend toward smaller expansion for smaller grain size was observed over the range of 5 to 100-μ grain sizes. Expansion did not appear to be influenced significantly by specimen density (which ranged from 2.6 to 2.9 g/cm^3), but strength retention was greatest in specimens of the lowest density. Specimens of 5-μ grain size increased as much as 40% in strength after the 900°C irradiation, whereas all specimens decreased in strength after the 800°C exposure.

An apparent saturation in volume expansion suggests that helium gas escapes in appreciable quantities in high-flux irradiation at 900 to 1000°C. Electron photomicrographs were obtained to assess helium-bubble formation in BeO specimens of 5-, 11-, and 15-μ grain size, all 2.9 g/cm^3 in density and irradiated to approximately 9×10^{20} neutrons/cm^2 (≥1 Mev) at 950°C. The photomicrographs suggested a progressive increase in the size and number of helium bubbles with increasing grain size. A similar trend was also noted from electron photomicrographs of 2.75 g/cm^3 specimens of 5-, 10-, and 20-μ grain size irradiated to approximately 1.6×10^{21} neutrons/cm^2 (≥1 Mev) at 900°C.

The use of a steady-state thermal-gradient method for growing single-crystal BeO in a molten flux of Li_2MoO_4-MoO_3 is under study at Atomics International.[39] Data have been reported on the influence of temperature, thermal-gradient, and flux-composition parameters on crystal growth characteristics. Growth rate for the best pyramidal crystals obtained under one set of conditions was approximately 1 mm/week. Growth rates observed for other habits, or poorer crystal quality, were frequently much higher. In spite of the use of the optimum growth conditions reported, crystal quality was not consistent. These continuing studies are investigating impurities in the flux system, which are instrumental in altering crystal habits and in suppressing the formation of interior voids.

The radiation-effects state-of-the-art report[3] for the period 1962-1963, issued by the Radiation Effects Information Center at Battelle, contains extensive summary data on the effects of neutron irradiation of BeO.

(M. C. Brockway)

Beryllium Compounds

The Australian AEC (Lucas Heights)[40] reports that reaction pressing is a suitable method for preparing $ThBe_{13}$, UBe_{13}, and $(U,Th)Be_{13}$. Good compacts were obtained at 1550°C, using 1 tsi of pressure, without maintaining maximum temperature for more than 1 min. Vaporization of beryllium and homogenization of the compact were found to be important and opposing variables encountered during reaction pressing.

Brush Beryllium,[41–44] in continuing studies of ternary-alloy additions to Zr_2Be_{17} and $ZrBe_{13}$, found that an addition of 0.35 wt.% aluminum to $ZrBe_{13}$ eliminates the rapid oxidation at intermediate (1100 to 1800°F) temperatures. To obtain this improvement for Zr_2Be_{17}, 1 to 3 wt.% aluminum is required.

As a follow-up of this work, the solubility of aluminum in these compounds was determined. The results are shown below.

Solvent compound	Solubility of aluminum, wt.% at indicated temperature			
	Room temp.	1500°F	2000°F	2500°F
$ZrBe_{13}$	Nil	Nil	0.05	0.23
Zr_2Be_{17}	1.13	1.14	1.06	1.65

Workers at Brush Beryllium believe that 0.25 to 0.30 wt.% aluminum in excess of the solubility limit is required for oxidation resistance.

Since the addition of aluminum causes a decrease in the mechanical properties, a search is under way for other additions that may improve the mechanical strength without impairing oxidation resistance. Titanium has been eliminated as a possible alloying element, since it reacts with $ZrBe_{13}$ to form $(Zr,Ti)_2Be_{17}$. Nickel is currently being studied in detail.

(R. W. Getz)

Solid Hydrides

Zirconium Hydride

The heat of combustion of ZrH_2 and of ZrD_2 has been determined at Argonne by oxygen-bomb calorimetry.[45] From these values the following heats of formation and free energies of formation were calculated.

	ZrH_2	ZrD_2
Heat of combustion, kcal/mole	−290.03 ± 0.24	−290.80 ± 0.18
$\Delta H°298$, kcal/mole	−38.90 ± 0.31	−40.22 ± 0.27
$\Delta F°298$, kcal/mole	−29.32 ± 0.31	−29.86 ± 0.27

The ΔH and the ΔF values for ZrH_2 given in the *Reactor Handbook* for the composition $ZrH_{1.8}$ are in good agreement with these determinations.

A British patent has recently been granted to General Dynamics,[46] for hydriding zirconium shapes without cracking. It describes the process for hydriding to H/Zr = 1.85 by slow addition of hydrogen so that the entire body undergoes one phase change before any part of it begins transformation to the next phase. This patent[47] apparently is the counterpart of one issued in the United States in December 1962.

Calcium Hydride

The dissociation pressure and the free energy of formation of calcium hydride as a function of temperature have been reported by Curtis and Chiotti.[48] From 600 to 789°C, they give:

$$\log P \text{ (atm)} = -9610/T + 7.346$$

In the range 780 to 900°C,

$$\log P \text{ (atm)} = -8890/T + 6.660$$

From 25 to 440°C,

$$\Delta F^\circ = -41{,}410 + 24.78\ T + 1.93\ T \log T$$

From 440 to 780°C,

$$\Delta F^\circ = -42{,}278 + 31.52\ T$$

Ternary Hydrides

The results of an extensive study of the hydriding of binary intermetallic compounds have been published by Denver Research Institute.[49] Experimental evidence indicates that the formation of hydrides that have predominantly metallic properties depends on two basic requirements: (1) that the hydrogen be occluded in tetrahedral interstices within the metal lattice, and (2) that the hydrogen be bound to the metal atoms predominantly by a mechanism of resonating covalent bonds. Two important conclusions are presented: (1) the potential existence of metallic hydrides which contain more than one kind of metal species and which exhibit a very high thermal stability at very high N_H levels is a definite possibility, and (2) the possibility of producing significant improvements in either the thermal stability or the N_H of presently used moderators such as zirconium or yttrium hydride by means of minor alloy additions seems very remote. Extensive tables of binary compounds examined, with their hydriding characteristics, are included. A computer program for the calculation of tetrahedral interstitials is also given.

(H. H. Krause)

References

1. P. R. Goggin, Some Effects of Electron Irradiation on the Young's Modulus of Graphite, British Report AERE-R-4364, June 1963.
2. W. N. Reynolds and P. A. Thrower, The Flux-Level Effect in Radiation Damage, British Report AERE-R-4316, April 1963.
3. Radiation Effects Information Center, Battelle Memorial Institute, Radiation-Effects State of the Art, REIC Report No. 28, June 30, 1963.
4. W. A. Gibeaut and H. R. Ogden, Summary of the Seventh Meeting of the Refractory Composites Working Group, Report DMIC-184, Battelle Memorial Institute, Defense Metals Information Center, May 30, 1963.
5. W. Bradshaw and J. R. Armstrong, Pyrolytic Graphite, Its High-Temperature Properties, Report ASD-TDR-63-195, Lockheed Missiles & Space Co., November 1962.
6. G. E. Spangler, M. Herman, E. J. Arndt, D. G. Hoover, V. V. Damiano, and C. H. Lee, Preparation and Evaluation of High Purity Beryllium, Quarterly Progress Report, April 15–July 14, 1963, Contract NOw 63-0500-d, Report AD-413120, The Franklin Institute.
7. A. G. Gross, Jr., and R. G. O'Rourke, Development of Fine Diameter High-Purity Wire from Zone-Refined Beryllium. Final Report. Technical Report No. 298-236, Contract NOw-62-0067-c, Report AD-297178, The Brush Beryllium Co., December 1962.
8. A. G. Gross, Jr., and R. G. O'Rourke, Development of High-Purity Wire from Zone-Refined Beryllium, Addendum to Final Report NOw 62-0067-c, The Brush Beryllium Co., January 1963.
9. E. A. Murphy, A. G. Gross, Jr., and R. G. O'Rourke, Fabrication of Ultrafine Beryllium Wire. Contract NOw-63-0137-c, Technical Report No. 314-240. Bimonthly Report No. 2, March 25, 1963–May 24, 1963, Report NP-12964, The Brush Beryllium Co., May 24, 1963.
10. E. M. Passmore, Solid State Welding Beryllium, *Welding J. (N. Y.)*, 42: 186S-189S, April 1963.
11. G. S. Hanks and R. W. Keil, Method of Brazing Beryllium, U. S. Patent 3,090,117, May 17, 1963.
12. Pressure Technology Corporation of America, A Study To Determine the Deformation Characteristics of Beryllium and Tungsten Under Conditions of High Hydrostatic Pressure, Interim Report No. 2 on Navy Contract N600 19 59430; AD 403144, April 1963.
13. M. I. Jacobson and E. E. Underwood, Fifth Quarterly Progress Report on Metallurgical Factors Affecting the Ductile-Brittle Transition in Beryllium, Report on USAF Contract AF 33(616)-7065, Lockheed Missiles & Space Co., Mar. 31, 1963.
14. A. S. Rabenstein, Tensile and Creep Properties of Beryllium Sheet and Block from Room Temperature to 1500 F, Report AD 299418; PR 281-3Q-2 on Air Force Contract AF 33(657)-8706, Marquardt Corp., Mar. 1, 1963.
15. New Beryllium is One-Third Stronger, *Mater. Design Eng.*, 58(2): 94 (August 1963).
16. Beryllium Turbine Wheel, *American Metal Market (New York)*, p.12 (Sept. 25, 1963).
17. F. Morrow and A. Moore, The Effect of Time and Temperature of Heat Treatment and Strain Rate on the Tensile Properties at 600°C of Beryllium-Iron Alloys Containing 0.04 to 0.40 Wt.% Iron, British Report AWRE-O-13/63, April 1963.
18. G. E. Spangler, M. Herman, E. J. Arndt, D. B. Hoover, V. V. Damiano, and C. H. Lee, Preparation and Evaluation of High Purity Beryllium, Quarterly Progress Report, January 15, 1963–April 14, 1963, Report Q-B2089-1, Contract NOw

62-0536-d, Report AD-406688, The Franklin Institute.

19. Nuclear Metals, Inc., Fundamental and Applied Research and Development in Metallurgy, Progress Report to United States Atomic Energy Commission, March 1963, USAEC Report NMI-2116, May 28, 1963.
20. D. F. Kaufman, E. D. Levine, J. J. Pickett, and L. R. Aronin, Fundamentals of Single Crystal Deformation in Zone-Refined Beryllium, Final Report, July 1, 1961–June 30, 1962, USAEC Report NMI-1256, Nuclear Metals, Inc., May 13, 1963.
21. G. P. Walters, C. M. Van Der Walt, and M. J. Makin, Burger's Vectors in Beryllium and Their Effect on Ductility, British Report AERE-R-4287, March 1963.
22. V. D. Scott, Electron Microscope Studies of Beryllium, British Report AWRE-O-59/62, October 1962.
23. K. J. H. McKay and N. A. Hill, Lattice Parameter and Hardness Measurements of High-Purity Beryllium (in English), *J. Nucl. Mater.*, 8: 263-264 (March–April 1963).
24. V. M. Amonenko, V. E. Ivanov, G. F. Tikhinskii, and V. A. Finkel', Solubility of Admixtures in Beryllium (in Russian), *Fiz. Metal. i Metalloved.*, 14: 128-130 (July 1962).
25. V. M. Amonenko, V. E. Ivanov, G. F. Tikhinskii, and V. A. Finkel', X-Ray Study of Solubility of Impurities in Beryllium (in Russian), *Fiz. Metal. i Metalloved.*, 14: 852-856 (December 1962).
26. The Beryllium Corp., *Beryllium Tech-Topics*, 9: 1, 2, and 4 (September 1963).
27. Nuclear Metals, Inc., Beryllium Research and Development Program, Quarterly Progress Report, October 1, 1962–December 31, 1962, USAEC Report NMI-9528, May 8, 1963.
28. J. A. Dukes, *Improvements in or Relating to Nuclear Reactor Fuel Elements*, British Patent No. 923,675, Apr. 18, 1963.
29. H. E. McCoy, Jr., Observations on the Oxidation of Beryllium in CO_2 by Use of $C^{14}O_2$ and Autoradiographic Techniques, USAEC Report ORNL-TM-622, Oak Ridge National Laboratory, Aug. 22, 1962.
30. P. C. S. Hayfield, Imperial Metals Industries, Ltd. (under Contract to UKAEA). (Unpublished)
31. Metallurgy Division Progress Report, September 1, 1961–April 30, 1962, British Report AERE-PR/M-2, 1962.
32. Metallurgy Division Progress Report, May 1, 1962–October 31, 1962, British Report AERE-PR/M-3, 1962.
33. T. Raine and J. A. Robinson, The Development and Properties of Beryllium-Calcium Alloys in Use in High Pressure Carbon Dioxide (in English), *J. Nucl. Mater.*, 7: 263-278 (December 1962).
34. R. A. Glass, Beryllium Nuclear Problem, private communication from M. A. Steinberg, Aug. 14, 1963.
35. J. H. Chute, Electron Microscope Studies of Irradiated Beryllium Metal, Australian Report AAEC/E-108, May 1963.
36. Atomic Energy of Canada, Ltd., 1963. (Unpublished)
37. General Electric Company, Advanced Technology Services, High-Temperature Materials Program, Progress Report No. 26, Part A, USAEC Report GEMP-26A, Aug. 16, 1963.
38. General Electric Company, Advanced Technology Services, High-Temperature Materials Program, Progress Report No. 24, Part A, USAEC Report GEMP-24A, June 28, 1963.
39. S. B. Austerman, Growth of BeO Single Crystals. III. Steady-State Thermal Gradient Method, USAEC Report NAA-SR-8056, Atomics International, Aug. 15, 1963.
40. G. L. Hanna and D. N. Turner, Preparation of the Beryllides of Uranium and Thorium, Australian Report AAEC-E-102, January 1963.
41. R. M. Paine, J. Booker, A. J. Stonehouse, and W. W. Beaver, Development of Intermetallic Compounds for Very High Temperature Applications, Summary Technical Report, January 1, 1962 Through August 31, 1962, USAEC Report BBC-116, The Brush Beryllium Co., Nov. 30, 1962.
42. R. M. Paine, A. J. Stonehouse, and W. W. Beaver, Research on Modified Beryllides as High-Temperature Nuclear Materials, Quarterly Progress Report, September 1, 1962 Through November 30, 1962, USAEC Report BBC-117, The Brush Beryllium Co., Dec. 31, 1962.
43. R. M. Paine, A. J. Stonehouse, and W. W. Beaver, Research on Modified Beryllides as High-Temperature Nuclear Materials, Quarterly Progress Report, December 1, 1962 Through February 28, 1963, USAEC Report BBC-118, The Brush Beryllium Co., Mar. 31, 1963.
44. R. M. Paine, A. J. Stonehouse, and W. W. Beaver, Research on Modified Beryllides as High-Temperature Nuclear Materials, Quarterly Progress Report, March 1, 1963 Through May 31, 1963, USAEC Report BBC-119, The Brush Beryllium Co., June 30, 1963.
45. D. R. Fredickson, R. L. Nuttall, H. E. Flotow, and W. N. Hubbard, The Enthalpies of Formation of Zirconium Hydride and Zirconium Deuteride, *J. Phys. Chem.*, 67: 1506-1509 (July 1963).
46. *Hydriding Zirconium Shapes Without Cracking*, British Patent No. 925,916, May 15, 1963.
47. Production of Zirconium Hydride, U. S. Patent No. 3,070,526, Dec. 25, 1962.
48. R. W. Curtis and P. Chiotti, Thermodynamic Properties of Calcium Hydride, *J. Phys. Chem.*, 67: 1061 (May 1963).
49. R. L. Beck, Investigation of Hydriding Characteristics of Intermetallic Compounds, Summary Report, November 1, 1960 to September 31, 1962, USAEC Report DRI-2059, Denver Research Institute, Oct. 15, 1962.

Section

III

Reactor Materials

Nuclear Poisons

Metallic Poison Materials

Specimens of 80 wt.% silver–15 wt.% indium–5 wt.% cadmium alloy plated with 1 mil of nickel or 1 mil of copper plus nickel have been examined after irradiation.[1] The specimens were irradiated to an integrated unperturbed thermal flux of 2.3×10^{21} neutrons/cm^2 at temperatures of 325 to 550°C. The mechanical properties of these specimens are given in Table III-1. The increase in elongation and reduction of area for the extruded powder alloy as a result of irradiation can be explained by the recrystallization that occurs at the irradiation temperatures.

The U. S. Bureau of Mines[2] has found that purification of hafnium by electron-beam melting at moderate energy inputs and low pressures shows considerable promise. Hafnium exhibits no brittle type fracture in the temperature range of –300 to +800°F, according to the Lawrence Radiation Laboratory.[3] (M. Kangilaski)

Nonmetallic Poison Materials

Boron compounds in powder form and wrought form were studied by General Electric (Vallecitos Atomic Laboratory),[4] in efforts to relate their crystal structures to helium retention and structural changes. It was found that the close-packed crystal structures retained more helium than did the more open crystal types. It was also found that mechanical restraint was an important parameter in limiting both swelling and/or fragmentation. The amount of swelling observed was found to be directly proportional to the volume of helium released and inversely proportional to the amounts of closed porosity and mechanical restraint.

Crystallographic changes in several irradiated metal boride systems were studied[5] by X-ray diffraction techniques. It was found that radiation damage can be related to structure. The relation does not depend primarily on the crystal system but rather on the structure bond strength. The metal diborides, with their tightly bonded hexagonal structures, were most resistant to radiation damage. The hexaborides, on the other hand, have a loosely bonded cubic structure and were extensively damaged by irradiation. The tetraborides were intermediate in bond strengths and also were intermediate in structure damage. A very limited study was made of irradiated dodecaborides. This face-centered cubic structure has an intermediate bond length between metal and boron atoms, but a long bond length between metal atoms. The radiation damage to this structure was quite extensive.

The use of mixed oxides for neutron-absorbing materials at ultrahigh temperatures has been studied by the Germans.[6] Among the more promising of these materials are Cd_2TaO_7 and $In_2Ta_2O_8$, which are relatively inexpensive and absorb neutrons by a simple (n,γ) reaction.

Efforts are under way at Combustion Engineering[7] to incorporate a burnable poison (B_4C) into high-density UO_2 fuel elements by means of powder-compaction techniques. Powder blending and loading techniques were studied to determine their effects on the uniformity of boron distribution in the UO_2 fuel matrix. Tubular elements were loaded incrementally with a UO_2–0.05 wt.% B_4C powder mixture and compacted to relative densities of up to 88%. The variation in boron content along the length of the elements was within ±20% of the mean value for all the elements loaded.

In a Euratom program[8] to develop shaped, burnable poisons, rods of gadolinia, alumina, and mechanical mixtures of these were formed

Table III-1 ROOM-TEMPERATURE TENSILE AND HARDNESS PROPERTIES OF IRRADIATED 80 Ag–15 In–5 Cd ALLOY SPECIMENS[1]

Specimen designation	Fabrication history	Irradiation history	Yield strength (0.2% offset)*		Ultimate tensile strength*		Elongation, %	Reduction in area, %	Hardness,† DPH
			1000 psi	kg/cm²	1000 psi	kg/cm²			
CR-6-A(A-5)	Extruded cast alloy, annealed 1 hr at 550°C	Unirradiated	19.5	1,370	41.6	2,920	45	45	
CR-6-B(B-5)	‡	Unirradiated	17.1	1,200	38.5	2,710	56	51	
CR-6-D(D-5)	‡	Unirradiated	16.2	1,140	42.7	3,000	55	56	55 to 61
CR-6-D(D-6)	‡	Unirradiated	19.9	1,400	46.1	3,240	56	50	55 to 61
CR-6-A(A-5)	‡	2.3×10^{21} thermal neutrons/cm² unperturbed at 325 to 550°C	16.2	1,140	40.9	2,880	62	53	45 to 52
CR-6-A(A-6)	‡	§	17.2	1,200	40.2	2,830	58	56	45 to 52
CR-6-B(B-5)	‡	§	13.6	960	41.1	2,890	66	57	36 to 39
CR-6-B(B-6)	‡	§	18.7	1,310	42.8	3,010	58	57	36 to 39
CR-6-C(C-5)	‡	§	21.4	1,500	42.5	2,990	62	55	
CR-6-D(D-6)	‡	§	17.4	1,220	42.9	3,020	59	54	
PCR-4-E(A-5)	Extruded powder alloy, annealed 2 hr at 600°C	Unirradiated	27.0	1,900	38.8	2,730	11	9	
PCR-4-H(D-6)	¶	Unirradiated	32.5	2,290	48.0	3,380	13	9	
PCR-4-E(E-5)	¶	2.3×10^{21} thermal neutrons/cm² unperturbed at 325 to 550°C	30.4	2,140	45.2	3,180	17	24	
PCR-4-E(E-6)	¶	§	34.5	2,430	46.2	3,250	19	30	
PCR-4-H(H-5)	¶	§	32.0	2,250	41.5	2,920	23	22	
PCR-4-H(H-6)	¶	§	32.2	2,270	43.7	3,070	20	14	

*The specimens were tested at a strain rate of 0.05 min^{-1}.
†A 1-kg load was applied.
‡Fabrication history: extruded cast alloy, annealed 1 hr at 550°C.
§Irradiation history: 2.3×10^{21} thermal neutrons/cm² unperturbed at 325 to 550°C.
¶Fabrication history: extruded powder alloy, annealed 2 hr at 600°C

and sintered at temperatures to 2700°F in air for 2 to 6 hr. These specimens will be used for compatibility studies and to develop fabrication techniques for these oxides to produce the desired shapes.

A recent annual report[1] issued by Argonne describes their studies with nonmetallic poison materials. The poison material for the control rods for the BORAX-V reactor is 50 wt.% B_4C dispersion in aluminum which is mechanically clad with type 304L stainless steel. A complete description of the fabrication and assembly of these rods is given.

Research on poison glasses for control-rod applications has been stimulated for two reasons: (1) to improve the fabricability of B_4C and (2) to provide a solvent for the rare-earth oxides to increase their stability and hydration resistance. It has been possible to vibratorily pack a glass-B_4C mixture and sinter the mixture to form a hard mass having 70 to 74% of theoretical density when using a mixture of 70 wt.% 60-mesh particles and 30 wt.% 325-mesh particles. Fabrication studies using several glasses were made to determine the properties of the resulting compacts. The solubility of Eu_2O_3, Gd_2O_3, Dy_2O_3, and Gd_2O_3-Sm_2O_3 mixtures in several glasses at 1500°C was found to be a maximum of 30 wt.% when using a soda-potassia-silica glass. Glasses containing rare-earth oxides were found to be very viscous and could not be poured at 1600°C. Hot pressing at 750°C yielded high-density samples, as did cold pressing and sintering at 900°C in air.

Phase-diagram studies were made for the urania-neodymia and urania-thoria systems. Information about crystal structure and physical properties of mixtures of these oxides is also reported.[6]

Specimens containing 30 wt.% Dy_2O_3 dispersed in cobalt have been compacted and then sintered at 1300°C for irradiation testing. No reaction between Dy_2O_3 and the cobalt was detected. Thermal cycling of sintered samples 125 times between 300 and 700°C produced only very slight dimensional changes and no reaction between the constituents.

The results of corrosion studies of stabilized Dy_2O_3, cobalt, and cobalt-Dy_2O_3 dispersions were reported[1] for several types of water corrosion environments at 250°C. (E. G. Smith)

References

1. Argonne National Laboratory, Metallurgy Division Annual Report for 1962, USAEC Report ANL-6677.
2. W. E. Anable and R. A. Beall, Electron-Beam Purification of Hafnium, Report USBM-U-929, Bureau of Mines, November 1962.
3. University of California, Lawrence Radiation Laboratory, Pluto Quarterly Report No. 16, USAEC Report UCRL-7442, July 19, 1963. (Classified)
4. E. W. Hoyt and D. L. Zimmerman, Radiation Effects in Borides. Part I. Helium Release and Swelling in Irradiated Borides, USAEC Report GEAP-3743 (Part I), General Electric Company, Vallecitos Atomic Laboratory, Feb. 13, 1962.
5. W. V. Cummings and W. I. Clark, Radiation Effects in Borides. Part III. Crystallographic Changes in Irradiated Borides, USAEC Report GEAP-3743 (Part III), General Electric Company, Vallecitos Atomic Laboratory, May 31, 1963.
6. F. Haessuer, G. Petzow, and E. Preisler, Control Materials for High Temperature Reactor Applications, Especially Mixtures of Oxides, *Kerntechnik*, 5: 153-156 (April 1963).
7. G. Zuronsky, R. C. Brayer, and W. P. Chernock, Summary Report — Burnable Poison Additions to UO_2, USAEC Report CEND-181, Combustion Engineering, Inc., November 1963.
8. Allis-Chalmers Mfg. Co., Shaped Burnable Poison Development Program Under the Euratom Program, Quarterly Progress Report, December 1, 1962 – February 28, 1963, USAEC-Euratom Report EURAEC-628 (ACNP-63012), Apr. 10, 1963.

Section

IV

Reactor Materials

Cladding and Structural Materials

Corrosion

Zirconium Corrosion

Zirconium ternary alloys were exposed for up to 292 days in 680°F water and 750 and 900°F steam by Illinois Tech Research Institute workers.[1] Zirconium–0.75 wt.% chromium–0.4 wt.% tellurium and zirconium–0.5 wt.% niobium–0.4 wt.% tellurium were found to have corrosion resistance, strength, and hydrogen pickup superior to those of Zircaloy-2 in 680°F water. Zirconium–0.5 wt.% niobium–0.25 wt.% tellurium exhibited lower corrosion rates and less hydrogen pickup in 750°F steam than did Zircaloy-2. The zirconium–0.5 wt.% niobium–0.25 wt.% molybdenum and zirconium–1 wt.% vanadium–0.25 wt.% molybdenum alloys looked promising in 900°F steam, exhibiting black adherent oxides but relatively high weight gain after 125 days of exposure.

Russian scientists[2] have found that hafnium alloys containing up to 30 wt.% zirconium additions possess high corrosion resistance in water at 350°C. Extended exposure to 400°C steam did not cause a marked deterioration of the physical properties of a hafnium–3 wt.% zirconium alloy.

Hanford[3] reports a marked increase in the corrosion of Zircaloy-2 under neutron flux of 2 to 4 × 10^{13} neutrons/(cm^2)(sec)(> 1 Mev) in loop tests conducted in 540°F, *p*H 9 to 10 (LiOH) water at the Engineering Test Reactor. Weight gains after 34 days of exposure to 4 × 10^{13} neutrons/(cm^2)(sec) were about 60 mg/cm^2, or an order of magnitude higher than for unirradiated specimens. Hydrogen pickup was slightly higher in irradiated specimens, but the percentage of theoretical hydrogen (from corrosion) was somewhat less in the irradiated specimens. Oak Ridge[4] also reports an increase in the corrosion rate of Zircaloy-2 with increasing radiation during in-pile loop tests in UO_2SO_4 solution at 280°C. Penetration rates at solution velocities of 10 to 40 ft/sec ranged from about 2.3 mils/year at a power density of 2.5 watts/ml to about 4.5 mils/year at 6 watts/ml.

Bettis[5] has found instances of hydriding of Zircaloy cladding at the inner hot surface at intentional defects in irradiated fuel elements, as well as at the cooler surface where hydriding normally occurs. Of all mechanisms studied, only the radiolytic decomposition of water was found to supply a sufficient hydrogen flux to cause hydriding of the hot surface. It was shown that H_2O_2, which is also produced by radiolysis, can be reduced by the fuel, thus accounting for the consumption of all the radiolytic decomposition products. However, not all defected fuel-element specimens exhibited severe hydriding, even for conditions that favored high radiolysis rates.

Oak Ridge[6] has studied deuterium pickup by zirconium alloys during exposure to thorium and thorium-uranium oxide slurries in toroid tests at 200 to 330°C. Deuterium pickup was kept to a minimum as long as oxygen overpressures were maintained above the slurries. Increasing the deuterium overpressure (in the absence of oxygen) resulted in increased deuterium uptake in the alloys. The abrasive action of the slurries was believed to be responsible for removal of protective oxide films, thereby permitting rapid hydriding (deuterium) of the zirconium alloys.

Thin films of zirconium have been oxidized inside an electron microscope using a calibrated heating stage at the Berkeley Nuclear Laboratory (England).[7] Films heated at 450°C oxidized uniformly, although the rates varied from one grain to another. Platelike precipitates extended into the metal at the oxide-metal

interface in $\langle 11\bar{2}0 \rangle$ directions parallel to $\{10\bar{1}0\}$ planes. The precipitates did not appear to be one of the three known forms of zirconia but were believed to be a lower oxide of the type observed in titanium.

Vallecitos workers[8] measured the hydrogen overvoltage in $1M$ H_2SO_4 for zirconium, Zr_2Ni, Zr_2Cu, ZrV_2, and zirconium–90 wt.% niobium. They also measured electrochemical potentials as functions of time for galvanic cells of zirconium with Zr_2Ni, Zr_2Cu, ZrV_2, $ZrFe_2$, $ZrCr_2$, or zirconium–90 wt.% niobium. Results showed that metals with a low hydrogen overvoltage are more susceptible to hydrogen pickup than metals with a high overvoltage; and alloying with low-overvoltage metals will promote high pickup fractions if the intermetallics that are formed are sites of hydrogen discharge. Intermetallics were not always found to be discharge sites, and during early stages of corrosion they varied between being oxidation and discharge sites. It was believed that if hydrogen-pickup fractions approached 100%, the bulk oxide properties, rather than intermetallic islands, would control pickup, since every hydrogen atom must be absorbed near its site of production.

(W. E. Berry)

Aluminum Corrosion

Canadian scientists[9] have conducted polarization studies on aluminum alloys corroding in pure water at 200 and 300°C. The oxide film on aluminum was found to have a much greater electronic resistance in the anodic direction and smaller (or about the same) resistance in the cathodic direction than special quaternary alloys containing 0.2 wt.% silicon, 0.5 wt.% iron, and 0.5 or 2.0 wt.% nickel. The alloying elements are believed to decrease the energy required for promoting electrons from the valence band to the conducting band of the oxide.

(W. E. Berry)

Stainless-Steel Corrosion

Oxidation studies conducted by Oak Ridge[10] at 1050°F in impure helium (10 ppm water plus other minor impurities) have revealed increasing oxidation rates with increasing thickness of nitride layers on type 304 stainless steel. Rates for a 0.0067-in.-thick nitride case were 4.39×10^{-4} mg/(cm^2)(hr), or about 14 times those for specimens with no nitride layer.

Hanford[11] has investigated the effect of sodium hydroxide–potassium permanganate decontaminating solutions on the stress-corrosion cracking of stainless steels. Cracks were detected in type 316 stainless-steel tubing connectors and in flared type 304 stainless-steel tubing after immersion in the decontaminating solution, followed by drying and exposure to steam at 275°C. A mild inhibiting effect was observed with increasing $KMnO_4$ (0.1 to 3.0 wt.%) in an aqueous 18% NaOH solution. Cracks occurred in less than one day at less than 0.5 wt.% $KMnO_4$ but were not evident until after several days at the 2 to 3 wt.% $KMnO_4$ levels.

Experiments conducted at Hanford[12] in high-purity deionized water at 300°C and 2000 psi have revealed concentrations of up to 200 ppm chloride and 1800 ppm fluoride in dissolved and redeposited aluminum corrosion product. The product was essentially aluminum monohydrate. Tests are under way with stressed stainless steel to determine whether this surface concentration of chloride will induce stress-corrosion cracking.

Vallecitos[13] has summarized the current status of development of cladding for nuclear superheat fuels, with particular emphasis on the stress-corrosion cracking of stainless-steel cladding on irradiated fuel elements. Intergranular cracking was found in sensitized zones, and transgranular cracking was found in nonsensitized areas. Cracking was attributed to high residual and operating stresses in conjunction with high oxygen levels and the concentration of chlorides carried over in the wet steam from the boiling-water reactor. Laboratory and in-pile tests have indicated that Inconel, Incoloy, and Inconel X are not subject to localized attack in the Vallecitos superheater environment.

Stress-corrosion cracking and intergranular pitting have been detected during hydrotesting of the N-Reactor stainless-steel heat exchangers at Hanford.[14] Examination of untested heat exchangers has revealed very little contamination, except for traces of vapor-phase inhibitor (VPI) and a very light black smut. Preliminary analyses of these products have given no indication of the cause of cracking. Accelerated corrosion tests are being conducted to determine whether the VPI is responsible for the cracking. (W. E. Berry)

Corrosion of Refractory Metals

Department of Defense-oriented efforts on protection of refractory metals from oxidation have been reviewed in a recent Defense Metals Information Center publication.[15]

The thermodynamic stability of oxygen in solution in niobium at 1832°F was determined by Russian investigators[16] by analyzing niobium-oxygen solutions in equilibrium with various oxides at this temperature. Their results are tabulated below:

Approximate dissolved oxygen content, wt.%	Free energy of solution at 1832°F, kcal/mole oxygen
0.01 to 0.02	242
0.2	224
0.5 (terminal solubility)	167.7

Thus niobium containing less than about 100 ppm oxygen would be contaminated by even the most stable oxides at 1832°F.

Studies recently completed at Battelle[17] showed the niobium–21 at.% titanium–12 at.% vanadium–9 at.% chromium alloy in the as-rolled condition to undergo only 2.27 mg/cm^2 weight gain when exposed for 189 days to 1500-psi steam at 1000°F, with no evidence of breakaway. This approaches the oxidation resistance of type 302 stainless steel (estimated as 1.15 mg/cm^2 under the same conditions) quite closely and provides an attractive material for potential use in a nuclear superheater. (Oxidation resistance of recrystallized alloys in this program was consistently and considerably inferior to that of as-wrought alloys.)

In continuing research at Denver Research Institute, the effects of silicon or tin additions on the oxidation resistance of titanium-containing $NbAl_3$, a potentially attractive coating material for niobium, are being investigated. Earlier studies[18] showed that, although substitution of 15 wt.% titanium for niobium in the $NbAl_3$ compound overcame the propensity for pest failure at 1400°F, the oxidation resistance of $NbAl_3$ at 2500°F was impaired by the titanium addition. Most recent results[19] suggest that a 20 wt.% tin addition to (Nb-15Ti)Al_3 provides superior oxidation resistance at all temperatures from 1400 to 2500°F, gaining a maximum of only 4 mg/cm^2 in 24 hr.

A recent report from Lawrence Radiation Laboratory[20] dealt with tests of intentionally defected coatings on F-48 niobium alloy at temperatures at or above those required for ignition of the bare substrate in a dynamic oxidizing environment. A ceramic coating (not otherwise specified) that contained a $^1/_{16}$-in.-diameter flaw inhibited ignition for 51 and 59 min in two tests. After 30 min test time, the flaw was enlarged to $^1/_8$ in.; after 45 min, its size was $^3/_{16}$ in., and the specimen showed "noticeable oxide heaving from the underside of the coating." A "packed-deposited" coating (not otherwise specified, but likely of the silicide type), containing $^1/_8$- by 1.8-in. flaws, sustained 60 min at 2650°F (50°F above the ignition temperature of uncoated F-48) without ignition. After this test, substrate oxidation had created $^1/_4$-in.-deep cavities at the original flaw sites.

(E. S. Bartlett)

Corrosion of Nickel-Base Alloys

Nuclear Superheat. Metallographic examination at Vallecitos[21,22] of superheat fuel-element claddings of Inconel X and type 347 stainless steel revealed no localized attack or leak after 29 days and 18 power cycles to 15 Mw in the VBWR at 840°F. However, a leak was suspected at operating temperature.

Out-of-pile general and stress-corrosion experiments showed Inconel, Incoloy, and Hastelloy X to be resistant under conditions where type 304 stainless steel failed by stress-corrosion cracking.

Deposits of corrosion products on various superheat fuel-element samples were examined by X-ray diffraction. This method was found to be too insensitive to detect traces of chlorides which were known to be present.

Harwell[23] finds nickel-base braze alloys superior to copper-base alloys for steam service. A maximum of 5 mils of attack was observed after 2000 hr in 650°C, 800-psi steam.

Argonne[24] has studied the electrical resistance of the corrosion film on TD nickel (2 wt.% ThO_2) to establish reasons for the greater protection in 650°C oxygenated steam compared to the film on wrought nickel. The thoria in the film on the TD nickel does not modify the electrical resistance of the film. The films on both TD and wrought nickel are semiconductors at the high temperature and insulators at room temperature.

Oxidation. The oxidation characteristics of TD nickel are being investigated at Hanford.[11,21]

At 900°C, the weight gain per unit area (W) for the first 150 min (t) follows the relation $W = K \ln (at + 1)$, where K and a are rate-law constants. After 200 min, the same linear rate is found for partial oxygen pressures of .5 to 700 mm. For comparison, INCO-270 (99.97 wt.% nickel–0.02 wt.% carbon-trace chromium) was studied at 700 to 1000°C. At 700°C in 25 mm oxygen pressure, TD nickel and INCO-270 behaved similarly, each showing a weight gain after 1400 min of 0.8 mg/cm^2; at 1000°C, TD nickel gained 2.0 and INCO-270 gained 6.5 mg/cm^2.

In a similar study at Pratt & Whitney,[26] the oxidation rate equation for TD nickel between 900 and 1400°C was determined as $W = K_p t^{0.55}$, where K_p is the parabolic rate constant and the other terms are defined as above. The film is composed of two layers, a dense outer oxide and a porous inner oxide. ThO_2 is absent in the outer layer. Less internal oxidation is found with TD nickel than with pure nickel.

At 1000°C, under a partial pressure of oxygen of 25 mm, Hanford workers demonstrated that Haynes 25 alloy oxidizes much slower than Hastelloy X. In air, the surface condition of the specimen affects its corrosion behavior, and, although the maximum observed rates are similar, Hastelloy X shows more consistent results than does Haynes 25 alloy.

In the Experimental Beryllium Oxide Reactor (EBOR),[27] simulated plateout of I^{131} from the coolant stream was studied. Results indicate that the iodine plateout rate was roughly proportional to absolute temperature and insensitive to substrate, regardless of whether it was type 304 stainless steel, SA-387B low-alloy steel, or type 1030 steel. Samples were placed in a quartz tube filled with helium containing 100 ppm oxygen, 370 ppm nitrogen, and 4 to 6 ppm H_2O. After controlled cooling from 750 to 235°C the amount of iodine deposited was found to range from 3.3 to 4.4 μg/cm^2 for the three materials.

In CO_2 + 10 vol.% CO at 650°C and 100 psi for 3500 hr, no leaks developed on brazed joints of nickel-base braze alloys tested at Harwell.[23]

(F. W. Fink)

Corrosion by Liquid Metals

In support of the development of 300- and 1000-kw boiling and condensing heat-transfer test loops, static-capsule, refluxing-capsule, and thermal-convection-loop experiments were conducted by General Electric[28] to examine the compatibility of L-605 alloy with 1800°F potassium. All three types of tests indicated mild surface corrosion after exposures of up to about 1100 hr. A noticeable condition was the migration of interstitials from the L-605; however, this seemed to produce no significant change in its mechanical strength. In some experiments, a niobium or niobium–1 wt.% zirconium liner was inserted in the L-605 tubing as a getter. The presence of the dissimilar metal had little or no influence on the overall compatibility behavior.

In another phase of this research, molybdenum was joined to L-605 by a 2150°F vacuum-brazing operation using H-33 (J-8400) brazing alloy (21 wt.% chromium–21 wt.% nickel–8 wt.% silicon–3.5 wt.% tungsten–0.4 wt.% carbon–0.8 wt.% boron, balance cobalt). Potassium (1850°F) exposures of test joints indicated excellent 100-hr resistance to attack. Some damage was accumulated after 250 hr, but helium tightness was still retained. After 1000 hr, the damage was severe and the ability to retain helium was lost. Thermal cycling during the longer time exposures appeared to contribute importantly to the damage. A behavior generally similar to that of the molybdenum–L-605 joints was found for specimens of molybdenum–0.5 wt.% titanium brazed to L-605 alloy.

The usefulness of Stellites Nos. 6 and 12 for 1850°F potassium-exposed valve-seat facings was also investigated. Although corrosion at this temperature level was not severe, considerable self-welding occurred. This self-welding effect was much less pronounced at 1650°F and virtually nonexistent at 1500°F.

Niobium alloys are being tested by Argonne[29,30] in flowing sodium for suitability as high-strength fuel claddings for fast reactors. The experimental materials contain alloying additions of either 1 or 5 wt.% zirconium, 5 wt.% molybdenum, 2.37 wt.% chromium, or 39 wt.% vanadium–1 wt.% titanium. Experiments of approximately 330-hr duration in which these materials were exposed to 650°C flowing sodium containing 140 ppm oxygen demonstrated that most of the alloys gettered oxygen from the sodium and were severely embrittled. Large weight losses (11 to 62 mg/cm^2) and thickness changes (+81 to −137 μ) were measured. The importance of the oxygen content of the sodium is evident from the con-

trast between these results and those from similar earlier tests[31] using sodium containing only 1 to 5 ppm Na_2O, as shown in Table IV-1. The 1.84 wt.% chromium and the 4.33 wt.% zirconium alloys still lost considerable ductility, particularly the welded specimens. However, the 5 wt.% molybdenum sample actually showed a slight softening after the test.

Elevated-temperature (2200°F) sodium corrosion is also under study at Brookhaven.[32] Nine 5000-hr (approximately) boiling-refluxing niobium–1 wt.% zirconium capsule tests were completed and subjected to preliminary examination. Variables were sodium purity (75 to 300 ppm oxygen), additions of barium or magnesium, and inserts of niobium, molybdenum, or tantalum. Less than ½ mil of corrosion was observed in all cases. The capsule inserts exhibited thin surface layers colored as follows: bright yellow on niobium, red-brown on molybdenum, and faint white on tantalum. There was reason to believe that the barium addition promoted roughening.

Harwell workers[23] were unable to detect any weight changes in nickel-base braze alloys after exposures to (1) sodium at 650°C, flowing at 0.5 ft/sec and containing 30 ppm oxygen or (2) sodium flowing at 10 ft/sec and containing 10 ppm oxygen for 1350 hr. However, there was some visual evidence of attack.

The effectiveness of zirconium alloying additions to niobium in preventing corrosion by lithium was found by Oak Ridge[33] to depend on their ability to tie up any oxygen present in the alloy. Proper heat-treatment is essential to allow the zirconium to react with any oxygen present in the alloy to form a stable phase that is not attacked by lithium. If this stable phase is ZrO_2, then about 3500 ppm oxygen could be tied up by 1 wt.% zirconium in niobium.

An extensive series of capsule type compatibility tests at Los Alamos[34] was designed to screen thermionic converter construction materials on the basis of their compatibility with liquid cesium to 500°C and cesium vapor to 1000°C. In liquid cesium, the materials apparently unaffected after 100 hr are Y_2O_3, Al_2O_3, Al_2O_3-UO_2, spinel, MgO, $UMoC_2$, tungsten–20 wt.% US, manganese-nickel, chromium, types 321 and 347 stainless steel, and all refractory metals. Silicon, gold, and seven commercial braze alloys were severely attacked. Tests of brazed joints in cesium liquid and vapor frequently resulted in failure or etching of the braze. The most promising joints were: (1) nickel to high-purity metallized alumina, using BT (72 wt.% gold–28 wt.% copper) braze alloy, (2) nickel to metallized BeO, using BT braze alloy, (3) niobium to metallized alumina, using Palco braze alloy, (4) molybdenum to UC : ZrC

Table IV-1 SOME RESULTS OF EXPOSURE OF NIOBIUM-BASE ALLOYS TO LOW-OXYGEN SODIUM AT 650°C FOR 21 DAYS[31]

Alloy composition (balance niobium), wt.%	Weight change, mg/cm²	Appearance
Unalloyed	−0.23	Dull, dark, adherent coating
1.84 Cr (with weld)	+0.02	Weld area dull metallic; remainder dull, dark, adherent coating
1.84 Cr	±0.00	Dull, heavy discoloration
3.21 Cr	±0.00	Bright metallic; small discolored areas
4.33 Zr	+0.01	Dull metallic; some discoloration
4.33 Zr (with weld)	−0.09	Weld area dull metallic, hairline crack; remainder dull, discolored
4.33 Zr	−0.07	Dull metallic, some discoloration
20 Ti–4.28 Cr	+0.23	Dull, iridescent tarnish
20 Ti–4.28 Cr (foil)		Dull, iridescent tarnish; severely embrittled and disintegrated on handling
20.5 Ti–4.28 Cr (with weld)	+0.29	Weld area dull metallic; remainder dull metallic with dark tarnish
20.5 Ti–4.28 Cr	−0.28	Dull metallic, dark tarnish
5 Mo	−0.03	Bright metallic
1 V	+0.21	Covered with dull, black adherent coating
3 V	−0.06	Covered with dull, dark gray adherent coating
5 V	−0.07	Covered with dull, light adherent coating
5.3 V	−0.10	Dull metallic with adherent dark coating

solid solution, using zirconium braze, and (5) niobium to UC:ZrC solid solution, using vanadium braze. In the last two joints listed, the bond was still good after 1 year at 700°C in cesium vapor.

Brookhaven[32] is investigating the corrosion resistance of certain materials in the presence of liquid mercury and mercury vapor. Long-term thermal-convection loop experiments are operated to obtain this information and, in addition, information relative to boiling and condensing phenomena. Materials under investigation include tantalum, zirconium-pretreated carbon steel, and niobium–1 wt.% zirconium. However, only information from one completed experiment—that from a niobium–1 wt.% zirconium system which ceased operation after 7698 hr owing to a faulty vacuum situation—is available. The boiling temperature during this period was 1200°F, with 200°F superheat. It was found that longitudinal cracks had developed in the superheater bend on the condensing side. Metallographic examination of the cracked area showed corrosive attack proceeding from the inside through nearly half of the 60-mil-wall tube. (J. H. Stang)

Radiation Effects in Nonfuel Materials

Defects: Structure and Properties

Metals. Transmission electron microscopy has been used[35] to measure the cluster density in copper irradiated with 2.5×10^{18} fission neutrons/cm^2. Annealing shows that recovery occurs at 275°C in two distinct stages. In the first stage, the density of the larger (>50 A diameter) cluster is reduced. This process occurs in a few tens of minutes with an activation energy of 1 to 1.5 ev. The second stage of recovery requires several thousand minutes at 275°C. In this stage, the smaller clusters (<50 A diameter) and the remaining larger loops disappear with an activation energy of ~2 ev. The small clusters are attributed to vacancies and the larger to interstitials. The first stage of recovery is explained as the thermal dissociation of submicroscopic vacancy clusters, with the consequent annihilation of a large proportion of the interstitials present in the larger loops and an increase in the size and stability of the larger vacancy clusters. The second stage is described as the thermal dissociation of the larger vacancy clusters and the annihilation of the remaining interstitial loops. A simple model in which each interstitial loop, irrespective of size, collects the same number of vacancies during a given anneal is shown to predict the correct shape of the size distribution throughout the annealing.

Fission damage in single-crystal gold films was studied with somewhat similar techniques by Merkle, Singer, and Hart.[36] The spots they observed are 20 to 300 A in diameter and show the contrast of both tensile and compressive type defects. They suggest that the spots are due to primary knock-ons with energies greater than 3×10^4 ev. Their observations indicate that each fission fragment produces, on the average, 25 primaries with energies above this value.

Prethinned foils of aluminum were bombarded[37] with 85-kev H^+, He^+, Ne^+, Ar^+, Kr^+, and Xe^+ ions. Electron microscopy was used to study the defect clusters formed. Contrary to observations reported elsewhere for neutron-irradiated copper, increasing the H^+ ion dose resulted in a reduction in the number of clusters. In general, the heavy ions produced damage that was dose-rate dependent. Only about 1 in 10^4 of the calculated number of point defects was observed as a cluster or loop (Table IV-2). This was attributed to extensive annihilation at the free surfaces. The heavier ions produced relatively more defects, in agreement with simple displacement theory. Damage due to Xe^+, Kr^+, and Ar^+ was retained even after annealing 1 hr at 400°C.

A number of studies are being made of the influence of impurities on defect production and annealing. Studies of iron[38] irradiated with neutrons at 78°K showed sharp effects of nickel (0.087 to 0.074 at.%) in the first stages of anneal, whereas antimony (0.03 to 0.3 at.%) affected the last stages of anneal. A theoretical description has been used to explain annealing in semiconductors,[39] assuming impurity atoms can capture vacancies from Frenkel pairs. Single-crystal molybdenum[11] rods (⟨1 1 0⟩ on the axis) showed no length increase at 10^{18} neutrons/cm^2 ($E > 1$ Mev). However, after exposure to 10^{19} neutrons/cm^2, the rods increased in length by about 0.007%, independent of carbon content from 10 to 500 ppm.

Annealing studies of point defects produced by quenching copper were made with small-

Table IV-2 CALCULATED AND OBSERVED NUMBERS OF DEFECTS FOR POSITIVE-ION BOMBARDMENT OF PRETHINNED ALUMINUM[37]

Ion	Ions/cm^2	Mean number of displacements per ion per cm^2 of foil (n_f)	Mean number of displacements per cm^2 of foil (N_f)	Observed displacements per cm^2 of foil (N^*)	N_f/N^*
H^+	5×10^{16}	1.6	8×10^{16}	2.7×10^{13}	2.9×10^3
He^+	5×10^{16}	30	1.5×10^{18}	5.8×10^{13}	2.5×10^4
Ne^+	5×10^{15}	7.8×10^2	3.9×10^{18}	2.4×10^{14}	1.6×10^4
Ar^+	1×10^{15}	2.0×10^3	2×10^{18}	8.9×10^{13}	2.2×10^4
Kr^+	5×10^{14}	3.3×10^3	1.65×10^{18}	5.6×10^{13}	2.9×10^4
Xe^+	5×10^{14}	3.9×10^3	1.95×10^{18}	8.6×10^{13}	2.2×10^4

angle X-rays scattering from single crystals and by resistivity measurements.[40] The energy of migration for a divacancy was found to be 0.67 ± about 0.05 ev; the binding energy, 0.19 ± 0.04 ev. The frequency factor for divacancy migration was determined to be 3×10^{13} sec^{-1}.

Hardening studies in irradiated copper[41,42] and molybdenum[43] were reported. In one case[41] a divacancy mechanism was proposed to explain the observations.

Defects in Metal Alloys. Various members of the Harwell group are studying radiation effects in steel. Higgins and Roberts[44] used prethinned foils of 0.1 wt.% carbon steel irradiated up to 4×10^{15} fission fragments/cm^2. At the lower doses, defects about 25 A in diameter are observed and, at the higher doses, the defects may be resolved as dislocation loops 50 to 150 A in diameter, together with an irregular network of dislocations. Smith[23] has used X rays to study the increase in unit cell size (Table IV-3). The results indicate that $\Delta a/a_0$ tends to saturate at about 5×10^{14} fission fragments/cm^2 by reason of the relatively large fraction of clustered interstitials. It is known that, as interstitial clusters increase in size, they are less effective in producing a lattice expansion than if the component interstitials are isolated and randomly distributed in the lattice.

Table IV-3 FRACTIONAL INCREASE IN LATTICE CONSTANT FOR IRRADIATED STEELS[23]

Dose, fission fragments per cm^2	Austenitic 18/12 +3 wt.% Mo	Austenitic EP-37	Ferritic FV-520
4×10^{14}	7.1×10^{-4}	9.3×10^{-4}	10.5×10^{-4}
6.5×10^{14}		10.2×10^{-4}	15×10^{-4}
16.8×10^{14}	9.1×10^{-4}	11.7×10^{-4}	
23.5×10^{14}			12×10^{-4}

Defects in Other Materials. Reynolds and Thrower[45,46] have continued to verify the homogeneous nucleation theory of the radiation damage produced in graphite. This theory suggests that interstitial atoms collect into clusters on a scale dependent on the temperature of the graphite and the damage flux to which it is exposed. Some experiments that have been conducted involved short irradiations (6 hr to 6 days) in a materials testing reactor at a lower temperature (150, 200, or 350°C) followed by irradiations of several months at a higher temperature (350 to 650°C). The long-term nucleation pattern has been shown, by transmission electron microscopy, to be profoundly modified by the short initial treatment, and the total rate of accumulation of interstitial atoms is considerably increased. The effects of the enhanced nucleation on macroscopic properties have been demonstrated by comparative measurements of dimensional changes and thermal-resistivity increases during 350°C irradiation of specimens seeded at 150°C. The authors point out that it is essential to ensure that isothermal irradiation experiments are not prejudiced by allowing material to accumulate appreciable doses below the specific irradiation temperature. Additional work[47] by the same authors on the microstructural changes in neutron-irradiated graphite confirmed the suggestions for growth mechanisms proposed elsewhere on the basis of macroscopic observations.

The changes in the physical properties of British Pile Grade A graphite, induced by high-flux fast-neutron irradiation under closely controlled conditions of temperature and flux, have been studied to higher doses than those previously published.[48] Irradiation-induced changes

in thermal conductivity, thermal-expansion coefficients, Young's modulus, electrical resistivity, and dimensions have been observed for irradiation doses of up to 3×10^{21} neutrons/cm^2, as measured by the reaction $Ni^{58}(n,p)Co^{58}$, at irradiation temperatures in the range 225 to 650°C. The results are discussed briefly in terms of the most recent theories of irradiation damage in graphite. In particular, it is shown that the observed dimensional changes can be entirely accounted for by crystallite growth in the c-axis direction and shrinkage in the a-axis direction. Some preliminary data on the changes in dimensions and coefficients of thermal expansion in highly oriented pyrolytic graphite are also described, and these are shown to be in reasonable agreement with the crystallite changes calculated from the observed behavior of the polycrystalline reactor-grade material.

Studies of the mechanical properties resulting from dislocation effects and neutron irradiation have been completed in MgO single crystals.[49] Microhardness measurements, followed by etching to reveal dislocations as well as three-point bending experiments, were used to determine that the fast-neutron damage itself did produce source hardening (higher stresses needed to produce dislocations) and friction hardening (higher stresses needed to move dislocations through the damaged lattice). Annealing to 900°C removes the effects caused by the radiation. The results indicate that individual vacancies or interstitials are producing the effects, whereas there is some indication that they must be related (as a Frenkel pair) to produce the observed results.

X-ray diffraction studies[50] of polycrystalline beryllium oxide irradiated to 1.5×10^{21} neutrons/cm^2 ($E > 1$ Mev) at 110°C showed selective symmetric or asymmetric broadening of reflections $hk \cdot l$ with $l \neq 0$. A unique a_3 spacing could not be defined. Various models were proposed, and the results indicate that the damage results from interstitial clusters.

Nelson[51] has now observed the sputtered patterns produced by 50-kev Xe^+ ion bombardment of UO_2 monocrystals. The preferential ejection from the ⟨1 1 0⟩, ⟨1 0 0⟩, and ⟨1 1 1⟩ directions is taken as evidence for the existence of focused-collision sequences that propagate along these directions. Analysis of the possible focusing mechanisms shows the damage to be very similar to that encountered in the fcc metals.

Direct electron-microscope observations show that fission fragments produce tracks of different types in single crystals of several heat-sensitive materials.[52] A thermal mechanism, based on the loss of energy of the fission fragment to electrons in the irradiated crystal, was proposed to explain the observations. Differences in the amount of damage are attributed to the different ranges of electrons in the various materials. This mechanism is contrasted with that which operates in more stable crystals where a considerable amount of the permanent damage may be due to displacement cascades. Fission tracks have also been observed in glasses,[53] silicon,[54] molybdenite,[55] polymers,[56] and LiF.[57] In the latter case, the mechanism proposed to explain the observations combines volume diffusion of material to the exposed surface and mechanical relaxation around the damage zone.

Theories of Radiation Effects

Lehmann and Leibfried[58] have presented analytical expressions for channeled atoms near the channel axis and hence near the maximum range. Numerical results are presented for a copper primary moving in a copper crystal, but the results can be easily extended to other cases. Two potentials are used. The first is an exponentially screened Coulomb potential (Bohr) thought to give an adequate description for relatively high energies and small interatomic distances, and the second is a purely exponential potential (Born-Mayer) better suited for relatively low energies and large atomic distances. The maximum ranges for a 10-kev copper primary is of the order of 10^3 lattice parameters for the Born-Mayer potential and 10^7 for the Bohr potential. Beeler and Besco[59] are also using a Bohr potential to study the range and damage effects of channeled atoms. They are now extending their machine calculations to include bcc and fcc metals.[25,60] Calculations are discussed for krypton bombarding aluminum and tungsten and for copper and iron atoms moving in their own lattices. Trajectories were simulated along ⟨1 0 0⟩, ⟨1 1 0⟩, and intermediate directions. In bcc materials ⟨1 0 0⟩ was the most prominent tunneling direction, with a minimum stopping power 39% that of ⟨1 1 0⟩. In fcc materials, ⟨1 1 0⟩ was the most prominent tunneling direction, with a minimum stopping power 62% that of ⟨1 0 0⟩. Stopping powers for perfectly tunneled atoms were in the range 0.4 to 2.5

ev/A. The number of defects created in cascades initiated by tunneling atoms was less than 10% that for normal trajectories, and the damage was confined to a region close to the tunnel trajectory.

A model, including directional and many-body effects without arbitrary assumptions, used to examine the kinetic energies transferred to successive atoms and the velocities in collision chains, as well as the displacement mechanism, has been presented.[61] The key mechanism of displacement at low energies is found to be a dynamic replacement by the knock-on (an atom replaces its neighbor). The associated replacement chains propagate with shock-wave velocities. The threshold energy for displacing an atom is found to depend heavily on direction. This dependence makes the integrated probability of displacement a slowly rising function of knock-on energy, in contrast to the step-function form of the simple displacement theory.

The basic assumptions of cascade theory have been discussed by Heinrich and Lenk.[62] A very general angular-dependent formulation of this theory is developed which contains, apart from the threshold energy, a further energy parameter. Angular integration gives the continuous displacement probability. This general model contains, as special cases, most of the models discussed by other authors and, therefore, interpolation is possible. The general continuous displacement probability can be reduced mathematically to give a sharp threshold energy. This procedure is quite general and allows a physical interpretation. As a test case, the hard-core approximation for the scattering law is applied to the present theory. Balarin[63] has prepared a general discussion of the production of defects arising from the correlative collision processes resulting from the irradiation of solids.

Fedulov[64] has developed formulas for the angular variation of the probability for formation of Frenkel pairs in copper crystals due to irradiation with energies near the displacement threshold. Experimental comparisons are satisfactory. A rather detailed discussion of the energy of vacancies in graphite crystals has been reported.[65] Unfortunately, the calculations do not agree with theory and suggest that the model of a vacancy in graphite might not be correct. In addition, Woolley[66] has suggested a modified method of describing the thermal resistivity of irradiated graphite.

A study[67] was made of the spatial distribution of atoms displaced by a primary atom generated by radiation and having a fixed energy and a known initial direction. Mean values were calculated for the products of the different powers of the components of the final position of the primary atom. For this purpose a correlation function was introduced for the distribution of the successive displacements of the primary atom, which includes the possibility of the atom stopping if its energy becomes less than E_d. A matrix method is used to find the recurrence formulas for the quantities corresponding with the nth displacement with respect to the $(n-1)$st displacement, which are expressions leading to Volterra integral equations in the case where n takes on very large mean values. These values are used to calculate the distribution function of the atoms displaced by a primary atom, which, in the third order of approximation, differ somewhat from a three-dimensional Gaussian function. (T. G. Knorr)

Effects of Radiation on Mechanical Properties

The Radiation Effects Information Center has issued a summary[68] of the recently reported work on radiation effects on materials. This, along with another survey report[68a] by Konobeevski, is worthy of note by personnel following the field.

Burst tests carried out by Westinghouse workers[69] on Zircaloy-2 cladding surrounding UO_2 fuel which had received an integrated fast flux of 10^{22} neutrons/cm^2 showed an increased burst strength after irradiation. The irradiation resulted in an 11 to 22% increase in the ultimate tensile strength. Evaluation of these data, along with other tensile data from irradiated Zircaloy-2 cladding, indicates that the increase in the tensile strength is proportional to the cube root of the integrated fast flux. Burst tests made at Hanford[11] on irradiated Zircaloy-2 tubing (PRTR) showed that the increase in hoop tensile strength is greater for annealed than for cold-worked material. These data also indicate that, although the ductility decreases with increased neutron exposure at room temperature, this effect disappears when irradiation is done at 550°F. The effects of cold work and dosage on the strength of Zircaloy-2 tensile specimens are shown in Table IV-4.

Studies made at Oak Ridge[70] using internal friction measurements indicate that nitrogen

Table IV-4 AVERAGE ROOM-TEMPERATURE TENSILE PROPERTIES[11] FOR IRRADIATED AND UNIRRADIATED ZIRCALOY-2

	Tensile strength, 1000 psi		Elongation in 2 in., %			Reduction in area, %	Plastic work, ft-lb
	Yield (0.2% offset)	Ultimate	Uniform	Necking	Total		
Annealed							
Unirradiated							
Longitudinal(3)*	47.9	68.0	16.8	16.2	33.0	51	78
Transverse(3)	54.4	63.1	12.4	22.0	34.4	55	73
0.84×10^{19} neutrons/cm^2							
Longitudinal(3)	64.8	75.2	5.3	10.0	15.3	46	43
Transverse(3)	74.0	74.7	1.1	10.4	11.5	57	31
1.1×10^{20} neutrons/cm^2							
Longitudinal(3)	72.1	78.3	4.2	9.8	14.0	49	40
Transverse(3)	77.5†	77.5	0.8	5.2	6.0		15
10% cold worked							
Unirradiated							
Longitudinal(2)	73.4	81.6	2.3	9.0	11.3	46	30
Transverse(3)	69.4	79.9	2.7	8.9	11.6	52	32
0.84×10^{19} neutrons/cm^2							
Longitudinal(2)	85.0	87.5	1.5	5.0	6.5		18
Transverse(2)	83.9	87.9	1.7	2.6	4.3	50	13
1.1×10^{20} neutrons/cm^2							
Longitudinal(2)	92.0	92.4	1.1	3.5	4.6		14
Transverse(2)	90.9	91.2	1.0	2.9	3.9	45	11
1.1×10^{21} neutrons/cm^2							
Longitudinal(1)	90.0	91.0	0.9	4.3	5.2	41	15
Transverse(3)	92.3	92.3	0.9	3.9	4.8	49	14
20% cold worked							
Unirradiated							
Longitudinal(3)	79.2	88.0	2.6	7.0	9.6	42	31
Transverse(3)	73.0	83.9	2.5	6.8	9.3	52	28
0.84×10^{19} neutrons/cm^2							
Longitudinal(2)	91.8	96.4	1.7	4.7	6.4		22
Transverse(2)	88.3	93.7	1.7	2.8	4.5		14
1.1×10^{20} neutrons/cm^2							
Longitudinal(3)	95.9	97.1	1.3	4.0	5.3	36	17
Transverse(3)	94.4	96.1	1.2	2.0	3.2	40–42	10
1.1×10^{21} neutrons/cm^2							
Longitudinal(3)	96.2	96.6	1.2	4.6	5.8	38–42	19
Transverse(2)	98.0	98.3	1.0	2.6	3.6	38–51	11
40% cold worked							
Unirradiated							
Longitudinal(3)	86.0	96.3	3.0	5.7	8.7	39	29
Transverse(3)	80.3	92.4	2.5	5.8	8.3	53	24
0.84×10^{19} neutrons/cm^2							
Longitudinal(2)	92.9	99.7	2.2	4.6	6.8	41	24
Transverse(2)	92.0	98.8	2.0	2.9	4.9		16
1.1×10^{20} neutrons/cm^2							
Longitudinal(2)	99.7	104	1.5	2.1	3.6	28	12
Transverse(2)	99.6	103	1.5	1.5	3.0	32	10
1.1×10^{21} neutrons/cm^2							
Longitudinal(2)	98.3	101	1.8	3.2	5.0	38	18
Transverse(2)	105	106	1.2	2.8	4.0	29 to 43	13
70% cold worked							
Unirradiated							
Longitudinal(3)	92.8	109	3.4	5.2	8.6	34	33
Transverse(3)	85.6	104	3.6	3.5	7.1	45	23
0.84×10^{19} neutrons/cm^2							
Longitudinal(2)	103	114	2.6	2.3	4.9		19
Transverse(2)	102	112	2.5	2.2	4.7		17
1.1×10^{20} neutrons/cm^2							
Longitudinal(3)	105	112	2.1	3.3	5.4	29	21
Transverse(3)	108	116	1.8	0.9	2.7	19 to 22	10
1.1×10^{21} neutrons/cm^2							
Longitudinal(1)	104	111	3.3	3.0	6.3	30	25
Transverse(3)	111	114	1.4	2.0	3.4	13 to 33	14

* Number in parentheses is number of specimens tested.
† Displayed yield point.

Table IV-5 ROOM-TEMPERATURE TENSILE PROPERTIES OF IRRADIATED STAINLESS STEEL[72]

(Average of Two Tests)

Material	Working direction	Material condition	Tensile strength, 1000 psi: Yield (0.2% offset)	Tensile strength, 1000 psi: Ultimate	% strain: Uniform	% strain: Necking	Reduction in area, %	Plastic work, ft-lb
Quadrants 37 and 38 (7.5×10^{20} neutrons/cm^2)								
AISI 348	TD	Annealed	95.80	111.54	14.0	6.9	53.8	66.5
AISI 348	TD	25% CW*	161.05	168.53	2.5	3.4	43.0	30.9
AISI 348	RD	Annealed	101.00	116.88	17.9	5.7	55.3	79.9
AISI 348	RD	25% CW	159.59	162.43	1.9	3.0	49.0	25.4
Quadrants 59 and 60 (4.5×10^{20} neutrons/cm^2)†								
AM-350	TD	ST	152.24	223.06	10.7	1.2	23.8	33.2
AM-350	RD	ST	152.17	233.31	12.7	1.7	25.2	56.2
AM-350	TD	DA‡	217.55	245.19	5.2	2.5	33.2	63.2
AM-350	RD	DA	216.70	240.40	5.2	2.7	27.9	63.9
AISI 410	TD	Annealed	105.80	106.30	5.4	2.2	51.9	15.4
AISI 410	TD	Martensitic	190.80	215.80	3.0	2.3	45.3	36.8
Quadrants 69 and 70 (5.2×10^{20} neutrons/cm^2)								
AM-350	TD	ST	137.9	244.3	3.8	2.1	45.0	30.0
AM-350	RD	ST	143.2	239.5	12.0‡	2.2	35.3	5.3
AM-350	TD	DA	215.6	245.3	4.8	1.2	20.1	48.6
AM-350	RD	DA	211.7	235.8	9.7	3.8	44.1	47.4
AISI 410	TD	Annealed	§	108.2		3.7	68.8	12.4
AISI 410	TD	Martensitic‡	204.81	215.62	2.5	2.3	43.8	32.4
Quadrant 91 (5.9×10^{19} neutrons/cm^2)								
AISI 410	TD	Martensitic	176.14	198.50	3.8	2.7	47.1	43.9
AISI 410	TD	Annealed¶	58.14	72.80	12.8	5.4	74.8	48.4

* 25% cold work as measured by reduction of area.
† Estimated exposure, neutrons/cm^2 (>1 Mev).
‡ One test only.
§ Yield decrement of $\sim 1000^3$ psi.
¶ Average of three tests.

Table IV-6 ROOM-TEMPERATURE TENSILE PROPERTIES OF STAINLESS-STEEL SPECIMENS AS-FABRICATED[73]

(Average of Three Tests)

Material	Working direction	% cold work	Tensile strength, 1000 psi: Yield (0.2% offset)	Tensile strength, 1000 psi: Ultimate	% strain: Uniform	% strain: Necking	Reduction in area, %	Plastic work, ft-lb
AISI 304	TD	Annealed	32.5	91.9	78.7	6.9	72.7	240.1
AISI 304	TD	25	104.3	133.9	16.3	5.0	65.2	97.7
AISI 348	TD	Annealed	37.8	89.5	58.0	6.3	63.6	144.3
AISI 348*	RD	Annealed	37.0	89.4	49.5	10.2	73.1	164.3
AISI 348†	TD	25	109.6	133.1	3.4	4.7	50.9	35.1
AISI 348	RD	25	112.4	129.2	3.6	7.6	57.1	54.3
AISI 410	TD	Annealed	35.9	66.6	21.1	9.2	74.5	64.5
AISI 410	TD	Martensitic	136.7	171.3	5.1	2.7	52.0	42.4

* One test only.
† Average of four tests.

Table IV-7 ROOM-TEMPERATURE TENSILE PROPERTIES OF STAINLESS-STEEL CONTROL* SPECIMENS[72]

(Average of Two Tests)

Material	Working direction	% cold work	Tensile strength, 1000 psi: Yield (0.2% offset)	Tensile strength, 1000 psi: Ultimate	% strain: Uniform	% strain: Necking	Reduction in area, %	Plastic work, ft-lb
			Quadrants 37 and 38 (Cycles 42 Through 52)					
AISI 348	TD	Annealed	39.50	91.00	57.2	9.7	67.7	173.3
AISI 348	TD	25	120.67	138.36	2.9	4.4	48.3	33.1
AISI 348	RD	Annealed	38.20	91.62	51.6	8.9	71.7	170.5
AISI 348	RD	25	123.28	131.65	2.6	7.2	60.6	43.6
			Quadrants 59 and 60 (Cycles 47 Through 50)					
AM-350	TD	ST	120.85	183.65	16.2	3.9	41.2	125.4
AM-350	RD	ST	114.96	180.31	17.3	4.3	54.5	127.9
AM-350	TD	DA	159.11	191.51	10.2	4.1	25.3	93.1
AM-350	RD	DA	160.92	190.17	8.5	4.4	40.0	84.3
AISI 410	TD	Annealed	38.54	65.97	25.4	11.2	76.0	79.9
AISI 410	TD	Martensitic	139.51	169.50	4.7	3.2	56.6	43.4
			Quadrants 69 and 70 (Cycles 48 Through 50)					
AM-350	TD	ST	118.88	187.29	16.1	4.3	41.4	127.6
AM-350	RD	ST	102.87	191.33	17.2	3.9	47.5	129.0
AM-350	TD	DA	163.84	196.36	8.8	3.2	20.0	80.1
AM-350	RD	DA	159.41	194.06	8.5	4.4	30.2	84.3
AISI 410	TD	Annealed	37.62	67.57	22.8	8.7	75.8	67.9
AISI 410	TD	Martensitic	138.12	127.40	5.3	3.9	63.1	50.7

*Specimens exposed in out-of-reactor loop.

Table IV-8 SUMMARY OF CREEP-RUPTURE TESTS[74] ON TUNGSTEN SPECIMENS IRRADIATED TO 6×10^{17} NEUTRONS/CM^2

Specimen	Condition	Temp., °C	Stress, 1000 psi	Rupture life, hr	Linear creep rate, min^{-1}
		Rod X Material			
84	Control	1100	27.5	5.85	0.00044
93	Irradiated	1100	27.5	6.74	0.00038
83	Control	1100	29.5	0.55	0.00457
82	Control	1100	30.8	0.15	0.0137
85	Control	1200	24	5.00	0.00065
88	Control	1200	25	2.10	0.00116
91	Irradiated	1200	25	2.10	0.00137
89	Control	1400	17.5	4.15	
92	Irradiated	1400	17.5	3.95	
95	Control	1400	18.5	2.60	
90	Irradiated	1400	18.5	2.55	
96	Control	1400	19.5	1.90	
		Rod Y Material			
22	Control	1400	17.5	6.30	0.000060
37	Control	1400	18.5	4.00	0.000360
38	Control	1400	18.5	4.00	0.000140
18	Control	1400	20.75	1.94	0.000171
41	Control	1400	21.5	0.75	

precipitation in iron is increased two- to three-fold during irradiation at −120°F after a 1-day irradiation. However, the nitrogen did not precipitate any faster after a 23-day irradiation than after the 1-day irradiation, thus suggesting a saturation effect. It has also been found[71] that martensite can be transformed by irradiation with electrons.

The stress-rupture properties of the British 20 wt.% chromium–25 wt.% nickel stainless-steel tubing were determined at Oak Ridge.[10] In comparing the results of unirradiated and irradiated specimens, it was found that irradiation caused little loss in rupture strength at 650 and 750°C; however, the average strains at fracture were 30 to 50% lower in the in-pile tests than in the out-of-pile tests. Preliminary results from Hanford's tensile tests of various stainless steels which had been irradiated at 540°F are given in Table IV-5.[72] By comparing the results obtained from unirradiated, as-fabricated specimens (Table IV-6)[73] with those from control specimens which were exposed in an out-of-pile loop at the same temperatures as the irradiated specimens (Table IV-7), it can be seen that slight property changes have been caused by thermal conditions alone.

Irradiated specimens of tungsten[74] have been tested, and some of the results are given in Table IV-8. (F. R. Shober)

Selected Mechanical Properties of Cladding and Structural Materials

Refractory Metals

A detailed evaluation of a single heat of F-48 alloy (niobium–15 wt.% tungsten–5 wt.% molybdenum–1 wt.% zirconium) was made at Battelle.[75] This evaluation includes measurements of mechanical properties (creep and tensile), impact behavior, thermal expansion, and thermal conductivity. From correlations of these properties by statistical analysis methods, the following conclusions were reached:

1. Ductile-to-brittle transition temperatures, either under slow-loading tensile testing or rapid-impact conditions, are substantially above room temperature.

2. Some tensile ductility is usually retained at room temperature, although microscopic ductility in certain areas of massive plates may be nil.

3. At temperatures above the transition-temperature region, tensile properties are consistent and reproducible.

4. Material chemistry from heat to heat is consistent and reproducible.

5. Creep strength at high temperatures (2200 and 2500°F) is erratic and far less reproducible (without closer control of fabrication operations) than is tensile strength.

6. Creep strength may vary from surface to central layers of rolled plate.

7. With close process control, heavy plate of F-48 having both good room-temperature ductility and a 1%, 10-hr creep strength at 2200°F of 15,000 psi can be produced. However, important processing variables have not yet been defined.

8. Collectively, for the heats of F-48 evaluated, design to greater than 9000 psi for a 10-hr, 1% creep life of 2200°F, or greater than 8500 psi for a total deformation of 1% in 10 hr at 2200°F would involve risk.

The tungsten-tantalum-molybdenum-niobium alloy system was investigated by Crucible Steel,[76] and several tungsten- and tantalum-rich alloys were developed and evaluated in the form of extruded bars. Many of these alloys exhibited very high strengths at 2000°F; in fact, the tensile strengths of some alloys were in excess of 20,000 psi. A continuation was made of this effort, aimed at producing and evaluating alloys from this system in the form of sheet and increasing their high-temperature strength by the formation of dispersed carbides. Small cylindrical ingots of six selected tungsten-tantalum-molybdenum-niobium alloys and unalloyed tungsten were vacuum arc melted by a multiple consumable-electrode technique and successfully extruded to sheet bars. Two alloys and unalloyed tungsten were rolled to sheet, and recrystallization temperatures, bend-transition temperatures, and high-temperature tensile properties were determined. The other four alloys could not be rolled to sheet by the techniques attempted in this program. A consumable-electrode technique for vacuum arc melting 88 wt.% tungsten–12 wt.% niobium alloys that contain small amounts of vanadium, zirconium, and carbon was developed. In the as-extruded condition, the alloys showed 3500°F tensile strengths of 49,000 to 57,000 psi. This con-

stituted a twofold increase in strength above that of the base solid-solution composition.

Zirconium

Long-term creep studies of Zircaloy-2 sheet are continuing at Battelle.[77] Table IV-9 summarizes the results of tests currently in progress. The creep rates as shown have reached second stage or constant rate. (J. A. DeMastry)

Selected Metallurgical Aspects of Cladding and Structural Materials

Aluminum

Investigators in Stockholm have conducted literature surveys dealing with aluminum-titanium alloys[78] and aluminum-zirconium alloys.[79] The surveys include references on structure, mechanical properties, corrosion, irradiation effects, and fabrication.

Miscellaneous

The scandium-yttrium and scandium-zirconium systems were studied at Ames[80] by thermal and X-ray methods. Both systems are characterized by complete solid solubility in the low-temperature hexagonal form and in the high-temperature bcc form. In the scandium-yttrium system, there is a minimum in the solidus at 50 at.% and 1365°C, whereas the solidus in the scandium-zirconium system follows a nearly straight-line relation between the melting point of scandium and zirconium. There is a minimum in the temperature of transition from hexagonal to bcc in the scandium-yttrium system at 43 at.% yttrium and 1175°C; whereas the temperature of transition is raised in the scandium-zirconium system to a maximum of 1415°C at 30 at.% zirconium.

Pressure, temperature, volume, resistance, and X-ray diffraction measurements have made it possible to establish a partial pressure-temperature phase diagram for metallic ytterbium by workers at Brigham Young University.[81] An electronic transition, previously indicated as occurring at 60 kbars, 25°C, is shown to occur at 39.5 kbars, 25°C. This transition pressure is lowered by increasing temperature, $\Delta P/\Delta T$ being -19.1 bars/°C, and is accompanied by a change in volume of -0.65 cm^3/mole simultaneously with a change in crystal structure from fcc to bcc. This is the first time a pressure-induced transition from a close-packed to a non-close-packed structure has been observed. Heat absorption at the transition is 89 cal/mole. A number of second-order transitions were discovered. Of particular interest are transitions in bond type from P-T regions in which directional bonds predominate to P-T regions in which metallic bonding predominates.

Refractory Metals

A systematic study was made on chromium-base alloys (by Russian investigators[82]) containing up to 47.5 wt.% niobium and 37.5 wt.% titanium, and niobium-base alloys containing up to 30 wt.% chromium and 30 wt.% titanium. The

Table IV-9 RESULTS OF LONG-TERM CREEP TESTS ON ZIRCALOY-2 SHEET[77]

Specimen	Temp., °F	Stress, psi	Time in progress, hr	Total deformation, %			Minimum creep rate, %/hr
				On loading	At 50 hr	At present	
15% Cold-Worked Material							
7-2-1	650	25,000	49,300	0.250	0.385	2.415	0.0030
7-4-3	750	12,500	46,900	0.134	0.290	3.568	0.0060
Annealed Material							
Zr-A-18	550	15,000	15,800	0.635	0.950	0.964	0.00003
Zr-A-17	650	17,500	34,400	1.778	1.852	4.300	0.0060
Zr-A-25	650	15,000	32,900	0.971	1.002	1.760	0.0020
Zr-A-28	650	12,500	23,250	0.321	0.370	0.475	0.00004
Zr-A-16	750	12,500	34,400	0.447	0.620	6.818	0.0060
Zr-A-26	750	9,000	29,800	0.082	0.120	0.900	0.0015

isothermal sections at 1250 and 1380°C are presented. In the chromium-rich corner (above 60 wt.% chromium), there are three one-phase regions (α-solid solution based on chromium, β-solid solution based on $NbCr_2$, and γ-solid solution based on $TiCr_2$), three two-phase regions ($\alpha + \beta$, $\alpha + \gamma$, $\beta + \gamma$), and one three-phase region ($\alpha + \beta + \gamma$) at 1250°C; at 1380°C only α, β, and $\alpha + \beta$ exist and a liquid phase (composition 25 wt.% titanium, 5 to 15 wt.% niobium) is observed. In the niobium-rich corner (above 70 wt.% niobium) there are a single-phase region δ (niobium-base solid solution) and a two-phase region $\beta + \delta$; the δ region is enlarged on heating to 1380°C, but both regions exist at 1250 and 1380°C. Although some of the alloys in the system studied are characterized by a high hardness (the alloy 30 wt.% chromium–70 wt.% niobium) and others are characterized by high resistance to scale formation at high temperatures (the alloy 25 wt.% chromium–5 wt.% titanium), there are no alloys that have both properties simultaneously.

The chromium-niobium, the quasibinary $NbCr_2$-Ni_3Nb, and the chromium-niobium-nickel systems were studied in detail by differential thermal analysis and X-ray diffraction. The phase diagrams derived by the Russians[83] are given. The chromium-niobium alloy that contained 47.18 wt.% niobium was found to undergo an allotropic transformation at 1590°C and to have a melting point of 1720°C; the allotropic transformation is associated with a transition from a low-temperature β structure of the $MgCu_2$ type to a high-temperature one (ϵ) of the $MgZn_2$ type with lattice parameters $a = 4.92$ and $c = 8.10$ kX. In the system niobium-chromium, a eutectoid transformation ($\epsilon \rightleftharpoons \alpha + \beta$) occurs at 1585°C in chromium-rich alloys, and a peritectoid transformation takes place at 1625°C in niobium-rich alloys. The addition of > 5 to 6 wt.% nickel to the $NbCr_2$, with tempering at 1100°C, causes the formation of a new phase that is assumed to consist of a solid solution of nickel in the ϵ modification of $NbCr_2$; the solubility of nickel in the ϵ phase is 36 wt.% at 1100°C. A four-phase peritectoid equilibrium, $\gamma + \epsilon \rightleftharpoons \alpha + \delta$ (where δ is Ni_3Nb), exists at 1160°C in the chromium-nickel-niobium diagram, in the section confined within the chromium-nickel-Ni_3Nb-$NbCr_2$ quadrangle; the composition at the peritectoid point is: 30.0 wt.% chromium – 23.5 wt.% niobium – 46.5 wt.% nickel. This quadrangle contains one quasi-binary section only, namely, the $NbCr_2$-Ni_3Nb.

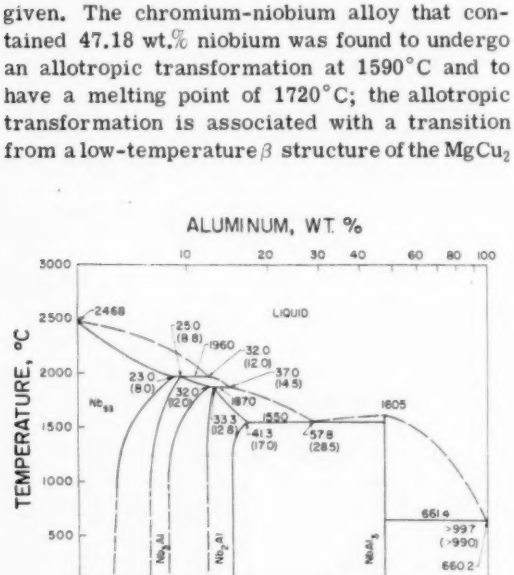

Fig. IV-1 The niobium-aluminum binary phase diagram.[86]

The radioactive isotope Mo^{99} was used by British investigators[84] to study self-diffusion in polycrystalline and single-crystal specimens of molybdenum in the temperature range 1850 to 2350°C. Diffusion-zone analysis was carried out by serial sectioning with a lathe and by X-ray activity measurements with a scintillation counter. The two kinds of specimens gave similar results; diffusion coefficients in the polycrystalline material are expressed by $D = 0.1 \exp(-92.2/RT)$.

The system niobium-ruthenium was investigated by X-ray diffraction and microscopy by German workers.[85] The tetragonal phase was found to be homogeneous between 41 and 46.5 at.% ruthenium. A second phase with a face-centered rhombic unit cell was observed between about 47 and 58 at.% ruthenium. The limits of mutual solubility were found at 17 at.% niobium and 40 at.% ruthenium, respectively. The ruthenium solid solution exhibited a B2 type superlattice, extending over part of the concentration range in analogy to the system vanadium.

The niobium-aluminum binary phase diagram shown in Fig. IV-1 was developed by workers at Denver Research.[86] Three intermediate phases are present: Nb_3Al, Nb_2Al, and $NbAl_3$. The Nb_3Al and Nb_2Al intermediate phases are formed peritectically at 1960 ± 10°C and 1870 ± 10°C, respectively, whereas the $NbAl_3$ phase forms congruently from the melt at 1605 ± 10°C. The maximum solid solubility of aluminum in

niobium is 23.0 ± 0.5 at.% (8.0 wt.%) aluminum at 1960 ± 10°C. A eutectic reaction occurs at 57.8 ± 0.5 at.% (28.5 wt.%) aluminum and 1550 ± 10°C between Nb_2Al and $NbAl_3$. The aluminum-rich end of the diagram has a peritectic reaction at 661.4 ± 0.5°C within less than 1 wt.% niobium. The maximum solid solubility of niobium in aluminum is less than 0.3 ± 0.1 at.% (1.0 wt.%) niobium.

A supplement to DMIC Report 152, which is a compilation of binary and ternary phase diagrams of niobium, molybdenum, tantalum, and tungsten, has been published by the Defense Metals Information Center.[87] Forty new binary and eighty new ternary diagrams are included.

Stress-rupture and creep testing of sintered tungsten at 2400 and 2800°C in hydrogen and argon atmospheres are reported by General Electric.[88] The major portion of the testing was performed at stress levels calculated to cause rupture between 20 and 100 hr. The test data obtained are given in Table IV-10, and the results of all tests on this material are shown in Fig. IV-2. The data indicate that good agreement is obtained in both hydrogen and argon atmospheres at 2800°C, whereas tests at 2400°C appear to show slightly longer times to rupture in hydrogen than in argon.

Similar stress-rupture and creep data were obtained by General Electric[88] from three sources of arc-cast molybdenum at 2200°C when tested in both hydrogen and argon atmospheres, whereas the data for sintered molybdenum varied, depending on the source. Since the results from arc-cast material are reproducible, stress-rupture tests of this material were performed between 1200 and 2200°C intervals in the 1- and 10-hr rupture range. Predictions of the stress-rupture curves at these temperatures were made from an isochronal plot (temperature vs. stress at constant time) using the data previously obtained at 1200 and 2200°C. The curves in Fig. IV-3 were obtained by using the 1- and 10-hr points from this plot at constant temperature. Experimental points obtained at each of the temperatures

Table IV-10 STRESS-RUPTURE–ELONGATION DATA FOR SINTERED TUNGSTEN SHEET[88]

Temp., °C	Atmosphere	Stress, psi	Time to rupture, hr	Percentage elongation in 1-in. gauge length
2400	H_2	960	37.52	10
2400	Ar	1000	23.02	5
		1400	2.30	14
		1600	1.56	18
		2000	0.54	24
2800	H_2	500	94.45	9
		550	62.25	12
		650	39.75	7
		900	3.18	18

are also shown with the curves and are tabulated in Table IV-11. Since it was demonstrated previously that similar results are obtained at 2200°C in both hydrogen and argon atmospheres, testing at the lower temperatures was performed only in hydrogen. The agreement between experimental and predicted data is fairly good.

Additional stress-rupture, as well as evaluation, tests of tantalum were performed[88] in an attempt to determine the source of, and the effect on, the strength caused by contamination

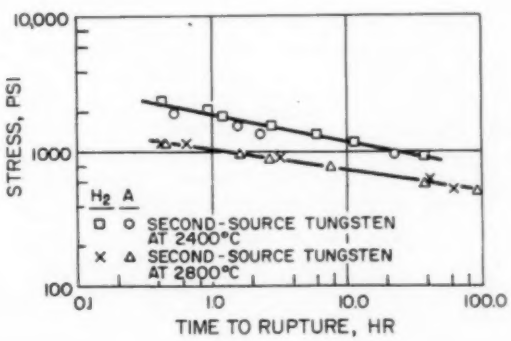

Fig. IV-2 Stress-rupture data for sintered tungsten sheet.[88]

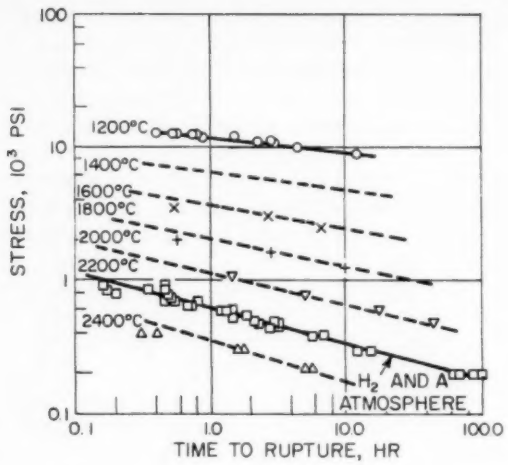

Fig. IV-3 Stress-rupture data for arc-cast molybdenum in hydrogen.[88]

Table IV-11 STRESS-RUPTURE–ELONGATION DATA FOR ARC-CAST MOLYBDENUM[88]

Material	Temp., °C	Atmosphere	Stress, psi	Time to rupture, hr	Percentage elongation in 1-in. gauge length
Mo-C	1600	H_2	2500	5.54	80
			3000	2.61	48
			3500	0.52	53
Mo-C	1800	H_2	1250	9.80	65
			1600	2.78	49
			2000	0.58	36
Mo-C	2000	H_2	650	17.28	88
			850	5.00	64
			1100	1.40	78
Mo-B	2000	H_2	500	44.10	44

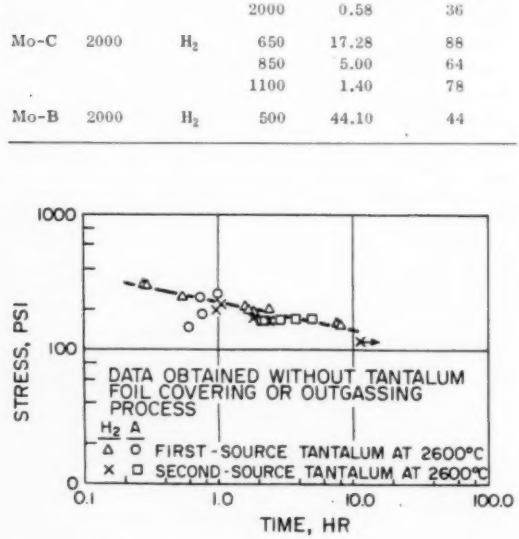

Fig. IV-4 Stress-rupture data for arc-cast tantalum sheet.[88]

of the material during the stress-rupture tests at 2400 and 2600°C in hydrogen and argon atmospheres. A tantalum protection foil was put around the sample and, prior to testing, the furnace was outgassed; these procedures decreased the test sample contamination (primarily oxygen and nitrogen) considerably but did not eliminate it. It was determined that the hardness (DPH) of the tantalum after test was primarily related to the amount of nitrogen in the sample.

The initial stress-rupture curve presented previously for tantalum at 2600°C was obtained using material from source Ta(1). Tests of a second source of material, Ta(2), employing a

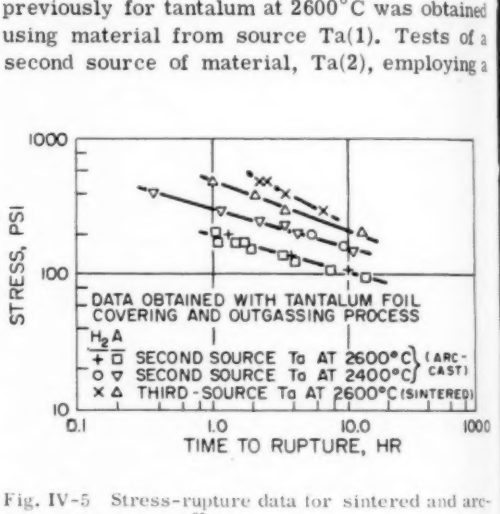

Fig. IV-5 Stress-rupture data for sintered and arc-cast tantalum sheet.[88]

tantalum foil getter around the sample as well as an improved furnace outgassing procedure prior to test, developed a stress-rupture curve that showed the Ta(2) material was not as strong as the Ta(1) material. This difference is attributed to the fact that the Ta(2) material was less contaminated with oxygen and nitrogen rather than to the fact that the materials were from different sources. Figure IV-4 shows the stress-rupture curve for both sources of tantalum obtained without the foil covering or outgassing process. Reasonably consistent results are obtained in a hydrogen atmosphere, but considerably more scatter is obtained when tests are conducted in an argon atmosphere. Figure IV-5 shows the results obtained with the Ta(2) material when the sample is covered with a tantalum foil and the furnace is outgassed prior to test. Good agreement was obtained in both hydrogen and argon at 2400 and 2600°C.

Zirconium

The body-centered cubic to hexagonal-close-packed transformations in titanium and zirconium were studied at the University of California[89] by means of differential thermal analysis at pressures in the range 0 to 65 kbars and at cooling and heating rates of 3 to 5°C/sec. The transitions occurred at different temperatures upon heating and upon cooling, and these hysteresis intervals did not appear to vary much with increasing pressure and/or contamination. Alloying with the tantalum containers and consequent lowering of the transition temperatures was unavoidable in most of the experiments. The titanium transition temperature decreases only slightly with increasing pressure. The zirconium transition exhibits a slope of about 2.4°C/kbar until a new transition is encountered near 58 kbars; the transition from body-centered cubic to the new zirconium polymorph is without much hysteresis, and the phase boundary exhibits a slope of about 0.6°C/kbar. Discontinuities of about 17% in electrical resistance with increasing pressure at room temperature are detected near pressures of 51 to 59 kbars for zirconium and 80 to 90 kbars for titanium, there being a decrease for zirconium and an increase for titanium.

Investigators at Oak Ridge[90] have found the low-temperature specific heats of titanium, zirconium, and hafnium to obey the relation $c = \gamma T + \beta T^3$ from 1.1 to 4.5°K. As with other transition metals, the electronic term is large, and for the Group IV-A metals it decreases with increasing atomic number, indicating a progressively larger degree of electronic interaction in the sequence titanium, zirconium, and hafnium. The Debye temperatures decrease with increasing atomic mass, as would be expected from the central-force model; however, the ratio of the Debye temperatures indicates that the average atomic force constant for hafnium is some 50% larger than for titanium and zirconium, in agreement with the unusually small atomic volume of hafnium.

A Russian paper[91] describes an experimental investigation of the thermal expansion of zirconium-base alloys in order to clarify the effect of hafnium additions on the $\alpha \rightarrow \beta$ transformation temperature of zirconium. Zirconium alloys with 1.1, 2.6, 7.6, and 18 wt.% hafnium were tested. Dilatometric measurements were made in vacuum over a temperature range from 20 to 1000°C. It was found that an increase in hafnium content increases the linear expansion coefficient of the alloys slightly, but the temperature of the inception of the $\alpha \rightarrow \beta$ transformation is increased. The linear expansion coefficient of the forged specimens of the alloy with 7.6 wt.% hafnium is substantially lower than that of the cast specimens throughout the entire temperature range covered. The alloys with 7.6 and 18 wt.% hafnium have similar coefficients up to 900°C.

A Soviet investigation[92] deals with the local character of the distribution of additive elements in zirconium, titanium, and their alloys. The investigation utilized the method of contact autoradiography with concurrent metallography. Radioactive C^{14} was introduced into the metal by drilling a blind hole into an ingot, depositing a suitable amount of radioactive $BaCO_3$, plugging the hole with a stopper of the parent metal, and remelting the ingot in an arc furnace in an atmosphere of argon. The resulting ingot was then subjected to various forms of high-temperature treatment. The amount of radioactive carbon thus introduced into iodide zirconium did not exceed 0.005 wt.%. Similar tests were made on technical titanium with a carbon (including C^{14}) content not exceeding 0.2 wt.%.

It was apparent from the autoradiographs and microstructural photos that the carbon distribution in the two alloys was extremely nonuniform. Hot forging reduced the grain size, but did not change the carbon distribution. Quick cooling after annealing above the $\alpha \rightarrow \beta$ phase-transformation temperature led to formation of a martensitic structure in both metals in which the carbon was said to be distributed along the boundaries of the β-phase grains and along the internal interfaces formed as a result of the $\beta \rightarrow \alpha$ transformation. Slow cooling after annealing in the β region of zirconium preserved the nonuniformity of the carbon distribution in the solid solution, with carbon remaining along the boundaries and subboundaries of the zirconium. This did not occur in titanium (with the greater carbon content). According to the phase diagram, a slow cooling from the β-phase region of titanium leads to the separation of a carbon-rich δ phase in which almost all the carbon of the alloy is concentrated. Thus a two-phase structure [which can be frozen by quick cooling from the $(\beta + \delta)$] region comes into being in titanium. Heat-treatment in the α region (e.g., 20 hr at 800°C) renders the carbon dis-

tribution in both zirconium and titanium uniform, since at that temperature the carbon is said to enter into solid solution in either metal. In the absence of an accurate zirconium-carbon phase diagram, somewhat hypothetical remarks are made on a peritectoid reaction, based on the greater solubility of carbon in the zirconium α phase, which has a closely packed hexagonal lattice, than in the body-centered cubic β phase.

(J. A. DeMastry)

Ceramic Technology

Studies of the brittle behavior of ceramic materials at Armour[93] are continuing in the third year. The results of mechanical testing to date show no clear relation between mean strength and volume of the test section—a surprising development, since the Weibull theory predicts that there should be a systematic relation between size and strength. It is recognized that the understanding of brittle fracture of ceramics is hampered by the present state of the technology of processing. Some new studies are being initiated on (1) chemical machining, (2) analysis of strength, grain size, and porosity relations, and (3) strength and slip activity in dilute solid solutions, concentrated solid solutions, dispersed phases in solid solution, and stably dispersed two-phase structures.

Honeywell[94] has prepared a review paper on the subject of microstructure and mechanical properties of ceramics. The scope includes elastic deformation, anelastic behavior, plastic deformation, brittle fracture, and high-temperature deformation and creep. The report deals almost exclusively with the simple oxide ceramics.

Lawrence Radiation Laboratory has published a bibliography[95] on the mechanical, physical, and thermodynamic properties of the carbides of chromium, hafnium, molybdenum, niobium, tantalum, titanium, tungsten, vanadium, and zirconium. The 1072 references cover the period from 1880 to 1963.

From equilibrium studies of the Nb_2O_5-Ta_2O_5 and the Nb_2O_5-WO_3 systems, a modified Nb_2O_5-Ta_2O_5 diagram has been prepared by A. O. Smith Corp.[96] They propose a tentative diagram of the Nb_2O_5-WO_3 system with the existence of two new possible compounds at the 60-40 and 50-50 (mole %) points.

National Carbon's investigations[97] of phase equilibria have led to a completed phase diagram for the zirconium-carbon system and a tentative diagram for the tantalum-carbon system.

Georgia Tech's[98] continuing work on the sintering of slip-cast fused silica has shown sintering to be enhanced by firing in steam atmospheres. The ultimate strength is higher and the strength development is much more rapid at steam pressures of 2-atm than in 1-atm steam. In another phase of their work studies of the reaction sintering of aluminum-U_3O_8 compacts are in an early stage, with considerably more work required.

Zirconium-pyrographite alloy produced by Raytheon[99,100] has exhibited flexural strengths on the order of that of steel. The strength increased with temperature to 2000°C, where plastic deformation occurred. The alloy has a microstructure unlike either parent material.

(D. J. Bowers)

References

1. D. Weinstein and F. C. Holtz, Improved Zirconium Alloys. Technical Progress Report, November 1, 1962–July 31, 1963, USAEC Report IITRI-B198-43, Illinois Institute of Technology Research Institute, July 30, 1963.
2. R. V. Grebennikov and S. P. Shamashov, Mechanical Properties and Corrosion Resistance of Hafnium-Zirconium Alloys in Steam-Water Media, *At. Energ. (USSR)*, 14: 290-295 (March 1963).
3. W. A. Burns and H. P. Maffei, Neutron Irradiation and Cold Work Effects on Zircaloy-2 Corrosion and Hydrogen Pickup, an Interim Report, USAEC Report HW-76636, Hanford Atomic Products Operation, December 1962.
4. G. H. Jenks and J. E. Baker, In-pile Radiation Corrosion Experiments with Zirconium, Titanium, and Steel Alloys in 0.17m UO_2SO_4 Solutions at 280°C, USAEC Report ORNL-3099, Oak Ridge National Laboratory, July 10, 1963.
5. J. M. Markowitz, Internal Zirconium Hydrate Formation in Zircaloy Fuel Element Cladding Under Irradiation, USAEC Report WAPD-TM-351, Westinghouse Electric Corp., Bettis Atomic Power Laboratory, May 1963.
6. S. A. Reed, W. J. Leonard, E. L. Compere, and L. Rice, Hydriding of Zirconium-Base Alloys During Exposure to Circulating Aqueous Thoria and Thoria-Urania Slurries, USAEC Report TID-7641 (pp. 353-366), paper presented at Third Conference on Nuclear Reactor Chemistry, Gatlinburg, Tennessee, October 9–11, 1962.

7. J. E. Bailey, On the Oxidation of Thin Films of Zirconium, *J. Nucl. Mater.*, 8(2): 259-262 (March-April 1963).
8. J. S. Armijo, Hydrogen Overvoltage and Electrochemical Potentials of Zirconium and Zirconium Intermetallics, USAEC Report GEAP-4192 (EURAEC-620), General Electric Company, Vallecitos Atomic Laboratory, Mar. 1, 1963.
9. J. H. Greenblatt and A. F. McMilland, Polarization Studies of Aluminum Alloys in Water at 200°C and 300°C, *Corrosion*, 19(4): 146t-155t (April 1963).
10. Oak Ridge National Laboratory, Gas-Cooled Reactor Program Semiannual Progress Report for Period Ending March 31, 1963, USAEC Report ORNL-3445, July 23, 1963.
11. Hanford Atomic Products Operation, Metallurgy Research Operation Quarterly Progress Report, January–March 1963, USAEC Report HW-77052, Apr. 15, 1963.
12. F. W. Albaugh, Reactor and Fuels Laboratory Monthly Report, June 1963, USAEC Report HW-78052A, Hanford Atomic Products Operation, July 15, 1963. (Classified; material cited is unclassified)
13. C. N. Spalaris, Finding a Corrosion-Resistant Cladding for Superheater Fuels, *Nucleonics*, 21(9): 41-49 (September 1963).
14. F. W. Albaugh, Reactor and Fuels Laboratory Monthly Report, July 1963, USAEC Report HW-78420A, Hanford Atomic Products Operation, Aug. 15, 1963. (Classified; material cited in unclassified)
15. W. A. Gibeaut and J. J. English, Review of Recent Development—Oxidation Resistant Coatings for Refractory Metals, DMIC Newsletter, Battelle Memorial Institute, Defense Metals Information Center, July 26, 1963.
16. G. A. Meerson and T. Segorcheanu, The Affinity of Niobium for Oxygen, USAEC Translation AEC-tr-5910 [translated from *At. Energ. (USSR)*, 13: 597-599 (1962)].
17. J. A. DeMastry, W. E. Berry, A. A. Bauer, and F. A. Rough, Development of Niobium-Base Alloys for Use in a Nuclear Superheater, USAEC Report BMI-1636 (EURAEC-744), Battelle Memorial Institute, June 27, 1963.
18. W. L. Wheatfall, D. T. Klodt, and C. E. Lundin, An Investigation of the Effect of Metallic Additions Upon the Oxidation Resistance of $NbAl_3$, Interim Report September 1, 1961–August 31, 1962, USAEC Report DRI-2061, Denver Research Institute, September 1962.
19. W. L. Wheatfall and D. T. Klodt, An Investigation of the Effect of Metallic Additions Upon the Oxidation Resistance of Titanium-Modified $NbAl_3$, Quarterly Progress Report No. 3, March 1, 1963–May 31, 1963, USAEC Report DRI-2104, Denver Research Institute, June 1963.
20. J. W. Cox and R. W. Werner, Engineering Testing of F-48 Columbium Alloy, USAEC Report UCRL-6187(Rev.), University of California, Lawrence Radiation Laboratory, Aug. 2, 1961.
21. W. L. Pearl and G. G. Gaul, General and Stress Corrosion of High Nickel Alloys in Simulated Superheat Reactor Environment, USAEC Report GEAP-4165A, General Electric Company, Vallecitos Atomic Laboratory, March 1963.
22. General Electric Company, Atomic Power Equipment Department, Nuclear Superheat Project, Thirteenth Quarterly Report, July 1962–September 1962, USAEC Report GEAP-4126.
23. Metallurgy Division Progress Report, May 1, 1962–October 31, 1962, British Report AERE-PR/M-3, Oct. 31, 1962.
24. Argonne National Laboratory, Reactor Development Program Progress Report, June 1963, USAEC Report ANL-6749, July 15, 1963.
25. Hanford Atomic Products Operation, Metallurgy Research Operation Quarterly Progress Report, January–March 1963, USAEC Report HW-77052, Apr. 15, 1963.
26. F. S. Pettit and E. J. Felten, The Oxidation of Ni-2ThO_2 Between 900° and 1400°C, paper presented at The Fall Meeting of the Electrochemical Society, New York, October 30, 1963.
27. General Atomic Division, General Dynamics Corp., Experimental Beryllium Oxide Reactor Program, Quarterly Progress Report, January 1–March 31, 1962, USAEC Report GA-3053, Apr. 25, 1962.
28. J. W. Semmel, Jr., W. R. Young, and W. H. Kearns, Alkali Metals Boiling and Condensing Investigations. Vol. II, Materials Support, Final Report Covering the Period January 1, 1961 to June 30, 1962, Report GE63-FPD-66, General Electric Company, Space Power and Propulsion Section, Missile and Space Division, Jan. 14, 1963.
29. Argonne National Laboratory, Reactor Development Program Progress Report, July 1963, USAEC Report ANL-6764, Aug. 15, 1963.
30. Argonne National Laboratory, Reactor Development Program Progress Report, August 1963, USAEC Report ANL-6780, Sept. 15, 1963.
31. Argonne National Laboratory, Metallurgy Division Annual Report for 1962, USAEC Report ANL-6677.
32. Jean H. Reynolds (Ed.), Nuclear Engineering Department Progress Report, September 1–December 31, 1962, USAEC Report BNL-782, Brookhaven National Laboratory, May 1963.
33. Oak Ridge National Laboratory Status and Progress Report, September 1963, USAEC Report ORNL-3517, Oct. 9, 1963.
34. E. S. Keddy, Compatibility Evaluation of Materials with Cesium, USAEC Report LAMS-2948, Los Alamos Scientific Laboratory, August 1963.

35. M. J. Makin and S. A. Manthorpe, The Annealing of Dislocation Loop in Neutron Irradiated Copper, British Report AERE-R-4355, June 1963.

36. K. L. Merkle, L. R. Singer, and R. K. Hart, Fission-Fragment Damage in Gold Films, *J. Appl. Phys.*, 34: 2800-2804 (1963).

37. C. J. Beevers and R. S. Nelson, The Formation of Defect Clusters in Aluminum by Ion Bombardment, *Phil. Mag.*, 8: 1189-1202 (July 1963).

38. C. Minier-Cassayre and D. Dautreppe, Resistivity of Doped Iron Irradiated with Fast Neutrons at 78°K, *Compt. Rend.*, 256: 2368-2371 (Mar. 11, 1963).

39. A. V. Spitsyn and L. S. Smirnov, Theory of the Annihilation of Radiation Defects in Semiconductors, *Soviet Phys.-Solid State (English Transl.)*, 4: 2529-2532 (June 1963).

40. A. Seeger, V. Gerold, K. P. Chik, and M. Rühle, Migration Energy and Binding Energy of Divacancies in Copper, *Phys. Rev. Letters*, 5: 107-109 (June 15, 1963).

41. H. Suzuki and A. Furusawa, Recovery of Irradiation Hardening of Copper Single Crystals Around 0°C, *J. Phys. Soc. Japan*, 18: 667-672 (1963).

42. J. N. Lomer, The Effect of Electron Irradiation on the Internal Friction of Copper Between 10°K and 80°K, *Phil. Mag.*, 8: 951-955 (1963).

43. A. S. Wronski and A. A. Johnson, A Hardening Effect Associated with Stage III Recovery in Neutron Irradiated Molybdenum, *Phil. Mag.*, 8: 1067-1070 (1963).

44. Metallurgy Division Progress Report September 1, 1961–April 30, 1962, British Report AERE-PR/M-2, 1962.

45. W. N. Reynolds and P. A. Thrower, Enhanced Nucleation of Radiation Damage in Graphite, British Report AERE-R-4345, May 1963.

46. W. N. Reynolds and P. A. Thrower, The Flux-Level Effect in Radiation Damage, British Report AERE-R-4316, April 1963.

47. P. A. Thrower and W. N. Reynolds, Microstructural Changes in Neutron-Irradiated Graphite, *J. Nucl. Mater.*, 8: 221-226 (1963).

48. H. Bridge, B. T. Kelly, and P. T. Nettley, The Effect of High-Flux Fast-Neutron Irradiation on the Physical Properties of Graphite, British Report TRG-Report-567, July 11, 1963.

49. P. F. Stablein, Dislocation Behavior and the Yield Stress in Neutron-Irradiated MgO, *J. Appl. Phys.*, 34: 1867-1871 (1963).

50. H. L. Yakel and B. Borie, Structural Changes in Irradiated BeO, *Acta Cryst.*, 16: 589-593 (July 10, 1963).

51. R. S. Nelson, The Observation of Collision Sequences in UO_2, British Report AERE-R-4283, April 1963.

52. L. T. Chadderton and H. M. Montagu-Pollock, Fission Fragment Damage to Crystal Lattices; Heat-Sensitive Crystals, *Proc. Roy. Soc. (London), Ser. A*, 270: 239-252 (1963).

53. R. L. Fleischer and P. B. Price, Charged Particle Tracks in Glass, *J. Appl. Phys.*, 34: 2903-2904 (September 1963).

54. D. P. Miller and H. L. Taylor, Nuclear Particle Tracks in Silicon, *J. Appl. Phys. Letters*, 2: 33-34 (Jan. 15, 1963).

55. K. Izui and F. E. Fujita, Electron Microscopic Study of Fission Fragment Damage in Molybdenite Crystals, *J. Phys. Soc. Japan*, 18: 467 (April 1963).

56. R. L. Fleischer and P. B. Price, Tracks of Charged Particles in High Polymers, *Science*, 140: 1221-1222 (June 14, 1963).

57. T. G. Knorr, Surface Structures Resulting from Fission-Fragment Damage in LiF Crystals, *J. Appl. Phys.*, 34: 2767-2773 (September 1963).

58. C. Lehmann and G. Leibfried, Long-Range Channeling Effects in Irradiated Crystals, *J. Appl. Phys.*, 34: 2821-2836 (1963).

59. J. R. Beeler and D. G. Besco, Range and Damage Effects of Tunnel Trajectories in a Wurtzite Structure, *J. Appl. Phys.*, 34: 2873-2878 (1963).

60. D. G. Besco and J. R. Beeler, Jr., Energetic Atom Tunneling in BCC-FCC Metals, USAEC Report CONF-46-40, General Electric Company, Advanced Technology Services, May 1, 1963.

61. C. Erginsoy, Dynamics of Atomic Displacement Processes. I. Primary Energies Near Threshold, USAEC Report BNL-7094, Brookhaven National Laboratory, 1963.

62. D. Heinrich and R. Lenk, Cascade Theory of Defect Production, *Phys. Status Solidi*, 3: 676-691 (1963).

63. M. Balarin, Korrelative Stossprozesse und die Erzeugung von Strahleneffekten in Festkörpern, German Report ZFZ-WK-15, March 1962.

64. M. V. Fedulov, Dependence of the Number of Defects in a Single Crystal on the Direction of Bombardment, *Phys. Metals Metallog. (USSR) (English Transl.)*, 14: 8-15 (1962).

65. C. A. Coulson, M. A. Herraez, M. Leal, E. Santos, and S. Senent, Formation Energy of Vacancies in Graphite Crystals, *Proc. Roy. Soc. (London) Ser. A*, 274: 461-479 (1963).

66. R. L. Woolley, Thermal Resistivity of Irradiated Graphite, *Nature*, 199: 684-685 (Aug. 17, 1963).

67. A. Korchovei, G. Gika, and D. Greku, Distribution of Displaced Atoms in a Solid Due to a Primary Atom Generated by Irradiation, *Soviet Phys.-Solid State (English Transl.)*, 4: 2037-2044 (April 1963).

68. Battelle Memorial Institute, Radiation Effects Information Center, Radiation-Effects State of the Art, 1962-1963, Report REIC-28, June 30, 1963.

a. S. T. Konobeevskii, The Modern State of the Studies of the Nature of Radiation Damage in Solids, *Kernenergie*, 6: 49-55 (February 1963).

69. L. R. Lynam, Examination of PWR Core I Blanket Fuel Rods for Microstructure Changes, Hy-

drogen Pickup, Burst Strength, and Fission Gas Release at the End of the Second Seed Life, USAEC Report WAPD-TM-326, Westinghouse Electric Corp., Bettis Atomic Power Laboratory, April 1963.

70. Oak Ridge Laboratory Status and Progress Report, August 1963, USAEC Report ORNL-3508, Sept. 9, 1963.
71. G. T. Nazarenko and F. Ya Zagarvura, Electron Irradiation as a Method of Strengthening a Steel Surface, *Dopovidi Akad. Nauk Ukr. RSR*, 1: 59-61 (1963).
72. Hanford Atomic Products Operation, Metallurgy Research Operation, Quarterly Progress Report, April-June, 1963, USAEC Report HW-77954 (to be published).
73. Hanford Atomic Products Operation, Metallurgy Research Operation, Quarterly Progress Report, October–December 1962, USAEC Report HW-76228, Jan. 15, 1963.
74. General Electric Company, Advanced Technology Services, High-Temperature Materials Program Progress Report No. 23, Part A, USAEC Report GEMP-23A, May 31, 1963.
75. A. G. Imgram, E. S. Bartlett, and H. R. Ogden, Process Development and Evaluation of Properties of F-48 Niobium Alloy, Final Report, USAEC Report BMI-X-249, Battelle Memorial Institute, July 1963.
76. R. C. Westgren, V. R. Thompson, and V. C. Petersen, Research on Workable Refractory Alloys of Tungsten, Tantalum, Molybdenum, and Columbium, Report WADD-TR-61-134 (Pt. II), Crucible Steel Co. of America, Mar. 1, 1963.
77. R. W. Dayton and R. F. Dickerson, Progress Relating to Civilian Applications During June 1963, USAEC Report BMI-1639, Battelle Memorial Institute, July 1, 1963. (Classified)
78. W. Uhlmann, Aluminum-Titanium Alloys. A Literature Survey, Swedish Report VDIT-73, April 1963.
79. W. Uhlmann, Aluminum-Zirconium Alloys. A Literature Survey, Swedish Report VDIT-74, April 1963.
80. B. J. Beaudry and A. H. Daane, The Scandium-Yttrium and Scandium-Zirconium System, *Trans. Met. Soc. AIME*, 227: 865-868 (August 1963).
81. H. T. Hall and L. Merrill, Some High Pressure Studies on Ytterbium, *Inorg. Chem.*, 2: 618-624 (June 1963).
82. V. N. Svechnikov, Yu. A. Kocherzhinskii, V. I. Latysheva, and V. M. Pan, A Study of Chromium-Niobium-Titanium Alloys, USSR Academy of Sciences, Institute of Metallurgy; *Research on Heat Resistant Alloys*, No. 8: 56-61 (1962).
83. V. N. Svechnikov and V. M. Pan, Phase Diagrams for the Systems Chromium-Niobium and Chromium-Niobium-Nickel, USSR Academy of Sciences, Institute of Metallurgy, *Research on Heat-Resistant Alloys*, No. 8: 47-56 (1962).
84. J. Askill and D. H. Tomlin, Self-Diffusion in Molybdenum, *Phil. Mag.*, 8: 997-1001 (June 1963).
85. E. Raub and W. Fritzsche, Niobium-Ruthenium Alloys, *Z. Metallk.*, 54: 317-319 (May 1963).
86. C. E. Lundin and A. S. Yamamoto, The Equilibrium Phase Diagram, Niobium-Aluminum. Final Report, USAEC Report DRI-2096, Denver Research Institute, April 1963.
87. J. J. English, Binary and Ternary Phase Diagram of Columbium, Molybdenum, Tantalum, and Tungsten, Report DMIC-183, Battelle Memorial Institute, Defense Metals Information Center, Feb. 7, 1963.
88. General Electric Company, Advanced Technology Services, High-Temperature Materials Program, Progress Report No. 25, Part A, USAEC Report GEMP-25A, July 31, 1963.
89. A. Jayoraman, W. Klement, Jr., and G. C. Kennedy, Solid-Solid Transitions in Titanium and Zirconium at High Pressures, *Phys. Rev.*, 131: 644-649 (July 15, 1963).
90. G. O. Kneip, J. O. Betterton, and J. O. Scarbrough, Low Temperature Specific Heats of Titanium, Zirconium, and Hafnium, *Phys. Rev.*, 130: 1687 (June 1, 1963).
91. K. S. Pridantseva, The Effect of Hafnium on the Thermal Expansion of Zirconium, *Sb. Tr. Tsentr. Nauchn.-Issled. Inst. Chernoi Met.*, No. 25: 298-302 (1962).
92. Yu. F. Babikova, G. G. Ryabova, and P. L. Gruzin, Distribution of Carbon Additions in Zirconium and Titanium, *Met. i Metalloved. Chistykh Metal., Sb. Nauchn. Rabot*, No. 3: 28-33 (1961).
93. N. M. Parikh and W. Rostoker (Eds.), Studies of the Brittle Behavior of Ceramic Materials, Quarterly Report No. 1, Report ARF B6012-1, Illinois Institute of Technology, Armour Research Foundation, May 31, 1963.
94. R. J. Stokes, Microstructure and Mechanical Properties of Ceramics, Technical Report No. 19, Report HR 63-264, Honeywell Research Center, May 1963.
95. J. E. Senkin and M. T. Milliken (Comp.), Some Physical, Mechanical, and Thermodynamic Properties of Transition Metal Refractory Carbides, USAEC Report UCRL-7284, University of California, Lawrence Radiation Laboratory, March 1963.
96. L. J. Fiegel, G. P. Mohanty, and J. H. Healy, Equilibrium Studies of Refractory Metal Oxides, USAEC Report LRR-41, A. O. Smith Corp., June 14, 1963.
97. R. V. Sara, C. E. Lowell, and R. T. Dolloff, Research Study To Determine the Phase Equilibrium Relations of Selected Metal Carbides at High Temperatures, Report WADD-TR-60-143 (Part IV), National Carbon Company, Feb. 28, 1963.

98. J. D. Fleming, J. W. Johnson, P. Boland, and S. H. Bomar, Materials for High Temperature Nuclear Engineering Applications, Quarterly Report No. 4, January 1, 1963 to April 1, 1963, USAEC Report TID-18891, Georgia Institute of Technology, Apr. 1, 1963.

99. Raytheon Co., High Temperature Materials Development, Progress Report No. 30, June 1962, AD-281769, July 15, 1962.

100. Raytheon Co., High Temperature Materials Development, Progress Report, August 1962, AD-285518, September 15, 1962.

Section V

Reactor Materials

Special Fabrication Techniques

Melting, Hot and Cold Working

There are many programs now in progress directed toward the development of techniques for the production of refractory-metal tubing. Among the sites with such programs in progress are Nuclear Metals, Argonne, and Du Pont. Nuclear Metals[1-3] is investigating the feasibility of producing tungsten and tungsten-rhenium tubing 0.375 in. in outside diameter by 0.030 in. in wall thickness. The extrusion of tube blanks has been conducted at temperatures of 1200 and 1800°C. It has been possible to extrude the unalloyed tungsten at either temperature, but attempts to extrude the tungsten–26 wt.% rhenium at the lower temperature were unsuccessful. Results to date indicate that the tungsten tubing extruded at 1200°C and annealed at 1450°C has better drawability at 480°C than does as-extruded tubing, and drawing reductions of 15 to 20% result in good surfaces and tolerances.

At Argonne[4] numerous alloys are being investigated for possible use at temperatures below 1000°C in the EBR-II Core II. The niobium–1 wt.% zirconium alloy is serving as the reference material. This alloy was purchased from the vendor in the form of 0.675-in.-diameter rods. Analyses at Argonne indicate that the zirconium content of this material is much lower than specified. A small quantity of this material has been fabricated to tubing. Other alloys being drawn to tubing include niobium–2.4 wt.% chromium, niobium–3.3 wt.% zirconium, niobium–5.2 wt.% vanadium, niobium–1.5 wt.% zirconium–1 wt.% chromium, and other niobium-base alloys. Other studies at Argonne[5] are concerned with the development of alloys for fast-reactor fuel jackets. Attempts to forge the niobium–9 wt.% titanium–8 wt.% vanadium, the vanadium–35 wt.% niobium, and the niobium–20 wt.% vanadium alloys at 850°C were unsuccessful. Attempts to roll the materials at 1150°C were also futile. Other breakdown methods may be required.

The program at Du Pont[6] is also concerned with niobium-base alloys, namely, B66 (niobium–5 wt.% molybdenum–5 wt.% vanadium–1 wt.% zirconium) and D-43 or X-110 (niobium–10 wt.% tungsten–1 wt.% zirconium–0.1 wt.% carbon). Both these materials have been extruded to tube blanks. Attempts to cold reduce the B66 alloy have been unsuccessful owing to cracking, and warm working may be required. The D-43 alloy has been reduced to 0.625-in.-OD by 0.073-in.-wall tubing by annealing at 2600°F and conditioning the internal surfaces after each reduction. As in most tube-drawing operations, the major problem is the condition of the internal surfaces.

Other programs concerned with the development and utilization of refractory alloys include a study of vacuum rolling, the production of ultrathin foils, and alloy preparation studies by powder metallurgical techniques and melting. The Materials Advisory Board[7] has issued a report concerning future requirements for rolling materials that can be expected to be developed within the near future. They have concluded that the most pressing need is a better understanding of the theories of rolling. The vacuum-rolling studies were conducted at Universal-Cyclops,[8] utilizing 10 refractory alloys for the purpose of ascertaining the degree and/or the effect of contamination incurred when the alloys were hot rolled in an atmosphere of 0.5 μ and 100 μ Hg pressure. Of the 10 alloys, only 5 were evaluated: tantalum–10 wt.% tungsten, F-48, D-31, TZM, and molybdenum–0.5 wt.% titanium. Lawrence Radiation Laboratory[9] has reported on the preparation of the F-48 alloy by vacuum arc melting. Both powder compaction and electron-beam melting have been

employed in the preparation of electrodes. It has been possible to extrude the alloy at 3000°F with a reduction ratio of 2.5:1, but attempts to upset-forge the ingots have been unsuccessful. Argonne[5] has produced tungsten foil ~7.8×10^{-5} in. thick and stainless-steel foils ranging from 3.9×10^{-5} to 5.0×10^{-5} in. thick. Even thinner foil requirements may necessitate an investigation of film deposition and stripping techniques. Argonne also has a need for 8000 ft of superconducting wire, <0.010 in. in diameter for solenoidal magnets operating at cryogenic temperatures. For this purpose they have been investigating techniques for making the wire of Nb_3Sn clad with the niobium–33 wt.% zirconium alloy. A small quantity of 0.025-in.-diameter wire has been prepared and will be evaluated.

Studies concerned with the melting and fabrication of uranium have continued at National Lead Co. of Ohio and Nuclear Metals. National Lead[10] has investigated the effects of electron-beam melting on uranium chemistry. Three types of uranium were melted at rates up to 22 in./hr in 3-in.-diameter molds. Analysis of the 8-in.-long ingots revealed that some aluminum, chromium, magnesium, manganese, and lead were volatilized from the melts. The carbon was reduced only in those ingots where the feed stock contained zirconium. Hydrogen was reduced in all ingots, but nitrogen was reduced only in materials where its original concentration was in excess of 100 ppm. These results strengthen the belief that the interstitials can be reduced only to the limit of their solubility at the partial pressure in the melt chamber.

Nuclear Metals[3] is continuing its study of splat-cooled uranium–1.2 wt.% copper and uranium–5 wt.% copper alloys. The technique consists of arc-melting a rapidly rotating consumable electrode so that fine molten particles are flung against the water-cooled mold wall and solidified almost instantaneously. Densification of the particles without altering the small grain size has been accomplished. Specimens are now being aged for periods up to 1000 hr at 800 and 950°C to determine the stability of the particles. (N. E. Daniel)

Cladding

Cladding by Rolling and Swaging

Five advantages in the swage process for fabricating UO_2-PuO_2 fuel elements have been reported by Hanford[11] investigators:

1. The fuel element is loaded with 1.2-in. increments comprising coarse UO_2 and a UO_2-PuO_2 mixture. This restricts gross deviations from the average plutonium concentration in the fuel rod to a length of one increment.

2. A simplified procedure was developed for decontaminating the weld zone.

3. A swageable end cap was developed which simplified loading and completely contained the plutonium throughout the subsequent operations.

4. A blend of particle sizes was developed which permitted the fuel rod to be loaded with fused oxide to a reproducible (±1%) high tapped density.

5. The rods were swaged to a prescribed length within $\pm 1/16$ in.

A process[12] was developed to produce Zircaloy-clad plutonium-zirconium core fuel-element plates by roll cladding. The potential application is in low-cost spike elements, as a means of keeping added plutonium enrichment separate from generated plutonium. The process eliminates external contamination on the finished plate by modifying the design of the Zircaloy sandwich.

The association BelgoNucléaire-CEN[13] has made an extensive study of sonic and ultrasonic compaction, to determine the fragmentation and segregation effects. They observed that intermediate annealing between swaging passes improved the homogeneity of the final densities.

Japanese researchers[14] have been establishing swaging techniques for the fabrication of UO_2 fuel elements for power reactors. Efforts have been directed toward economical fabrication methods for hollow type UO_2 fuel elements to be used in high-temperature reactors, including superheat reactors. Their swaging process produced a fuel rod from fused UO_2 powder; feasible dimensions were 6 to 20 mm in diameter, 0.3 to 0.5 mm in sheath wall thickness, and 1500 mm in length. Maximum swaged densities achieved were 91% and 96% of theoretical by cold and hot swaging, respectively.

Fundamental studies of UC and UC_{2-y} powders and the fabrication of UC and UC_{2-y} fuel elements by both swaging and vibration compaction have been carried out as a part of the Japanese high-temperature reactor fuel development program. Microstructures of the powders and swaged compacts were studied. Swaged densities were more than 91% of theoretical.

An interesting new high-energy-rate metal-working process has been investigated at

Atomics International.[15] Called magnetic-pulse swaging, its potential is the elimination of the fuel-cladding annulus in fuel rods made of UO_2 pellets clad with APM (7 wt.% Al_2O_3 in an aluminum matrix) tubing. A collapsing magnetic field is discharged from a capacitor back through a coil, inducing eddy currents in the fuel element. The resulting repulsive force between the coil and the fuel element produces the swaging action. Radiographic inspection of the rods made this way revealed intimate contact between the cladding and the simulated fuel pellets. In one of the fuel rods containing UO_2 pellets, this contact was maintained after thermal cycling and heat-treatment to 900°F. The author concluded that magnetic pulse swaging is a feasible method for fabrication of APM-UO_2 fuel rods with fuel-cladding contact. (R. J. Diersing)

Pressure Bonding

Hanford and Battelle[16,17] have continued a joint effort to produce clad, high-density UO_2 fuel rods. Pressure bonding is considered a promising fabricating technique because it can densify the UO_2 and clad the fuel during a single operation. Stainless steel was used as the cladding material for most of the studies; subsequently some work was done with Inconel X. For both materials, the bonding parameters were 2100°F and 10,000 psi for 3 hr.

Of the various types of stainless steel evaluated, type 347 provided the best properties. Studies showed that the desired fine-grain structure in the cladding could be obtained if the stainless steel had been subjected to cold working before pressure bonding. Fortunately there was only a little carbide precipitation as a result of gas-pressure bonding.

Some pressure-bonded tungsten-to-tungsten joints, sectioned and examined under a light microscope at Battelle,[18,19] showed what appeared to be poor bonding on the basis of a visible bond line at the original interface. However, these joints were surprisingly strong when mechanically tested, so the bonds were examined under an electron microscope. These revealed that over 50% of the grains had indeed formed metallurgical bonds across the interface but that most of the grain boundaries were still fairly close to the original surfaces, giving an appearance, at low magnification, of poor bonding. The electron micrographs also indicated the presence of tiny voids at the interface, some appearing isolated and others appearing in closely spaced rows. Apparently, at least part of these holes were originally contaminant sites from which loosely held inclusions had been pulled out during metallographic polishing.

(G. R. Goetsch)

Nonelectrolytic Chemical Plating

Interest in the use of chemical vapor deposition as a technique for preparing refractory-metal shapes has promoted several research investigations.

Chemical vapor deposition (CVD) was discussed by Cornell Aeronautical[20] as an applicable technique in a general study of processes for material transfer, joining, and removal. At American Machine & Foundry,[21] a small quantity of tungsten–12 wt.% niobium alloy was prepared by CVD methods. On the basis of an incomplete evaluation, the properties of this alloy appear promising for high-temperature high-strength service.

New Union Carbide data[22] on the mechanisms of reaction occurring during the deposition of pyrolytic carbon were presented. Boron Pyralloy (trade name for pyrolytic carbon alloys with 0.5 to 1.0 wt.% boron) is a CVD material which, because it is deposited in highly ordered form, maintains dimensions and resists the delamination resulting from postdeposition heating that occurs in ordinary pyrolytic graphite.[23] The material can be readily deposited in the form of thick plates.

Rhenium coatings, of nearly theoretical density, were deposited by the Soviets[24] on molybdenum strips and tungsten filaments by thermal dissociation of rhenium chlorides. The range of substrate temperatures was 1000 to 1400°C. A diffusion layer was observed between the rhenium coating and the molybdenum substrate when the deposition temperature exceeded 1300°C.

Metallic coatings, deposited by CVD methods, are useful in joining applications. A U. S. Patent[25] describes the use of a carbonyl nickel layer on graphite as an intermediate which permits subsequent bonding of the graphite to nickel and to zirconium. Molybdenum and tungsten coatings deposited on tungsten substrates by pyrolysis of their respective carbonyls yield thorough metallurgical bonds when the coated parts are heated for 2 hr at 2350°C in hydrogen at 1400 psi.[26] Bond strengths in tension of 30,000 psi were obtained.

Protection of refractory metals from oxidation at elevated temperatures still presents a challenging problem to materials scientists. An investigation by Thompson Ramo Wooldridge[27] was directed toward optimization of processing conditions for the formation of chromium-titanium-silicon diffusion alloy coatings on niobium-base alloys. Pack silicide coatings on 60 wt.% vanadium–1 wt.% niobium–titanium alloy, in a thickness range of $2\frac{1}{4}$ to $2\frac{3}{4}$ mils, appear to offer optimum oxidation protection on the basis of static air oxidation tests[28] at 2200°F. Pack-diffusion coating processes for aluminizing[29] and combined chromizing-aluminizing[30] were patented. Various metallic and nonmetallic coating systems currently under development were reviewed.[31,32]

(E. M. Sherwood)

Ceramic Coatings

During the seventh meeting of the Refractory Composites Working Group,[32] coatings for superalloys were discussed. Armour reported that plasma-sprayed zirconia or hafnia protected tungsten for 5 min at over 3800°F in a torch test, but the tungsten spalled or cracked on reheating. Boeing found that an Inconel-MgO composite containing 2 wt.% Cr_2O_3 would withstand a hot-face temperature of 4600°F. Lockheed noted that a metal-reinforced coating of plasma-sprayed zirconia is superior to one containing only the oxide and could withstand five 3-min exposures at 4500°F. The total hemispherical emittance and normal spectral emittance of a few commercial oxidation-resistant coatings have been measured by the Naval Radiological Defense Laboratory with the following results:

Coating	Substrate	Temp. range, °F	Range of total hemispherical emittance
Pfaudler	Molybdenum	1300–3200	0.6 to 0.7
Chance Vought IV	Molybdenum	1300–3000	0.6 to 0.75
Chromizing Durak B	Molybdenum	1300–3300	0.4 to 0.55

Allison (Division of General Motors) has found that a 10-mil layer of HfN was ample to prevent carbon from diffusing into tungsten in 180 sec at 5400°F. A 6-mil layer was inadequate.

(B. W. King)

Welding and Brazing

Aluminum

Wollaston,[33] in a study of methods of making closures on SAP fuel cans found that argon-arc welding, as well as torch and furnace brazing, gave unsatisfactory results because of low strength, internal fissures, and external blisters. Spot welding also was unsatisfactory because of segregation and weld-line porosity. Pressure welding gave closures that were helium-leak tight and withstood 2000-psi pressure at room temperature. However, the degree of deformation necessary for welding may be intolerable in many applications. Akeret[34] reports that SAP can be successfully flash welded. The requirements for welding involve extremely careful control of the welding procedure to give a very thin fusion zone.

The Budd Company[35] has developed a successful electrical system that will feed back joint resistance changes during resistance welding of aluminum. The device permits automatic control of the weld size and strength. Demonstrations were made on 0.051-in.-thick alloy 5056-H343.

Steels

Heavy steel plate welding is the subject of much research and development to establish materials and processes suitable for pressure vessels and similar devices. Euratom has several studies in progress. In one of these,[36] the electroslag process is being examined to determine the effect of slag composition. Contrary to expectations, it was discovered that slag powders made from pure metals gave poorer results than did commercial powders. The sulfur and phosphorus in the commercial powders would be expected to cause weaker joints.

Grotke[37] has reported on a comprehensive program on the heat-affected-zone portion of a 150,000-psi minimum-yield-strength (HY-150) steel developed for the Navy. His studies indicate that steels of this high strength can be obtained without a corresponding drop in either notch toughness or restraint cracking.

Another class of high-strength steels, the so-called maraging steels, will, if the development work now in progress is successful, provide materials of construction having yield points in the range of 200,000 to 300,000 psi. They can be welded in the heat-treated condi-

tion without preheating, and weld-joint efficiencies of about 90% can be obtained by using postweld treatments as low as 900°F. The biggest problem at the moment is the fracture toughness of welds, which is poorer than that of the base metal.

Tungsten

Hanford[11] has succeeded in welding tungsten end caps to tubes, with essentially no recrystallization of the parent metal. Magnetic-force resistance welding involving weld times of less than 20 msec was used. A very narrow recrystallized bond was found in the joint area, but the recrystallized grains were smaller than those in the parent metal. Thus it might be expected that the welds were stronger than the parent metal.

Martin-Orlando[38] has also developed a technique for joining tungsten with a minimum effect on the parent metal. The parts to be joined are heated to about 1200°F in an inert atmosphere, and a mixture of tungsten hexafluoride and hydrogen is passed over the joint area. The resulting reaction causes pure tungsten to deposit in the joint. This thermochemical welding technique avoids any degradation of the parent-metal properties.

Dissimilar-Metals Joining

A study of considerable interest is in progress at Hanford[39] on the production of dissimilar-metal joints to be used in the high-temperature ATR gas loop. With only three exceptions, all possible combinations of Hastelloy X, Hastelloy C, Haynes 25 alloy, AISI 316, and AISI 347 were welded together by the tungsten-electrode inert-gas process. The only dissimilar-metal joint not made was Hastelloy X to Hastelloy C. Hastelloy W was used to make butt joints in pipe. Most of the joints passed face- and root-bend tests. On the basis of room-temperature tensile strength, the joints showed essentially full efficiency. The work is continuing to determine the stress-rupture properties of the superalloy joints at elevated temperatures.

Brazing

Brazing as a method for joining dissimilar materials and hard-to-weld metals continues to receive much attention. Oak Ridge[40] is in the midst of a fundamental development program to find brazing alloys for beryllium. In this work wetting tests were run on beryllium with the following metals and alloys: silver, gold, germanium, aluminum, copper, palladium–2.1 wt.% beryllium and titanium–6 wt.% beryllium. All but gold, copper, and zirconium–5 wt.% beryllium wet better *in vacuo* than in argon. Little difference was noted with the other metals. Wetting, as expected, increased with temperature. It was found that those metals which showed the least tendency to wet also had the highest calculated liquid-vapor and solid-liquid surface tension. (R. M. Evans)

Explosive Forming

A study to determine the factors that govern the deformation of metals by shock loading and the parameters affecting component production has been conducted by the Royal Armament Research and Development Establishment in England.[41] Up to 12-in.-diameter hemispherical molds and 6-in.-diameter cylindrical molds were employed to establish the relation between the explosive charge, standoff distance, and workpiece for a variety of materials and material thicknesses. The effects of explosive forming on the properties and microstructures of these materials were also studied. The materials investigated included mild steel, alloy steels, stainless steels (including precipitation-hardening stainless steels), Nimonic alloys, aluminum alloys, titanium, and titanium alloys. Of these materials, only the titanium alloys presented difficulties in forming. It is anticipated, however, that these problems may be circumvented by forming the material at an elevated temperature.

Free-forming experiments were conducted with these materials to determine the rate and geometry of deformation. These experiments were photographed with a high-speed camera at 14,000 frames/sec. The results revealed that, for the experimental conditions employed, the velocity of deformation was constant during most of the deformation. The total time of deformation was found to be longer than anticipated from previous claims for the process. The rate of deformation for $^1/_{16}$-in. and $^3/_{16}$-in.-thick copper plates, for example, was found to be 226 and 148 ft/sec, respectively, with a maximum estimated strain rate of 300 ft/sec. The material moved forward as a free body until constrained by the bending wave. The velocity

of bending was essentially constant for varying metal thicknesses. In the tests conducted with each type of material, an increase in impulse resulted in an increase in depth of deformation. When the wall thinning reached its maximum, rupture occurred at the center of the specimen. From the data on depth of deformation and wall thinning obtained during this testing, a linear relation between impulse and depth of deformation was found to exist. This relation is expressed as

$$d = \frac{mW^{2/3}}{R} + c = mI + c$$

where d is the depth of deformation, W is the weight of charge, R is the standoff distance, I is the maximum impulse, and m and c are constants. The values derived for m and c for the materials tested are given in Table V-1.

A linear relation between depth of bulge and volume was found, and the amount of deformation (wall thinning) was controlled by the mechanical and metallurgical properties of the material. The relation between wall thinning and shape of the formed specimen was, however, much more complex. The degree of work hardening experienced during these tests, as assessed by hardness measurements, varied across the wall thickness, being harder on the exterior surface and decreasing toward the interior surface. Typical work-hardening curves for some of the materials tested are shown in Fig. V-1.

A comparison of the work hardening experienced during explosive forming with that experienced in stretch forming or pressing was obtained. It was found that mild steel and commercially pure, soft, titanium body-centered cubic and close-packed hexagonal structures work hardened more during pressing than explosive forming. The difference in hardness with the titanium was quite small, however. Face-centered cubic structures, stainless steel, Nimonic 75 and 90, and superannealed aluminum alloy HS-15 were found to work harden more by explosive forming. With the HS-15 aluminum alloy, the hardness difference was only slightly less. The data obtained during these tests are shown in the curves in Fig. V-2.

An attempt was made to correlate static tensile-test properties with explosive formability. The relation obtained between elongation (measured on a 2-in. gauge length) and maximum

Table V-1 EXPERIMENTALLY DERIVED DATA FOR BULGING OF DIAPHRAGMS[41]

Material	Thickness, in.	Constants of equation $d = mI + c$: m, $g^{-2/3}\,cm^2$	c, cm	Max. impulse, I, $g^{2/3}\,cm^{-1}$	Max. deformation, cm	Max. thinning at rupture, %	Max. increase in HV5 number*
Mild steel	0.063	8.40	+0.16	0.78	6.12	49.1	88
	0.105	5.96	−0.27	1.03	4.93	48.9	79
	0.128	4.92	−0.02	1.22	5.58	53.3	80
Stainless steel	0.048	8.37	−0.001	0.61	5.60	56.0	198
	0.063	6.83	+0.08	0.70	5.75	55.5	202
	0.128	3.68	+0.51	1.08	5.0	54.0	200
Titanium I.C.I. 130	0.050	6.23	0	0.72	5.0	53.0	93
Nimonic 75	0.048	7.95	−0.46	0.68	5.37	60.4	154
	0.125	3.85	−0.046	1.14	4.8	45.6	145
Nimonic 90	0.050	7.99	−0.44	0.70	6.2	63.0	216
	0.129	3.24	+0.42	1.67	5.95	43.4	193
Aluminum alloy HS 15, annealed	0.065	17.9	−0.89	0.33	5.29	60.0	26
	0.125	8.89	−0.83	0.57	4.70	57.0	29
	0.253	6.48	−0.51	1.04	5.64	62.7	35
HS 15 WP condition	0.064	10.65	−0.97	0.33	2.59	28.1	11
	0.126	5.14	−0.030	0.57	2.95	35.0	13
	0.245	2.67	+0.051	0.97	2.75	21.2	12

*Probably refers to Vickers hardness (5-kg load).

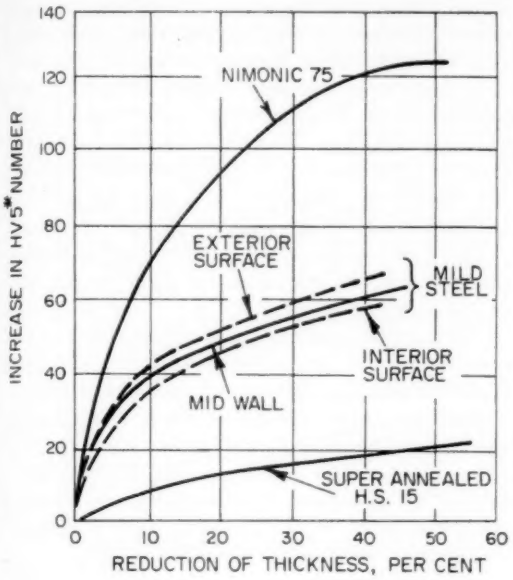

[*Probably refers to Vickers hardness (5-kg load).]

Fig. V-1 Work-hardening curves of $\frac{1}{8}$-in.-thick materials explosively formed.[41]

deformation during explosive forming is shown in Fig. V-3. Of the materials tested, stainless steel was the only one that did not fall on the curves derived. The supposition is that this was due to a breakdown of the austenite during forming. Since elongation values vary only slightly with an increase in strain rate, such a relation may be valid.

A slight increase in elongation values is usually experienced with aluminum at higher strain rates, whereas mild steel appears unaffected, and titanium and its alloys experience a slight decrease.

A study was conducted on the microstructures of explosively formed specimens. The maximum effect, observed as twinning and/or slip, was found to occur near the surface of the tension side of the formed shapes, and much less was found at the surface nearest the charge. The twinning was observed as Neumann Bands in the mild steel which increased in severity up to about 30% reduction in thickness, after which slip lines were also visible. Lath-shaped streaks, thought to consist of a form of martensite, were found in the 18-8 stainless steel. The amount present was much greater than that present during an equivalent amount of deformation by pressing. Annealed Nimonic 90 that possessed large, twinned, solid-solution grains prior to explosive forming showed strain markings after 32% reduction. Pronounced twinning and grain elongation were observed with commercially pure titanium, whereas at 30% reduction some very distorted microstructures were observed.

The results of this metallographic study indicated that with body-centered cubic metals, twinning is predominant on explosive forming and, providing their ductile-brittle transition temperature is sufficiently low, they should form successfully at room temperature. Slip and twinning have been observed in face-centered cubic metals. Other research with single crystals of copper has shown that, by selecting different orientations, any one of four types of defects could be produced by explosive forming: (1) slip on octahedral planes, (2) slip on cube planes, (3) intersecting twins, or (4) par-

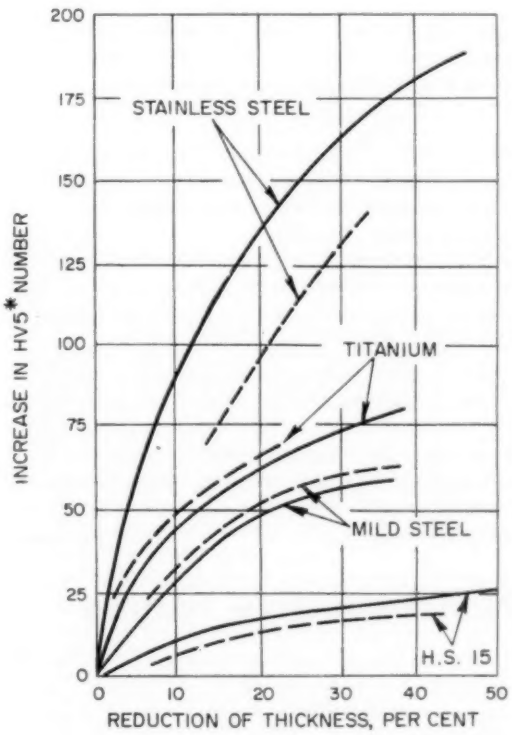

[*Probably refers to Vickers hardness (5-kg load).]

Fig. V-2 Comparison of work-hardening arising from explosive forming and from pressing: —, explosively formed; – –, pressed.

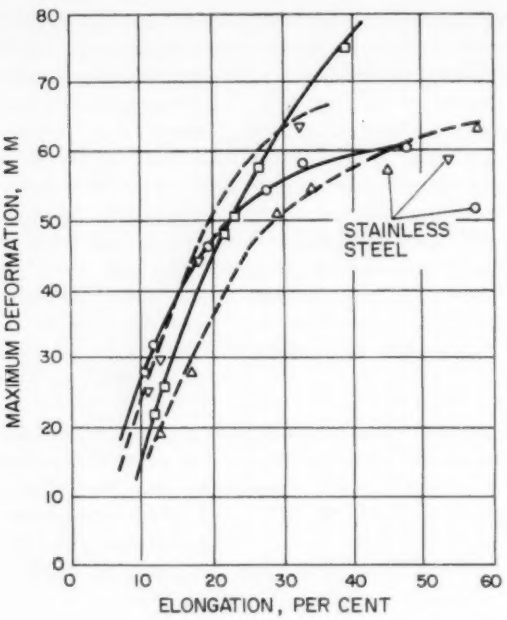

Fig. V-3 Relation between maximum deformation and "static" elongation value.[53] Sheet thickness: △, 0.048 in.; ▽, 0.063 in.; ○, 0.120 in.; □, 0.252 in.

allel twins. The practical application of this work suggests that, for explosive forming, sheet material should have an orientation that favors slip on octahedral planes.

The conclusions that can be drawn from the results of this research are, in general, that during explosive forming, materials behave in a manner that can be predicted from a knowledge of their microstructures, work-hardening characteristics, and mechanical properties, particularly under high rate of strain. Post-forming heat-treatments will be required when undesirable internal stresses, microstructures, or mechanical properties are introduced during explosive forming. (C. C. Simons)

Nondestructive Testing

Armour Research,[42] in continuing studies to evaluate ceramic coatings on metallic substrates, had anticipated that the coating would be sufficiently thin to cause no pronounced alteration in the effective elastic constants of the surface and, therefore, would have little effect on the velocity of a Rayleigh wave. However, the elastic properties of the coatings do vary with depth so that the angle of incidence necessary to produce a Rayleigh wave by mode conversion in a coated material differs from that necessary to generate a Rayleigh wave in uncoated metal. The incident angle also varies with the condition of the coating, i.e., whether it is cracked or not. These conditions present a problem in choosing the wedge angles for generating a Rayleigh wave by mode conversion.

The ratio of the wavelength to coating thickness is a dominant factor in determining the modes of propagation.

The closures and jackets of Hanford[43] AlSi canned reactor fuel elements are brazed and welded to prevent water from entering the cores. Cracks or other defects in these weld beads and brazed layers are the most likely routes for water to enter the core. Hanford has developed an automatic ultrasonic tester, called the UT-4, for inspecting these fuel elements for leaks. Of several test modes tried, the longitudinal wave system gave the best results. The tester is capable of resolving the first-return echoes from a 16-mil-diameter or larger defect located 30 mils or more from the exterior surface of the jacket. The system automatically measures the defect, passes or rejects the fuel element, and records the test results. The pulse repetition rate is 5 kc/sec. Hanford claims the unit detects flaws of 22 mils or greater with nearly 100% reliability.

(D. Ensminger)

References

1. Nuclear Metals, Inc., Fundamental and Applied Research and Development in Metallurgy, Progress Report, February 1963, USAEC Report NMI-2115, Apr. 23, 1963.
2. Nuclear Metals, Inc., Fundamental and Applied Research and Development in Metallurgy, Progress Report, March 1963, USAEC Report NMI-2116, May 28, 1963.
3. Nuclear Metals, Inc., Fundamental and Applied Research and Development in Metallurgy, Progress Report, April 1963, USAEC Report NMI-2117, July 2, 1963.
4. Argonne National Laboratory, Metallurgy Division Annual Report for 1962, USAEC Report ANL-6677.
5. Argonne National Laboratory, Reactor Development Program Progress Report, August 1963, USAEC Report ANL-6780, Sept. 15, 1963.
6. E. I. du Pont de Nemours & Co., Inc., Columbium Alloy Extrusion Program. Phase V. Tubing Program. Interim Report VIII, January 15–April 15, 1963, Report AD-403514.

7. National Research Council, Materials Advisory Board, Recommended Research Program for Rolling, Report MAB-139-M(R3), May 2, 1963.
8. F. R. Cortes, Determination of the Effects of Processing Refractory Metals Under Vacuum, Report ASD-TDR-62-618, Universal-Cyclops Steel Corporation, June 1962.
9. J. W. Cox, R. W. Werner, and J. L. Morris, Engineering Testing of the F-48 Columbium Alloy, USAEC Report UCRL-6187(Rev.), University of California, Lawrence Radiation Laboratory, Aug. 2, 1961.
10. H. M. Eikenberry, Electron Beam Melting of Uranium, USAEC Report NLCO-881, National Lead Co. of Ohio, June 14, 1963.
11. Hanford Atomic Products Operation, Ceramics Research and Development Operation Quarterly Report, January–March 1963, USAEC Report HW-76301.
12. Hanford Atomic Products Operation, Ceramics Research and Development Operation Quarterly Report, October–December 1962, USAEC Report HW-76300.
13. Minutes of Ceramic Fuel Meeting Held in Brussels, October 3–5, 1962, United States–Euratom Joint Research and Development Program, USAEC Report TID-7666.
14. S. Takahashi, Y. Honda, et al., Oxide and Carbide Fuels, Japan–US Research Newsletter No. 1, February 1963.
15. E. C. Supan, Magnetic Pulse Swaging of APM-UO_2 Fuel Rods, USAEC Report NAA-SR-8263, Atomics International, Sept. 30, 1963.
16. E. S. Hodge, S. W. Porembka, C. B. Boyer, and R. J. Diersing, Use of Agglomerated UO_2 in Pressure-Bonded Stainless Steel-Clad Fuel Rods, USAEC Report BMI-1640, Battelle Memorial Institute, July 23, 1963.
17. S. W. Porembka, C. B. Boyer, and J. J. Hauth, Fabrication of UO_2 Fuel Rods by Vibrational Compaction and Pressure Bonding, USAEC Report BMI-1637, Battelle Memorial Institute, June 28, 1963.
18. R. W. Dayton and R. F. Dickerson, Progress Relating to Civilian Applications During May 1963, USAEC Report BMI-1632(Del.), Battelle Memorial Institute, June 1, 1963.
19. R. W. Dayton and R. F. Dickerson, Progress Relating to Civilian Applications During June 1963, USAEC Report BMI-1639(Del.), Battelle Memorial Institute, July 1, 1963.
20. P. Rosenthal, A General Study of Processes for the Realization of Design Configurations in Materials, Report AD-403142, Cornell Aeronautical Laboratory, Inc., April 1963.
21. M. E. Browning, W. H. Webster, Jr., and B. A. Macklin, Deposition for the Production of Structure, American Machine & Foundry Co. Interim Progress Report No. 7, February 1–May 1, 1963.
22. R. Lowrie, Research on Physical and Chemical Principles Affecting High Temperature Materials for Rocket Nozzles, Quarterly Progress Report, Union Carbide Research Institute, June 30, 1963.
23. High Temperature Materials, Inc., Development of Boron Pyralloy for Rocket Motor Hardware, Final Report on Contract NOw 60-0292(FBM), May 6, 1963.
24. A. N. Zelikman and N. V. Baryshnikov, Obtaining Rhenium Coatings by Thermal Dissociation of Rhenium Chlorides, *Tsvetn. Metal.*, (2): 120-126 (1963).
25. H. W. Davidson and J. W. Ryde, Methods of Joining Graphitic Surfaces, U. S. Patent 3,097,931 (to General Electric Company, Ltd.), July 16, 1963.
26. R. I. Batista, G. S. Hanks, and D. J. Murphy, Elevated Temperature Diffusion Bonding of Tungsten to Tungsten Under Pressure, USAEC Report LADC-5262, Los Alamos Scientific Laboratory, 1962.
27. Thompson Ramo Wooldridge Inc., Advancement of High Temperature Protective Coatings for Columbium Alloys (II), First Interim Technical Progress Report, February 16–June 16, 1963, on Contract AF 33(657)-7396 S2.
28. L. I. Kane, J. J. Rausch, and F. C. Holtz, High-Temperature Oxidation Protective Coatings for Vanadium-Base Alloys, Bimonthly Report No. 4, March 13–May 12, 1963, Illinois Institute of Technology, Armour Research Foundation, June 7, 1963.
29. R. B. Puyear, Vapor Diffusion Coating Process, U. S. Patent 3,096,160 (to Union Carbide Corp.), July 2, 1963.
30. C. A. de Guisto, Diffusion Coating of Metals, U. S. Patent 3,096,205 (to Chromalloy Corporation), July 2, 1963.
31. W. L. Aves, Jr., High Temperature Aerospace Coating Systems, Paper No. 13 presented at Fifth National SAMPE Symposium on Materials and Processes for Space Power and Primary Propulsion, June 2–5, 1963.
32. W. A. Gibeaut and H. R. Ogden, Summary of the Seventh Meeting of the Refractory Composites Working Group, Report DMIC-184, Battelle Memorial Institute, Defense Metals Information Center, May 30, 1963.
33. K. H. Wollaston, End Sealing of Experimental S.A.P. Fuel Element Cans by Pressure Welding, *Welding and Metal Fabrication*, 30: 319-323 (August 1962).
34. R. Akeret, The Bonding of S.A.P., *J. Nucl. Mater.*, 8: 126-137 (January–February 1963).
35. R. P. Hurlebaus, Development of Automatic Quality Control for Resistance Welds in Aluminum Alloys, Phase II, The Budd Company, Contract No. DA-36-034-ORD-3217 RD, Nov. 20, 1962.
36. Schweisstechnische Lehr- und Versuchanstalt, Research into Electroslag Welding of Reactor

Steels, Quarterly Report, October 1 to December 31, 1962, USAEC-Euratom Report EURAEC-585, Jan. 31, 1963.

37. G. E. Grotke, Weldability and Heat-Affected-Zone Toughness of HY-150 Steel, paper presented at the 44th Annual Meeting of the American Welding Society, Philadelphia, Pa., April 1963.
38. Refractory Metal Weld Developed, *Aviation Week and Space Technol.*, 79(2): 85 (July 8, 1963).
39. R. L. Knecht, Hanford Atomic Products Operation, May 15, 1963. (Unpublished)
40. Oak Ridge National Laboratory, Gas-Cooled Reactor Program Semiannual Progress Report for Period Ending March 31, 1963, USAEC Report ORNL-3445, July 23, 1963.
41. S. W. Hollingum, High Energy Rate Forming of Metals—I, *Metal Ind. (London)*, 102(23): 801-804 (June 6, 1963).
42. A. M. Baumanis and W. E. Lawrie, Ultrasonic Methods for Nondestructive Evaluation of Ceramic Coatings, Report WADD-TR-61-91 (Part III), Illinois Institute of Technology, Armour Research Foundation, Feb. 28, 1963.
43. D. O. Hunter and M. F. Zeutschel, UT-4—An Automatic Ultrasonic Tester for Closures of Hanford I & E Fuels, USAEC Report HW-74625, Hanford Atomic Products Operation, May 1963.

LEGAL NOTICE

This document was prepared under the sponsorship of the U. S. Atomic Energy Commission. Neither the United States, nor the Commission, nor any person acting on behalf of the Commission:

A. Makes any warranty or representation, expressed or implied, with respect to the accuracy, completeness, or usefulness of the information contained in this report, or that the use of any information, apparatus, method, or process disclosed in this report may not infringe privately owned rights; or

B. Assumes any liabilities with respect to the use of, or for damages resulting from the use of any information, apparatus, method, or process disclosed in this report.

As used in the above, "person acting on behalf of the Commission" includes any employee or contractor of the Commission, or employee of such contractor, to the extent that such employee or contractor of the Commission, or employee of such contractor prepares, disseminates, or provides access to, any information pursuant to his employment or contract with the Commission, or his employment with such contractor.

NUCLEAR SCIENCE ABSTRACTS

The U. S. Atomic Energy Commission, Division of Technical Information, publishes *Nuclear Science Abstracts (NSA)*, a semimonthly journal containing abstracts of the literature of nuclear science and engineering.

NSA covers (1) research reports of the U. S. Atomic Energy Commission and its contractors; (2) research reports of government agencies, universities, and industrial research organizations on a world-wide basis; and (3) translations, patents, books, and articles appearing in technical and scientific journals.

Complete indexes covering subject, author, source, and report number are included in each issue. These are cumulated quarterly, semiannually, and annually providing a detailed and convenient key to the literature.

Availability of *NSA*

SALE *NSA* is available on subscription from the Superintendent of Documents, U. S. Government Printing Office, Washington, D. C., 20402, at $30.00 per year for the semimonthly abstract issues and $22.00 per year for the four cumulated-index issues. Subscriptions are postpaid within the United States, Canada, Mexico, and all Central and South American countries, except Argentina, Brazil, British and French Guiana, Surinam, and British Honduras. Subscribers in these Central and South American countries, and in all other countries throughout the world, should remit $37.00 per year for subscriptions to semimonthly abstract issues and $25.00 per year for the four cumulated-index issues.

EXCHANGE *NSA* is also available on an exchange basis to universities, research institutions, industrial firms, and publishers of scientific information. Inquiries should be directed to the Division of Technical Information Extension, U. S. Atomic Energy Commission, P. O. Box 62, Oak Ridge, Tennessee, 37831.